AFML-TR-78-158

EVALUATION OF YTTRIATED TITANIUM 6Al-4V PLATES AND FORGINGS

A. W. Gunderson
R. F. Geisendorfer

Materials Integrity Branch
Systems Support Division

January 1979

TECHNICAL REPORT AFML-TR-78-158

Final Report for Period June 1975 to August 1978

AIR FORCE MATERIALS LABORATORY
AIR FORCE WRIGHT AERONAUTICAL LABORATORIES
AIR FORCE SYSTEMS COMMAND
WRIGHT-PATTERSON AIR FORCE BASE, OHIO 45433

NOTICE

When Government drawings, specifications, or other data are used for any purpose other than in connection with a definitely related Government procurement operation, the United States Government thereby incurs no responsibility nor any obligation whatsoever; and the fact that the government may have formulated, furnished, or in any way supplied the said drawings, specifications, or other data, is not to be regarded by implication or otherwise as in any manner licensing the holder or any other person or corporation, or conveying any rights or permission to manufacture, use, or sell any patented invention that may in any way be related thereto.

This report has been reviewed by the Information Office (OI) and is releasable to the National Technical Information Service (NTIS). At NTIS, it will be available to the general public, including foreign nations.

This technical report has been reviewed and is approved for publication.

Allan W. Gunderson

ALLAN W. GUNDERSON
Engineering and Design Data
Materials Integrity Branch

C J Harmsworth

C. L. HARMSWORTH, Technical Manager
Engineering & Design Data
Materials Integrity Branch

FOR THE COMMANDER

T. D. Cooper

T. D. COOPER, Chief
Materials Integrity Branch
Systems Support Division

"If your address has changed, if you wish to be removed from our mailing list, or if the addressee is no longer employed by your organization please notify AFML/MXA *,W-PAFB, OH 45433 to help us maintain a current mailing list".*

Copies of this report should not be returned unless return is required by security considerations, contractual obligations, or notice on a specific document.

AIR FORCE/56780/19 July 1979 — 460

UNCLASSIFIED
SECURITY CLASSIFICATION OF THIS PAGE *(When Data Entered)*

REPORT DOCUMENTATION PAGE		READ INSTRUCTIONS BEFORE COMPLETING FORM
1. REPORT NUMBER AFML-TR-78-158	2. GOVT ACCESSION NO.	3. RECIPIENT'S CATALOG NUMBER
4. TITLE *(and Subtitle)* EVALUATION OF YTTRIATED TITANIUM 6Al-4V PLATES AND FORGINGS		5. TYPE OF REPORT & PERIOD COVERED FINAL June 75 - August 78
		6. PERFORMING ORG. REPORT NUMBER
7. AUTHOR(s) A. W. Gunderson and R. F. Geisendorfer(18*) Air Force Materials Laboratory Wright-Patterson AFB, Ohio 45433		8. CONTRACT OR GRANT NUMBER(s)
9. PERFORMING ORGANIZATION NAME AND ADDRESS Air Force Materials Laboratory Wright-Patterson Air Force Base, Ohio 45433		10. PROGRAM ELEMENT, PROJECT, TASK AREA & WORK UNIT NUMBERS 2418
11. CONTROLLING OFFICE NAME AND ADDRESS Air Force Materials Laboratory (AFML/MXA) Air Force Systems Command Wright-Patterson Air Force Base, Ohio 45433		12. REPORT DATE January 1979
		13. NUMBER OF PAGES 123
14. MONITORING AGENCY NAME & ADDRESS*(if different from Controlling Office)*		15. SECURITY CLASS. *(of this report)* Unclassified
		15a. DECLASSIFICATION/DOWNGRADING SCHEDULE

16. DISTRIBUTION STATEMENT *(of this Report)*

Approved for public release; distribution unlimited.

17. DISTRIBUTION STATEMENT *(of the abstract entered in Block 20, if different from Report)*

18. SUPPLEMENTARY NOTES

*Currently Staff Member
Battelle-Northwest
Richland, Washington 99352

19. KEY WORDS *(Continue on reverse side if necessary and identify by block number)*

Titanium
Mechanical Properties
Yttria
Rare Earth Alloying
Fatigue
Fracture
Fatigue Crack Growth

20. ABSTRACT *(Continue on reverse side if necessary and identify by block number)*

This program evaluated the effects of yttrium additions to titanium 6Al-4V alloy by means of mechanical property testing and metallurgical studies. Product forms evaluated which contained yttria (yttrium oxide) included hand forgings, die forgings, and plate material which were compared to baseline plate material which had no yttria additions. The summary of results of the mechanical property evaluations are presented below. Certain heats and specimens did appear as outliers from the norm and these have been noted.

DD FORM 1 JAN 73 1473 EDITION OF 1 NOV 65 IS OBSOLETE

UNCLASSIFIED
SECURITY CLASSIFICATION OF THIS PAGE *(When Data Entered)*

Block 20 continued.

Metallographic evaluations of the yttriated material demonstrated the yttria particles are readily observable by optical and scanning electron microscopy. Fracture surface analysis on the failed fatigue and tensile specimens did not establish a direct correlation between specimen performance and yttria particles or clusters. These results indicate the effects of yttria additions are indirect and more subtle, and that the variations in data are more likely to be a consequence of the differences in mill processing procedures due to the greater hot workability of the yttriated titanium.

SUMMARY MECHANICAL PROPERTY COMPARISONS OF YTTRIATED TITANIUM TO NON-YTTRIATED BASELINE PLATE.

Material	Specimen Orientation	UTS, ksi	YS, ksi	% Elong.	% RA	E, psi x 10^6	Fracture* Toughness, ksi-$in^{1/2}$	Fatigue Crack Growth Rate	Fatigue N	Fatigue S
Baseline Plates-No Yttria	ST	143.1	128.4	10.6	16.2	15.0		=**	=	=
	L	145.4	138.3	16.9	27.4	17.8	66.2			=
Plates with Yttria	ST	141.8	129.6	11.5	24.1	15.1		+	=	-
	L	138.6	131.5	18.8	40.7	16.1	63.5			=
Forgings with Yttria	ST	141.6	128.6	14.0	27.6	15.6		+	=	=
	L	140.9	131.9	16.0	30.3	16.8	56.7			=***
BCL/AFML No. 14 Die Forging w/Yttria	ST	140.4	128.7	8.0	12.9	16.3		+	=	-
	L						62.8			=

* Fracture toughness measurements were made on less than optimum size specimens; therefore, the values should be used only for relative comparisons. S-L specimen orientation.

** KEY: =, equal to baseplate
+, improvement over baseplate
-, degraded from baseplate

*** Compare favorably except for BCL/AFML No. 12, and one outlying data point from No. 13.

FOREWORD

This report describes a joint inhouse/contractor effort under Work Unit 24180703 "Engineering and Design Data". The work reported herein was performed during the period of July 1975 to August 1978 under the direction of Mr. A. W. Gunderson and Mr. R. F. Geisendorfer of AFML/MXA. A major portion of the testing effort was conducted at Battelle-Columbus Laboratories under Contract F33615-75-C-5065, directed by Mr. O. L. Deel. This report was submitted by the authors for publication in October 1978.

The authors thank Dr. D. N. Williams, Battelle-Columbus Laboratories, Columbus, Ohio, for the initial metallographic analysis, Mr. A. L. Wingert, Boeing Materials Technology, the Boeing Company, Seattle, Washington, for the pole figure determinations, and Mr. B. Strope, Systems Research Laboratories, Research Applications Division, Dayton, Ohio, for the X-ray spectroscopy and scanning electron microscopy. Additionally, the authors appreciate the cooperation of industrial users and producers of titanium in supplying the materials for this investigation and in sharing their test results during the course of this study, and the numerous helpful discussions, in particular, those with Dr. H. B. Bomberger, RMI, Inc., Mr. H. Turner and Dr. S. Shastry, McDonnell-Douglas, St. Louis, Missouri, Dr. B. Rath, Naval Research Laboratory, Washington, D. C., and Mr. W. Kerr, Dr. P. Bania, and Mr. L. Clark of the Air Force Materials Laboratory, Wright-Patterson AFB, Ohio. A special thank you to Ms. Debra Patten for her assistance in assembling and typing this report.

TABLE OF CONTENTS

TABLE OF CONTENTS (CONT'D)

LIST OF ILLUSTRATIONS

LIST OF ILLUSTRATIONS (CONT'D)

LIST OF ILLUSTRATIONS (CONT'D)

LIST OF ILLUSTRATIONS (CONT'D)

LIST OF TABLES

LIST OF TABLES (CONT'D)

LIST OF TABLES (CONT'D)

SECTION I

INTRODUCTION

1. BACKGROUND

Rare earth* additions to titanium have been of interest to researchers at least since the infancy of the titanium industry, and for a variety of reasons. Schwartzberg (Reference 1), in 1958, surveyed the literature then existing and found information on phase diagrams, deoxidation, fabricability, corrosion resistance, strength, and neutron-absorption properties. However, most efforts involved cerium and lanthanum additions. Interestingly, although some grain refinement was shown in early investigations of rare earth additions to titanium, decreased fabricability was also shown for several alloys. Still further, at a symposium in 1956, sponsored by Watertown Arsenal, one producer working with misch metal (the naturally occurring ratio of rare earths in the particular mineral used as the starting material) additions to titanium reported hot shortness, while another reported that higher working temperatures were necessary. Most additions were 0.5 weight percent or greater and apparently did not include yttrium.

Conversely, during the late 1960's, Bomberger, et al (Reference 4), invented a method of improving the macrostructure (reducing the prior beta grain size) of titanium-base alloys by small additions of yttrium (.03 to .40 weight percent). Although greater sonic inspectability and increased workability were shown, tensile properties were adversely affected. However, by adjusting (increasing) the amount of the interstitial strengtheners, oxygen and/or nitrogen, to compensate for the oxygen gettering effect of yttrium, the loss in strength could be regained.

*The rare-earth elements (References 2, 3) are commonly called the lanthanides or lanthanons and include elements of atomic number 57 through 71. Scandium (21) and yttrium (39), while not strictly rare earths are very similar in properties to and often occur in nature with the rare earths, and hence are usually included.

As a result of the foregoing promising effect of yttrium additions to titanium, the Air Force Materials Laboratory in 1973, funded an exploratory development program to determine the optimum additions for grain refinement in both an alpha-beta and a beta titanium alloy, and to establish both the positive and negative effects of such additions to titanium.

The program (Reference 5) evaluated 3-inch diameter forged bar stock made from 8-inch diameter laboratory prepared ingots of Ti-6Al-4V and Ti-3Al-8V-6Cr-4Mo-4Zr. The evaluation included room and elevated tensile tests, fracture toughness, creep, K_{ISCC}, smooth and notched fatigue, and Charpy impact determinations. Improved ultrasonic inspectability was shown for both alloys with additions of yttrium as low as 0.03 weight percent. However, grain refinement at the 0.03 yttrium level was shown only for Ti-6Al-4V. Improved tensile ductility was also shown with some loss in toughness. Other properties were little affected; furthermore, similar results were obtained for additions of yttrium as a metal or as an oxide. Further work to determine the most effective level of yttrium additions to commercially important titanium alloys was recommended; unfortunately, no additional optimization or scale-up studies were funded by the Air Force.

In early 1974, one titanium producer, apparently without customer knowledge, began making minor additions of yttria to production heats of Ti-6Al-4V and Ti-5Al-2.5Sn to improve the mill fabricability of their products with attendant cost benefits. These additions were well within the trace element limits specified in MIL-T-9046 and MIL-T-9047 for titanium and were apparently based upon proprietary work (6). A considerable tonnage amount (some 400 production heats) has been produced with yttria additions with only a limited amount of data generally available on the effect of such additions on properties.

In late 1974, a Ti-6Al-4V die forging, scheduled for inclusion in an Air Force aircraft, exhibited low tensile ductility in a specimen taken from a prolongation region of the forging. Both the forger

and the aircraft manufacturer conducted additional tests on this forging and discovered inclusions or clusters of particles high in yttrium and of a size believed to be large enough to affect the mechanical properties.

2. OBJECTIVES

As a result of ensuing discussions between the titanium producer, forger, aircraft manufacturer, and the Air Force, it was determined that additional data would be required to make usage disposition of yttria-containing titanium in the industrial pipeline. This program was subsequently established and conducted with three primary objectives: 1. to clarify the major unknowns about the effects of yttria additions to titanium plate and forgings on mechanical properties; 2. to provide guidance for any subsequent disposition and/or design adjustments necessary for incorporating, where appropriate, yttria-containing titanium in aerospace hardware; and 3. to make recommendations on the desirability and guidelines for further work to establish the conditions, if any, under which the benefits of yttria (or yttrium) additions to titanium may be realized without serious detrimental effects.

3. SCOPE

Some 14 plate and forging materials from 13 production heats were evaluated during the present study, three of which were non-yttriated plates for baseline property comparisons. The room temperature mechanical properties evaluated selectively were tensile strength and ductility, fracture toughness, notched and smooth fatigue, fatigue crack growth (da/dn), and stress corrosion (K_{ISCC}). The metallurgical evaluation included optical and electron metallography/fractography, energy and wavelength dispersive x-ray analysis, and crystallographic texture determinations.

SECTION II

MATERIALS AND TESTING PROCEDURES

1. COMPOSITION

The program was planned to give comparisons between normal titanium 6Al-4V plate materials purchased to MIL-T-9046 and MIL-T-9047 and the yttria containing titanium plate and forged products purchased to the same specifications. The chemical compositions for each of the heats of materials tested are shown in Table 1 along with the product form. Note, that BCL/AFML Sequence Numbers 1, 2, and 3 are the baseline plate materials not containing yttria.

Note, also that the potent strengtheners nitrogen and oxygen are at higher levels in yttriated materials. The nitrogen contents of yttriated materials are two to three times those of the two RMI baseline plates, while oxygen contents average 250 ppm higher in the yttriated materials. The mean (arithmetic average) yttrium content for materials with intentional yttria additions is .026 weight percent with a standard deviation (measure of the dispersion around the mean) of .0056 weight percent. One material evaluated, BCL/AFML No. 12, hand forged billet, had an yttrium content higher than the calculated standard deviation.

2. TESTING

Mechanical testing was conducted as outlined in Table 2. The die forging that prompted this investigation, BCL/AFML No. 14, is given a more extensive examination as is a single material from each of the following groups: the baseline plates; the plates containing yttria; and remaining forgings with yttria. Note, that a major portion of the test program was concentrated on the short transverse loading direction since previous testing by both the producer and the user had indicated that properties in this orientation were most affected. Fatigue and fracture properties were also emphasized following the more recent trends in aerospace design.

The fatigue, fracture, and tensile specimens were tested at the Battelle-Columbus Laboratories, whereas, the fatigue crack growth specimens were tested at the AFML.

All tests were run in accordance with current applicable ASTM Methods. Specimen and testing description are as follows:

a. Tensile tests were conducted using the specimen shown in Figure 49. The length of the specimen was dictated by the short transverse thickness available in the materials tested. Procedures used for tensile testing were those recommended in ASTM Method E8. These procedures were followed to determine tensile ultimate strength, 0.2 percent offset yield strength, elongation, and reduction in area. The modulus of elasticity was obtained from load strain curves plotted by an autographic recorder during each test. The strain rate in the elastic region was maintained at 0.005 inch/inch/minute. After yielding occurred, the head speed was increased to 0.1 inch/inch/minute until fracture.

b. Fatigue tests were conducted using the specimens shown in Figures 50 and 51. All fatigue tests were accomplished using electro-servohydraulic fatigue machines operating in load control mode. These machines were equipped with load limiters and error detectors to prevent specimen overload and are normally accurate to within 2% of maximum load. Extreme care and accuracy in testing was deemed necessary to "sort out" subtle variations. All fatigue tests were run at a nominal frequency of 20 Hertz.

c. The fracture toughness tests were conducted using the compact specimen (Figure 52) per ASTM Test Method E399. It was recognized at the program offset that insufficient specimen dimensions would likely invalidate some data as plane strain fracture toughness (K_{IC}) values, therefore, all specimens were made to the same size so a relative comparison could be made on the conditional (KQ) fracture values.

d. Stress corrosion cracking tests were conducted using the bolt loaded specimen shown in Figure 53. The specimens were precracked under fatigue loading, similar to the fracture specimens and then were loaded with the bolts until the crack started to grow. An alternate immersion cycle of 10 minutes in and 50 minutes out of the 3.5% NaCl test solution was used for the environment.

e. The fatigue crack growth testing was accomplished using the center cracked panel (CCP) specimen. In a recent ASTM Committee E-24 Round Robin this specimen was found to exhibit very little testing "scatter" in comparison to the modified compact specimen. The CCP specimen would, therefore, be more discriminating in sorting out anticipated slight variabilities. In order to obtain specimens in the ST orientation, it was necessary to electron beam weld extension tabs on to the machined test sections. Electron beam welding was used to minimize the heat input to the test section material. The starter notch in the specimens was put in by electric discharge machining in order to get a very thin notch. A traveling micrometer was used to observe the crack length changes as a function of the cyclic load applications. The CCP specimen is shown in Figure 54.

The data reduction technique used on the fatigue crack growth data was the seven point incremental strip. This is one of the methods included in the ASTM Tentative Test Method, E-647-78T; details on this method and this testing area in general are presented in AFML-TR-78-40.

3. SPECIMEN LAYOUTS

Details on the specimen orientation within each lot of material are shown in Figures 55 through 62. The orientation nomenclature used is as shown in Figure 48. The fracture, stress corrosion, and crack growth specimens used the two letter designation for loading direction and crack direction, whereas the fatigue and tensile specimens use the single designation of longitudinal, transverse, or short transverse to indicate the test specimen orientation.

SECTION III

RESULTS AND DISCUSSION

1. MECHANICAL PROPERTIES

A summary comparison of the mechanical properties of yttriated titanium plate and forging materials to those of the yttria-free baseline plates is given in Table 3. It can be seen that yttriated materials, in general, compare favorably with the non-yttriated baseline plates. Tensile properties of yttriated materials are equivalent to those of the baseline plate with two exceptions. Tensile ultimate and yield strengths in the longitudinal test direction are lower, and secondly, the ST ductility of the die forging (BCL/AFML No. 14) that prompted this investigation is lower and that of BCL/AFML No. 6 plate is marginally equal to the baseline plate ductility. Fracture toughness is somewhat lower for yttriated plate and considerably lower than the baseline plate for yttriated forgings. Notched fatigue properties of yttriated materials are equivalent to baseline plate; whereas, smooth fatigue properties of yttriated plate and die forging No. 14 in the ST direction are inferior to those of the baseline material. However, yttriated materials were superior in crack growth characteristics.

Tensile, toughness, and fatigue property compilations for individual test specimens are displayed graphically in Figures 1 through 20, and given in tabular form in Appendix B.

a. Tensile

Tensile test results are presented in Tables 4, 5, and 6, Appendix B. By averaging the data for sequence numbers 4, 5, 9, and 10, for which both short transverse (ST) and longitudinal (L) properties were obtained, and comparing to the average values of baseline sequence numbers 1, 2, and 3, the following observations are made.

Average ST tensile ultimate (UTS) and 0.2% yield strengths (YS) of yttria-containing material are essentially the same as the non-yttria

baseline material; whereas, both UTS and YS for the L orientation is 5 to 6 ksi lower than the baseline material. Within the yttria-containing heats, somewhat lower yield strength in the ST direction is noted as compared to the L test direction; however, the opposite effect pertains to ultimate strength in three of the four heats compared.

Directionality effects as indicated by yield strength and modulus of elasticity are less pronounced in the yttriated material. Yttriated material exhibits a 3.3 ksi average difference in YS between ST and L oriented specimens versus a 10 ksi spread in YS for non-yttria containing baseline material. The average directional differences in Young's modulus of elasticity are 0.9 and 2.8 X 10^6 psi for yttria and non-yttria containing materials, respectively. Texture effects are more fully discussed in the Metallurgical Evaluation Section III-2 of this report.

The most striking difference in properties is shown in tensile ductility (with the exception of BCL/AFML No.'s 14 and 6 as mentioned earlier). Yttria containing heats exhibit nearly a two-fold increase in percent reduction in area in the ST direction and a more moderate increase in the L test direction, as compared to the baseline material. Short transverse tensile properties of yttria-containing heats are compared with the baseline materials in Figure 1. Note, that a wider variability exists within baseline materials and furthermore, BCL/AFML No. 2 baseline plate shows the lowest tensile properties.

b. Fracture Toughness

Results of fracture toughness tests, using compact-tension specimens in the S-L and S-T orientations, are presented in Appendix B, Table 7. The average fracture toughness of yttriated material is, in general, lower than that of the baseline material for both specimen orientations evaluated. Short transverse toughness for yttriated plate was, however, considerably lower than that of the baseline plate (55.3 ksi $\sqrt{in}$ versus 69.4 ksi $\sqrt{in}$, respectively). Forgings with yttria exhibited the lowest toughness but less directionality effects: 54.9 ksi $\sqrt{in}$ in the S-T orientation and 56.7 ksi $\sqrt{in}$ for the S-L orientation. Yttriated titanium

exhibited consistently less scatter in toughness values for any given group of specimens, as shown in Figure 2. Orientational effects on toughness will be discussed under the Metallurgical Evaluation Section III-2.

c. Stress Corrosion Cracking (K_{ISCC})

Tests were conducted to determine the stress corrosion cracking threshold using the bolt-loaded double cantilever beam specimen shown in Appendix A. The specimens were precracked under fatigue loading similar to the fracture toughness specimens and then bolt loaded until the crack started to grow. The specimens were then exposed to a 3.5 percent NaCl solution in an alternate immersion cycle of 10 minutes in and 50 minutes out. No appreciable crack growth was noted in any of the specimens. It is felt that this test procedure is not the optimum for evaluating the materials of this study. The large plastic zone likely occurring from bolt loading plus the possible corrosive blunting action from the environment may have produced a biased result. Therefore, no conclusion has been drawn as to the adequacy or applicability of this data.

d. Fatigue

Smooth fatigue test results are presented in Figures 3 through 14, while notched fatigue results are presented in Figures 15 through 18. Individual test specimen results are given in Appendix B, Tables 8 through 16. Baseline plate data are presented first, for each set of test conditions, followed by the data for yttriated plate and forgings. No attempt to analyze the data statistically was made nor is it considered justified. It should also be noted that the data from yttriated forgings (pancake, hand, and die) are compared to a different product form, namely plate; however, differences due to product form would not be expected to be large since relatively thick plates with a similar degree of working were evaluated, with the possible exception of die forging No. 14 which exhibited large amounts of working in some areas of the forging (Figure 29).

(1) Notched Fatigue

One plate (BCL/AFML No. 4) and two forgings (No's 9 and 14) were evaluated in notched fatigue (K_t=3) in the short transverse direction at two R ratios. Interestingly, both yttria containing forgings exhibited properties equivalent to or exceeding the notched fatigue properties of the baseline plate. The yttriated plate (No. 4) at an R ratio of 0.1 exhibited lower fatigue properties than did the baseline plate; however, at an R ratio of -0.25 the data are at least equivalent. Although the above inconsistent results for yttriated plate No. 4 appear to be questionable, the original specimens and data were rechecked and are believed to be correct.

(2) Smooth Fatigue

Smooth longitudinal fatigue properties are equivalent to those of the baseline material except for BCL/AFML No. 12 and one outlying data point of No. 13 (Figure 13). Smooth (K_t=1) short transverse fatigue properties of the yttriated plates and die forging No. 14 exhibited consistently lower fatigue properties as compared to the baseline plate, particularly at the higher maximum stress levels (low cycle fatigue region). Note that hand forgings 11, 12, and 13 were of insufficient thickness to permit ST testing; consequently, only longitudinal fatigue specimens were used for comparison, as displayed in Figure 12. Note, also that the comparison is made with baseline ST data but at the same R ratio since baseline longitudinal data was, unfortunately, not obtained. The longitudinal baseline scatterband, had it been generated, would most likely have encompassed the data shown in Figure 12 for the yttriated materials.

(3) Fatigue Crack Growth Rates

Fatigue crack growth rates were obtained at two R ratios, one with all positive stresses and one with both positive and negative stresses. These R ratios were chosen to provide the most severe range appropriate for normally tensile loaded aircraft structure. The negative R ratio was also chosen to amplify any detrimental effects of yttria inclusions.

The data were reduced from the "raw crack length versus cycles" inputs by the seven point incremental strip method contained in the ASTM tentative standard method of test for determining fatigue crack growth rates. (ASTM E 647-78T published in the 1978 Book of Standards.)

The data for an R ratio of 0.1 are presented in Figure 19, while the R ratio of -0.25 data are displayed in Figure 20. Only the positive stresses were used in calculation of delta K. In both instances it can be seen that the yttria containing materials have a lower crack growth rate than the baseline plate. The negative stress ratio tends to emphasize the differences in the crack growth rates. In the low crack growth rate region, the differences between the various materials and product forms were the most pronounced, and are indicative of microstructurally controlled growth. At the higher delta K region (faster crack growth regime), where toughness of the material is more of a consideration, the differences in rates were not as pronounced. It should be pointed out, however, that the baseline plate exhibited higher crack growth rates than are usually obtained for current high toughness plate. The relative crack growth rates (ranking) were the same for both R ratios evaluated, namely, in order of increasing crack growth rate, BCL/AFML No.'s 14, 4, 9, and 1. This same ranking in crack growth rate compares with the relative roughness of the fracture surfaces as shown in the macrographs of Figure 40. The rougher the macroscopic fracture surface appearance, indicative of a more tortuous fracture path, the slower the crack growth. The macroscopic crack growth rates shown in Figures 19 and 20 were confirmed by microscopic striation counting using replicas of the fracture surfaces, in conjunction with transmission electron microscopy, taken at locations adjacent to the initial growth region, in the center region, and in the region of fast fracture near the specimen hinge area. Good (order of magnitude) agreement was obtained.

2. METALLURGICAL EVALUATION

The metallurgical evaluation of this investigation included extensive metallography including both optical macroscopy and microscopy, scanning

electron microscopy, fractography of tensile and smooth fatigue specimens, and a crystallographic texture analysis. The results from each technique used will be discussed below.

a. Metallography

Yttria-Free Baseline Plates - The three yttria-free hot rolled baseline plates, BCL/AFML No.'s 1, 2, and 3, examined in this study were first metallographically sectioned parallel to the rolling plane at mid-thickness and examined for grain elongation to permit positive identification of the rolling direction. The plates had apparently been rolled an appreciable amount above the beta transus and, although obviously finished in the alpha-beta field, showed a very large, but only moderate elongated, prior beta grain size. The prior beta grain size was so large at mid-thickness in Plate No. 3 that the section examined, about 0.7 square inches in area, contained fewer than six grains. The grain size was somewhat smaller toward the plate surface. The prior beta grain sizes of Plates No.'s 1 and 2, although smaller than that of Plate No. 3, were still moderately large (Figure 40).

A second metallographic specimen was prepared to permit examination of the microstructure at a quarter-thickness location in a plane perpendicular to the transverse direction of each rolled plate. Plate No. 1 contained a few small spherical inclusions but all three baseline plates were completely free of yttria inclusions. The alpha-beta structure of these baseline plates, as shown in Figure 21, was typical of Ti-6Al-4V hot worked a moderate amount in the alpha-beta field. Plate No. 3 showed slightly more acicularity of the alpha phase than the other two, suggesting less work below the beta transus. The large prior beta grain size is not obvious at the magnification shown in these micrographs. (The sections shown in Figure 21 are perpendicular to the rolling plane such that the beta grain structure appears much more elongated than described previously).

Yttriated Plates - Five hot-rolled and annealed yttriated plates, BCL/AFML No.'s 4, 5, 6, 7, and 8, were examined by sectioning. Each sample for metallographic examination measured 1 X 1/2 inch X thickness. This piece was then sectioned at mid-thickness parallel to the rolling plane and examined to confirm that the rolling direction was correctly identified. A second section was prepared at a quarter thickness location perpendicular to the transverse direction. This section was used to compare the microstructure and yttria distribution in the five plates.

Figures 22 through 26 show the microstructural characteristics and the distribution of yttria. All plates show evidence of having been fabricated in the beta field followed by some alpha-beta working. There are appreciable differences in the alpha particle size and shape; however, plates 6, 7, and 8 appear to have received considerably more alpha-beta fabrication than the other two. The prior beta grain size did not appear excessive in any of the yttriated plates as contrasted to the baseline plates. Yttria distribution, in the cross-sections evaluated, appeared to be quite variable among the five plates. Plate No. 6 exhibited the most uniform yttria distribution and the finest yttria particle size, while Plate No. 4 exhibited the largest particle size and was the most heavily stringered with yttria. Yttria appeared to be located along alpha-beta interfaces in most cases as can be seen by comparing the yttria location in the etched and as polished micrographs. Stringered yttria distributions were common. A few spherical yttrium-free particles, such as the three particles polished in relief which are visible in Figure 26, were present in most of the plates. These could not be positively identified, however, subsequent energy dispersive x-ray analysis of specimen fracture surfaces detected yttria-free particles high in aluminum and some particles high in calcium as well. These observations are not surprising since, historically, inclusions have been observed in a variety of wrought titanium alloys with no apparent harmful documented effects on properties.

The yttria particles showed, by optical metallographic observations, a rather characteristic gray color. Typical examples are shown in Figure 27. In many cases, the particles appeared to consist of a mixture

of phases with distinctly different regions within the particles such as seen in the large particle in Figure 27a. Although this aspect was not pursued, these regions likely represent different compositions, possibly suboxides of yttrium. Microprobe analysis of the gray particles showed all of them to be rich in yttrium. Considerable fluorescence was evident during the x-ray examination of the yttrium-containing particles indicating that the particles were oxides.

Yttriated Forgings - Six yttriated forgings were examined and included two upset pancake forgings (BCL/AFML No.'s 9 and 10), both from the same production heat, three hand forged billets (No.'s 11, 12, and 13), and one die forging (No. 14).

Sections were cut from each forging and macroetched to show the grain flow pattern resulting from the forging process. Sections were cut from the pancake forgings near the edge of the forging along a plane containing the radial and thickness directions. (Forging No. 9 was 3 inches thick X 14-1/2 inches in diameter. Forging No. 10 was 2 inches thick X 17 inches in diameter). Sections were cut from the billet forging along a plane containing the thickness and length of the billet about one-half inch from one side of the billet. (The hand forged billets were approximately 1-1/2 inches thick X 7 inches in width X 14 inches long). The die forging supplied for this investigation was part of a moderately large bulkhead forging. The section for macroscopic examination was cut in an area which was expected to show extensive metal flow. The macrostructures of three of these forgings are shown in Figures 28 and 29.

Both pancake forgings showed the anticipated mild grain flow pattern, indicative of a lesser amount of working in the thickness direction, following the contour of the part, as shown in the photograph of the section from No. 10 in Figure 28a. A very obvious grain flow pattern was also apparent in forging No. 14, the die forging, as shown in Figure 29. In contrast to this, the three hand forgings showed a

large equiaxed grain structure as macroetched and no evidence of a grain flow pattern. The structure shown for forging No. 12 in Figure 28b is typical of that shown by all three hand forgings.

Metallographic specimens were prepared from the macroetched sections and examined as-polished for the presence of yttria inclusions. All six forgings contained appreciable amounts of yttria distributed in stringers or clusters much like those seen in the rolled plates previously described. The yttria stringers were oriented parallel to the flow pattern in forgings 9, 10, and 14, and large yttria particles originally present in the alloy appeared to have been fragmented during fabrication to a considerable degree. There was very little evidence of alignment of the yttria particles in the hand forged billets, however, and that which was seen suggested that the yttria was aligned parallel to the thickness direction. The absence of a significant amount of yttria alignment in these billets suggests that they were not extensively hot worked. The alignment seen presumably could have developed during the casting operation or early in the ingot breakdown process. Yttria variability was also indicated during efforts to correlate the microstructurally observed amounts of yttria with the heat analysis of the forgings. Forging No. 13 was judged during metallographic examination to contain appreciably more yttria than forgings 11 and 12, while analysis suggests that forging 12 contained the most yttria. Similarly, metallographic examination suggested that forging 9 contained more yttria than forging 10 although both forgings were prepared from the same heat.

The six forgings showed appreciably different alpha-beta microstructures as illustrated in Figures 30 through 35. The two pancake forgings had been forged well below the alpha-beta transus as evidenced by the presence of moderately equiaxed alpha grains contained in a transformed beta matrix. Forging No. 10, Figure 31, showed appreciably more elongation in the alpha grains than did Forging No. 9, Figure 30, suggesting a greater amount of forging. Both pancake forgings showed clearly evident variations in microstructure from surface to center of the forging. The surface contained more transformed beta, indicating

it was finished closer to the beta transus than the center. Since it is unlikely that the surface was hotter than the center at the conclusion of forging, some variability in composition is probable. Forging No. 14 had also been finished below the beta transus, but as shown in Figure 35, this forging contained more transformed beta than did forgings 9 and 10 indicating that it was forged closer to the beta transus temperature.

In marked contrast to the appearance of the above three forgings, the three hand forgings exhibited a coarse acicular alpha microstructure typical of beta annealed Ti-6Al-4V as shown in Figures 32 through 34. Forging No. 13 may have received a small amount of deformation below the beta transus, as evidenced by some curvature in the alpha platelets and a suggestion of deformation at the alpha-beta interface, but the other two obviously did not. These forgings were either beta annealed following forging or they were forged well above the beta transus. In view of the evidence of a small amount of deformation in the acicular alpha present in Forging No. 13, the latter is believed more likely.

The scanning electron microscopy images of Figures 36 through 39 serve to better illustrate that yttria particles and clusters tend to reside at alpha-beta interfaces, as had been determined by the optical metallographic examination discussed previously. No evidence of the particles bonding or reacting with the adjacent matrix was found. The x-ray area scans shown in Figures 36c and 37c confirm that the particles observable in the microstructure are high in yttrium and are typical of all yttria-containing plates and forgings studied. There is some evidence of yttria particle pullout during specimen preparation. Note in particular that some yttria particles have fractured (Figure 38b) apparently during the hot working operations. Also note that the yttria particles bear little resemblance to those of the starting yttria powders. Compare the particle morphologies shown in Figures 36 through 39 with those of the yttria powders in Figure 43.*

*The yttria powder sample was provided to the AFML by H. B. Bomberger, RMI, Inc., and was manufactured by the Moly Corporation.

From the above observation that the starting yttria particle morphology is most often cubical, somewhat tabular or laminated in appearance, and exhibits multiple cracks, as shown in Figure 43, rather than the rounded shape and smooth surfaces of particles always observed in the yttria containing material of this investigation, the question arises as to whether the yttria dissolved completely, partially, or not at all in the melt during ingot preparation.

It is obvious that at least partial dissolution of the yttria occurred by virtue of the aforementioned change in external morphology; however, it is not obvious, nor has it been established, that full dissolution occurred followed by precipitation during solidification by solute rejection, or precipitation from solid solution during ingot cooling. Hoch (Reference 7), in a recent thermodynamic analysis using available data, calculated that the solubility at equilibrium of Y_2O_3 in liquid and solid titanium, containing 1500 ppm oxygen, at the melting point of titanium (1943°K), is at least 5400 and 2000 ppm, respectively. For titanium containing 2000 ppm oxygen, the liquid and solid solubilities of Y_2O_3 were calculated to be 4600 and 1700 ppm, respectively.

Simpson (Reference 8), in a recent experimental study of weld pool solidification structures in Ti-6Al-6V-2Sn resulting from yttrium metal inoculation, has shown that precipitates of Y_2O_3, identified by electron microprobe fluorescence analysis were clearly visible at 500 magnifications if the yttrium addition was .06 weight percent (600 ppm), but were rarely seen at the .03 w/o level, and further, were never observed (at 500X) if the yttrium addition was less than .03 w/o, thus indicating either an extremely fine (submicroscopic) precipitate and/or some solid solubility of yttrium in titanium. His results show that the precipitates strengthen the weld metal but reduce ductility and toughness of weldments after heat treatment, apparently as a result of a refinement of the alpha platelet structure within the transformed beta grains that occurs at the .03 w/o yttrium level and above but not at the .016 w/o level.

Simpson postulates that the yttria precipitates are dragged by advancing solid/liquid interfaces during solidification as evidenced by the high concentration of precipitates observed at grain boundaries and in rows parallel to them. The drag effect increases as the solidification continues; the yttria particle content builds up at the solid/liquid interfaces resulting in increased undercooling and heterogeneous nucleation sites for the last metal to solidify, i.e., the center of the weld. The increased number of nucleation sites tends to reduce the prior beta grain size, often dramatically.

Lyon, et al (Reference 9), have shown that under certain conditions of molten titanium in contact with Y_2O_3 crucible material (at 1780°C, 100°C superheat, for ten minutes followed by step-wise furnace cooling), reaction and dissolution does occur at the crucible-titanium interface leading to precipitation of flower shaped yttria dendrites and dendrite-like particles in prior beta grain boundaries of titanium; however, precipitation of fine particles within alpha grains or at alpha grain boundaries was not observed. They interpret this observation as indicative of yttria particle formation near or above the solidus temperature of titanium. The above experimental evidence of dissolution and precipitation possibly explains why in the study of Bomberger, et al., previously cited, comparable results were obtained whether the yttrium addition was as the metal or as the oxide. Yttrium metal would very likely get the oxygen (combine preferentially) from the molten titanium and subsequently precipitate as the oxide during cooling as explained above. Still further, Kerr (Reference 10) upon examining material from a more recent study by Schuyler, et al. (Reference 11), in which a low melting titanium-beryllium alloy was cast in a high yttria crucible, similarly found yttria idiomorphs residing primarily in those microstructural regions last to freeze, i.e., the material of eutectic composition, and infrequently, enveloped by an alpha grain.

Yet others (References 12, 13) have concluded that Y_2O_3 is essentially insoluble in titanium, citing as evidence a limited evaluation showing

identical particle size distributions of the starting yttria powder and the yttria particles in the matrix of titanium after melting and solidification.

Unfortunately, no information was found in the literature search of this study pertaining to the reaction kinetics, i.e., the rates of solution and dissolution of yttria (and yttrium) in molten and solid titanium, nor are the actual production melting and solidification conditions sufficiently well known to make valid conclusions about such important aspects as the residence time available to yttria particles in the melt, local temperature gradients and solidification rates, and oxygen partial pressures.

b. Fractography

Fractographic examinations were performed on both tensile and smooth fatigue specimens exhibiting low or questionable properties. The fracture surfaces of three tensile specimens, Numbers 6-ST-1 (Table 5) and 14-ST-1 and 14-ST-2 (Table 6) having unusually low ductility, were examined at magnifications from 10 to 5000 times by optical microscopy and scanning electron microscopy for evidence of unusual yttria concentrations or other features that could conceivably contribute to low ductility. In addition, both wavelength and energy dispersive x-ray spectroscopy (line and area scans) were used to aid in chemical identification. Although yttria particles were detected (using the yttrium L-alpha characteristic x-ray line) on each fracture surface, no unusually high concentrations, as compared to specimens with normal properties, were found; however, banding was evident in specimen 14-ST-2 with alternating regions of small and large alpha grains. Yttria particles were often observed residing at the base of cusped void regions on fracture surfaces indicative of ductile rupture; however, this phenomena, in a qualitative sense at least, was no more pronounced in specimens exhibiting low ductility than in specimens with normal ductility. X-ray analysis failed to detect yttrium in some of the particles observed at the base of ductile voids.

All smooth fatigue specimen fracture surfaces were screened visually for evidence of internal fatigue crack initiation sites. Those specimens questionable upon this initial visual examination were further examined with the aide of a stereomicroscope at 10 to 80 magnifications. On the basis of this second stage examination, nine specimens, all from yttriated materials, were selected for further examination by scanning electron microscopy. Specimen fracture surfaces for SEM examination were deliberately not cleaned to prevent the loss of any loosely adhering yttria particles. The results indicate that no yttria clusters or particles observable at up to 5000X could be associated with fracture initiation sites. Still further, in every case examined, fatigue cracking was initiated at or very near the specimen surface, with most specimens exhibiting multiple initiation sites. Examples of the results are shown in Figures 41 and 42. Cleavage-like fracture (transgranular) is associated with each crack initiation region illustrated, particularly specimen 14-ST-16 tested in low cycle fatigue (maximum stress of 85 ksi, R=-.25, life=3.8 X 10^4 cycles) and specimen 12-L-4 tested in high cycle fatigue (maximum stress of 40 ksi, R=-.25, life=1.45 X 10^6 cycles). Note also in Figures 42a and b the banding as shown by the region of large alpha grains (smooth cleavage regions) indicative of alpha colonies of similarly oriented grains and corresponding to a prior beta grain. Although yttria particles were not observed at crack initiation sites, clusters of yttria particles were readily observable at interior regions of the same fracture surfaces, as shown in Figures 42c and d. The lack of yttria particles in the immediate vicinity of initiation sites indicates that yttria particles, per se, likely do not directly affect fatigue crack initiation or early (Stage I) crack propagation. Yttria particles also appeared to have little effect on crack propagation during the later stages of growth since a detailed examination of fatigue striations and yttria particles in interior regions of specimen fracture surfaces failed to show an observable effect on either the striation spacing or changes in the crack propagation direction. From the above observations, coupled with the fact that yttriated titanium materials exhibited low crack growth rates but lower fatigue life in some cases, the logical conclusion must be that any effect yttria may have on early crack

initiation or subsequent crack growth must be indirect and result from subtle changes in the beta transformation products, recrystallization kinetics, local deformation mode, or different mill processing, such as lower rolling or forging temperatures and fewer reheats, as well as other as yet unidentified effects. It is well known and recently documented by Sommer, et al. (Reference 14), that changes in processing can sometimes exert considerable changes in the metallurgical structure and/or crystallographic texture. These changes can enhance or diminish the mechanical properties depending upon the thermomechanical history of the specific titanium alloy plate and forging.

c. Texture Analysis

Information about the degree of texture can be obtained from comparisons of properties such as strength and modulus measured in different directions within the material. For example, modulus measurements relate to preferred orientation in that the elastic properties of the alpha phase (hexagonal crystal structure) of titanium are anisotropic, i.e., vary with direction. In fact, Young's modulus can range from a minimum of 14.5×10^6 psi for directions within the basal plane to 21.0×10^6 psi for a direction perpendicular to the basal plane in titanium.

Nonetheless, the most generally accepted method of describing preferred crystallographic orientation, or texture, of polycrystalline metals is the pole figure derived from measured diffracted x-ray intensities. Pole figures are stereographic projections showing the density of crystallographic poles of selected planes as a function of orientation within the material, usually related or referenced to the rolling (or forging) direction.

The Kula-Lopata (Reference 15) reflection technique as adapted by Olsen (Reference 16) was used to generate the pole figures of this study. This technique, using a specimen cut from the material at an oblique angle to the rolling plane, overcomes the usual reflection limit for

plane normals (70°) and permits one to generate the entire quadrant of an x-ray pole figure (90°). The cut surface normal is equidistant (54° 44') from the rolling plane normal, the rolling direction, and the transverse direction, as shown in Figure 44. The alternative to this technique would require two separate determinations, one in reflection for angles to 70 degrees and another in x-ray transmission (requiring a thin specimen) for pole angles greater than 70 degrees. Another perhaps not so obvious advantage to the oblique plane technique used for this study is that a greater thickness of the original plate is sampled and hence the preferred orientation is averaged over the reflection surface representing a considerable volume of the material. Historically, as pointed out by Bowen (Reference 17), texture in titanium is known to vary, sometimes considerably, with thickness (surface to center) due to temperature gradients and the resultant nonuniform deformation during rolling or other hot working operation. Larson and Zarkades (Reference 18) have given a comprehensive review of current (1974), albeit limited, knowledge of the properties of textured titanium.

For this study, pole figures of both basal (0002) and prism $\{10\bar{1}0\}$ planes were obtained to derive maximum benefit for subsequent correlation with properties. Copper x-radiation generated at 35KV and 28 milliamps was used throughout this investigation. Pole figures were generated for all three non-yttriated baseline plates, as well as for three of the five plates with yttria, a single pancake forging, a hand forged billet, and the die forging, all containing yttria additions. The pole figure results are presented in Figures 45 through 47. The "contour lines" displayed on each pole figure represent iso-intensity lines of the poles of the plane examined, i.e., (0002) or $\{10\bar{1}0\}$, whereas, the numbers associated with each "contour line" correspond to the various multiples of random intensity as indicated below each pole figure. The number one represents half random intensity, two represents one times random, four represents two times random and so forth.

Although none of the materials of this study for which pole figures were obtained exhibited extreme texturing--the maximum texture was

4 times random as compared to 20 or 30 times random that can be experienced with titanium plate and sheet materials--significant differences in texture are observable, as will be discussed.

The texture or preferred orientation in Ti-6Al-4V produced as a result of plastic deformation, such as occurs during the rolling of plate or forging operations, is primarily controlled by the resulting alpha phase and hence the mechanical property anisotropy is related to the available slip (and twinning) systems in the hexagonal alpha phase. The major slip planes are the basal (0001), prism $\{10\bar{1}0\}$, and the pyramidal $\{10\bar{1}1\}$ planes.

The directions of easy slip lie in the basal plane and accordingly, even though non-basal slip directions such as (1123) active on $\{10\bar{1}1\}$ and $(11\bar{2}2)$ planes have been shown to exist (Reference 19), basal or basal related slip is often dominant.

Pole figures of the baseline plates are displayed in Figure 45. Although BCL/AFML baseline Plate No.'s 1 and 2 were from the same producer (RMI), each exhibited a different texture. Plate No. 1 exhibited the strongest texture (four times random), a basal texture in the rolling direction (RD) which is confirmed by the $\{10\bar{1}0\}$ pole figure shown directly below the basal (0002) pole figure in Figure 45. The $\{10\bar{1}0\}$ prism planes are aligned about the rolling direction. Such a texture as that displayed by Plate No. 1 is likely the result of rolling primarily in one direction as opposed to extensive or uniform cross-rolling. In contrast, baseline Plate No. 2 shows a texture consistent with alpha plus beta cross-rolling. Baseline Plate No. 3, from a different producer (TIMET), also exhibits a cross-rolled texture but its texture is not so strong as those of Plates 1 and 2. This observation is supported by the lesser differences in mechanical properties between the two directions evaluated. Note that the "L" tensile test direction corresponds to the "RD" direction on the pole figure; whereas, the "ST" test direction is equivalent to the direction perpendicular to the plane of the pole figures.

Yttriated titanium plates (BCL/AFML No.'s 4, 5, and 6) exhibited a remarkable uniformity in texture plate-to-plate as shown in Figure 46. The basal poles are oriented primarily in the long transverse direction (TD). The $\{10\bar{1}0\}$ pole figures confirm that crystallites oriented with their basal poles toward the TD direction (three o'clock position on pole figure) of the plates are the primary contributors to the $\{10\bar{1}0\}$ texture. Both the basal and prism textures of the yttriated plates are very similar to the texture of the non-yttriated baseline Plate No. 2. Compare Figures 45 and 46. The spread between tensile ultimate and yield strength of each yttriated plate is less than the baseline plate however, and may be indicative of a twinning deformation mode component since twinning produces little or no strain hardening as does deformation by slip. A good correlation between toughness and texture is also shown for yttriated and non-yttriated plate materials. Toughness is consistently highest when the crack propagation direction lies in the basal plane, i.e., at 90° to the basal-pole high intensity regions of the pole figures. Compare the pole figures of Plate 1 in Figure 45 with those of Plate 4 in Figure 46.

The pancake forging (BCL/AFML No. 9) shows very little texture (Figure 47.) In particular, note the more random pattern of the $\{10\bar{1}0\}$ poles. Property directionality effects are also very minimal. (Note that the "RD" direction on the pole figures of Figure 47 is the forging direction and the "TD" direction corresponds to a radial direction at 90°.)

The hand-forged billet (BCL/AFML No. 12) exhibits a two times random texture in both the RD and TD directions for the basal (0002) pole figure of Figure 47; however, only the TD component contributed to the $\{10\bar{1}0\}$ texture. Considerable texture remains in this forging even though microstructural analysis indicated that the forging had either been beta annealed following forging or forged primarily in the beta phase field. The texture of forging No. 12 is similar to those of the yttriated plate materials.

The die forging (BCL/AFML No. 14) exhibited basal pole maxima at two positions 90° from both the forging direction and one another; however, crystallites or grains with their basal poles at the "TD" position were the primary contributors to the $\{10\bar{1}0\}$ texture shown. It should be noted that the specimen for pole figures analysis was taken from a region of the forging that was not as heavily worked as some other regions, (Figure 29), and hence, is likely not representative of the entire forging.

The relationships between the textures displayed and the fatigue test results (including crack growth rate measurements) of this study are not obvious but likely complex and could be the topic of a separate future study.

SECTION IV

CONCLUSIONS

1. Tensile ultimate and yield strengths of yttriated materials tested in the short transverse direction are equivalent to the baseline material strengths; longitudinal tensile ultimate and yield strengths are, however, 5-6 ksi lower than those of the baseline plates. Directionality effects are much less pronounced in the yttriated materials, particularly with respect to yield strength and modulus of elasticity. Yttria containing heats also exhibit substantial increases in tensile ductility over that of the baseline plate, with two exceptions, BCL/AFML No.'s 6 and 14.

2. Fracture toughness is somewhat lower in yttriated plate and considerably lower than the baseline plate for yttriated forgings. However, less scatter in the data is shown for yttriated material.

3. Notched fatigue properties of yttria containing heats are equivalent to those of the baseline material at both R ratios evaluated, with the sole exception of BCL/AFML No. 4 plate material, tested at an R ratio of 0.1, which is lower over the entire range tested.

Unnotched longitudinal fatigue properties are at least equivalent to those of the baseline material, except BCL/AFML No. 12, the data points of which are at or near the lower region of the baseline scatterband, and one outlying data point of BCL/AFML No. 13.

The most significant degradation in fatigue properties is exhibited in plate material tested in the short transverse direction (unnotched) and in BCL/AFML No. 14 (die forging) which exhibited consistently lower fatigue properties as compared to baseline plate material.

4. Yttriated materials consistently showed lower fatigue crack growth rates (da/dN) at a given stress intensity than did the baseline material. The tests included a compressive load component (R= -0.25) which tended to magnify the differences between materials.

5. Although the die forging (BCL/AFML No. 14) that prompted this investigation exhibited the lowest ST ductility, it also exhibited the lowest crack growth rate of the materials evaluated as well as higher toughness with equivalent strength as compared to the other yttriated forgings evaluated. Material from an additional three heats (represented by BCL/AFML No.'s 4, 6, and 12) of the ten yttriated titanium production heats evaluated displayed somewhat lower properties, i.e., ductility and/or fatigue, than did the remaining six heats.

6. The metallographic evaluation demonstrated that yttria particles and clusters of particles are readily observable by both optical and scanning electron microscopy, reside primarily at alpha-beta interfaces, and are nonuniformily distributed and bear little morphological resemblance to the starting yttria powders. The latter finding is indicative of at least partial dissolution of yttria during melting; however, a number of questions still remain from not only the fundamental standpoint of solidification, precipitation, and particle distribution, but also from the practical aspects of how best to make the addition and the cost benefits to be derived relative to specific alloys and product forms.

7. No direct effect of yttria particles or clusters of particles observed in this study on tensile or fatigue properties could be definitely established by fractographic analysis. Rather, the results indicate that the effects of yttria additions to titanium are indirect and more subtle, and are likely to a large extent, a consequence of different mill processing due to the greater hot workability of yttriated titanium, i.e., fewer reheats, lower working temperatures, etc. and the resulting changes in the macrostructure, microstructure and texture (including changes in the beta transformation products or recrystallization kinetics).

8. Yttriated plate exhibited a basal transverse texture that was highly consistent plate-to-plate in contrast to the considerable variation in texture shown by the three non-yttriated baseline plates. Most of the property differences shown between yttriated and non-yttriated materials were consistent with the differences in crystallographic texture.

SECTION V

RECOMMENDATIONS

1. Disposition of yttriated titanium presently in the industrial pipeline should be made on a case by case basis considering the specific application requirements and using the data of this report for guidance. User generated data should also be used where appropriate and available. Yttriated titanium exhibits adequate properties for most Air Force applications except those with critical requirements such as certain rotating engine components, or those few applications where loading in the short transverse direction is likely and/or a slight reduction in toughness or fatigue life cannot be tolerated.

2. Any material on hand from RMI Heat Numbers 891479, 891567, 892019, and 901975 should be closely scrutinized for possible lower tensile ductility and/or fatigue life. These four heats of the ten yttriated titanium heats evaluated exhibited the greatest loss in those properties.

3. Present limitations (50 ppm maximum) on yttrium levels in AMS titanium materials specifications should remain in effect until the technology for adding yttria (or yttrium) in a reproducible, reliable, and uniform manner without serious diminution in important properties has been demonstrated and documented systematically with production scale heats.

A near-term need for an evaluation of the effects, if any, of lower yttrium levels (10 - 100 ppm) on critical properties is shown to provide guidance on the use of yttriated titanium presently in the scrap cycle.

4. As a precursor to production scale documentation, a need for further exploratory development is indicated from both a fundamental solubility/solidification standpoint and from the practical standpoint of how best to make the addition and which alloys and product forms benefit most from such additions.

Any exploratory development effort should be designed to bracket actual production melting conditions as well as to permit separation of processing effects from those of yttria on resulting properties as well as the interactions. The latter aspect should be addressed by evaluating identically melted and processed ingots with and without yttria additions.

TABLE 1

COMPOSITIONS OF PROGRAM MATERIALS

BCL/AFML Sequence(Heat) Number	Producer Heat Number	AFML Source	Product Form	Composition, Weight Percent[a]						
				C	N	Fe	Al	V	Y	O
1	992141	RMI[b]	2.2" Plate	.02	.006	.19	6.3	4.1	-	.145
2	902099	RMI[b]	2.2" Plate	.02	.005	.17	6.1	3.9	-	.148
3	K7787	TIMET	2.1" Plate	.03	.014	.14	6.3	4.1	-	.16
4	892019	Boeing	2.9" Plate	.02	.015	.18	6.5	3.9	.021	.162
5	801533	Rockwell	3.0" Plate	.03	.018	.17	6.3	4.0	.030	.170
6	901975	RMI	2.15" Plate	.03	.010	.19	6.0	3.9	.017	.162
7	901777	RMI	2.15" Plate	.02	.013	.19	6.1	3.8	.026	.169
8	991899	RMI	2.15" Plate	.03	.014	.18	5.9	3.8	.022	.154
9	801645	Wyman-Gordon[c]	Pancake Forging	.03	.015	.18	6.6	3.9	.028	.168
10	"	G.E.	"	.03	.015	.18	6.6	3.9	.028	.168
11	801623	Alcoa	Hand Forged Billet	.02	.013	.20	6.6	4.0	.026	.190
12	891567	Alcoa	"	.01	.013	.16	6.1	3.9	.037	.177
13	801445	Alcoa	"	.03	.019	.20	6.0	4.0	.029	.171
14	891479	McDonnell-Douglas	Die Forging	.02	.014	.17	5.9	3.9	.020	.173

a - From producer test reports in most cases.
b - These plates were annealed 1 hour at 1450°F after hot rolling.
c - Forged from 6.375" diameter billet at 1750°F, annealed 2 hours at 1300°F after forging.

TABLE 2

TEST PROGRAM OUTLINE TO EVALUATE YTTRIATED TITANIUM 6Al-4V PLATE AND FORGINGS

Test	Specimen Orientation	Test* Conditions		BCL/AFML Sequence(Heat) Number												
				1	2	3	4	5	6	7	8	9	10	11	12	13	14
				Product and Number of Specimens													
				Baseline Plates			Plates with Yttrium					Forgings with Yttrium					Forging 61550
TENSILE	ST			3	3	3	3	3	3	3	3	3	3	3	3	3	3
	L			3	3	3	3	3				3	3				
K_{IC}	SL			3	3	3	3	3				3	3				3
	ST			3			3					3					
K_{ISCC}	ST			3	3	3	3	3				3	3				3
FATIGUE	ST	R=-0.25	K_t=1	12	4	4	12	4	4	4	4	12	4	4	4	4	12
			K_t=3	6			6					6					6
		R=0.1	K_t=1	12	4	4	12	4	4	4	4	12	4	4	4	4	4
			K_t=3	6			6					6					6
FATIGUE	L	R=-0.25	K_t=3	12			12					12		4	4	4	12
da/dn	ST	R=-0.25		3			3					3					3
		R=0.1		3			3					3					3

* All testing was conducted at room temperature in laboratory air.

TABLE 3

SUMMARY MECHANICAL PROPERTY COMPARISONS OF YTTRIATED TITANIUM TO NON-YTTRIATED BASELINE PLATE

Material	Specimen Orientation	UTS, ksi	YS, ksi	% Elong.	% RA	E, psi x 10^6	Fracture* Toughness, ksi-$in^{1/2}$	Fatigue Crack Growth Rate	Fatigue N	Fatigue S
Baseline Plates-No Yttria	ST	143.1	128.4	10.6	16.2	15.0		=**	=	=
	L	145.4	138.3	16.9	27.4	17.8	66.2			=
Plates with Yttria	ST	141.8	129.6	11.5	24.1	15.1		+	=	-
	L	138.6	131.5	18.8	40.7	16.1	63.5			=
Forgings with Yttria	ST	141.6	128.6	14.0	27.6	15.6		+	=	=
	L	140.9	131.9	16.0	30.3	16.8	56.7			=***
BCL/AFML No. 14 Die Forging w/Yttria	ST	140.4	128.7	8.0	12.9	16.3		+	=	-
	L						62.8			=

* Fracture toughness measurements were made on less than optimum size specimens; therefore, the values should be used only for relative comparisons. S-L specimen orientation.

** KEY: =, equal to baseplate
+, improvement over baseplate
-, degraded from baseplate

*** Compare favorably except for BCL/AFML No. 12, and one outlying data point from No. 13.

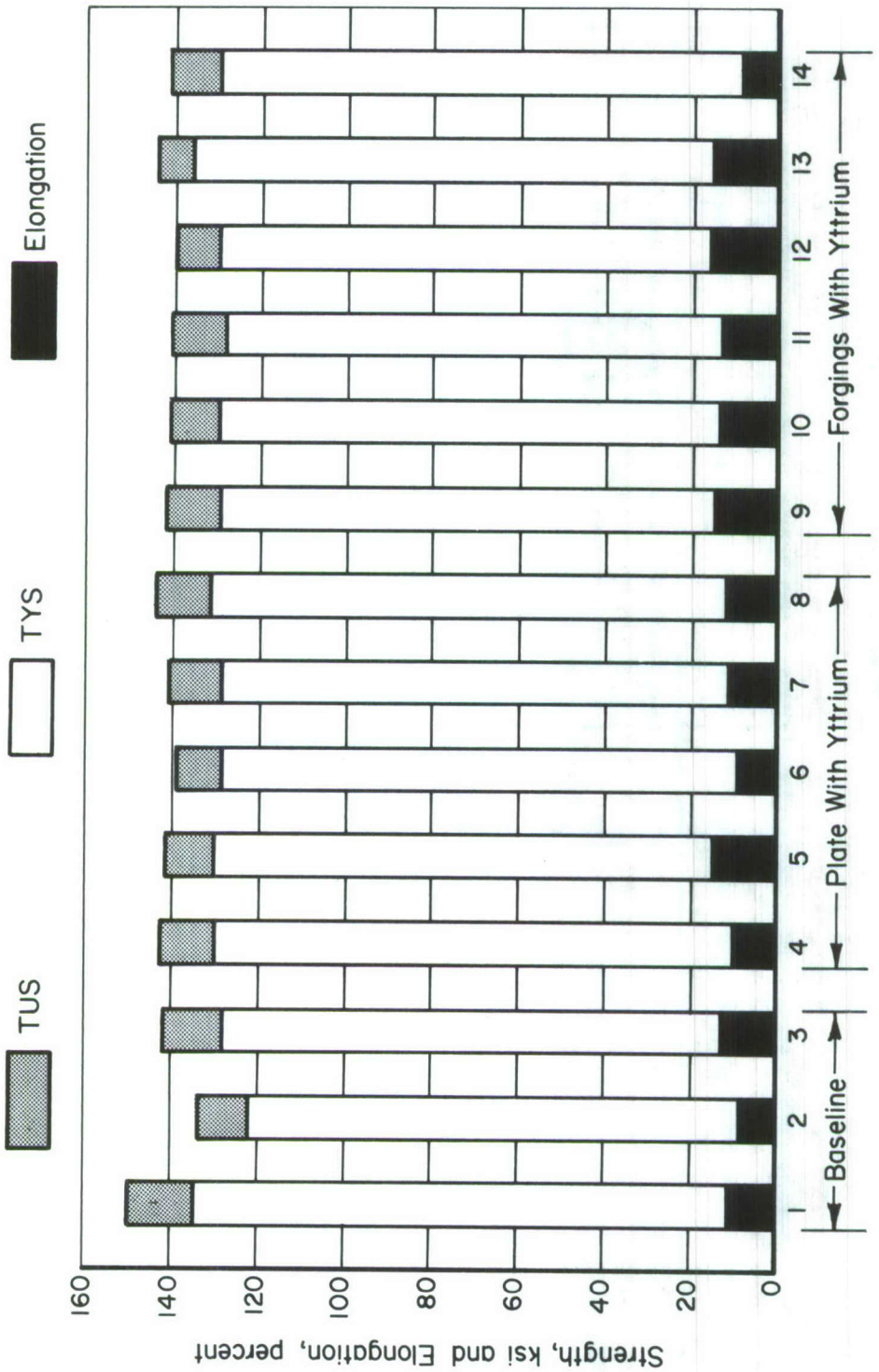

Figure 1. Average Short Transverse Tensile Properties of Program Materials

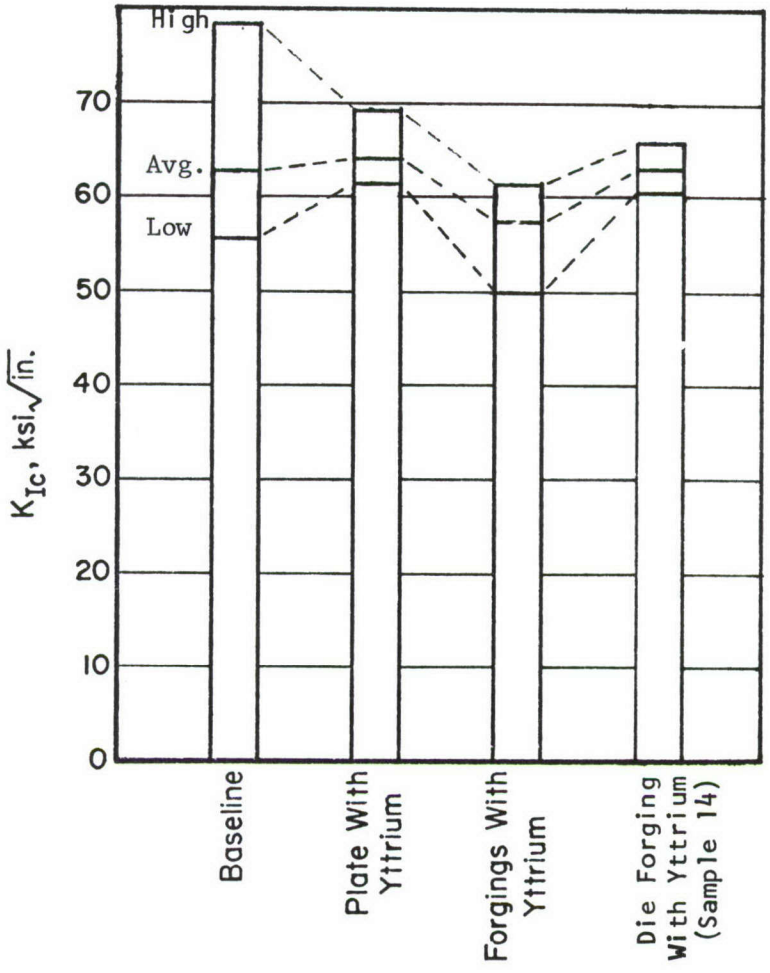

Figure 2. Range of Fracture Toughness Values Obtained for Program Materials

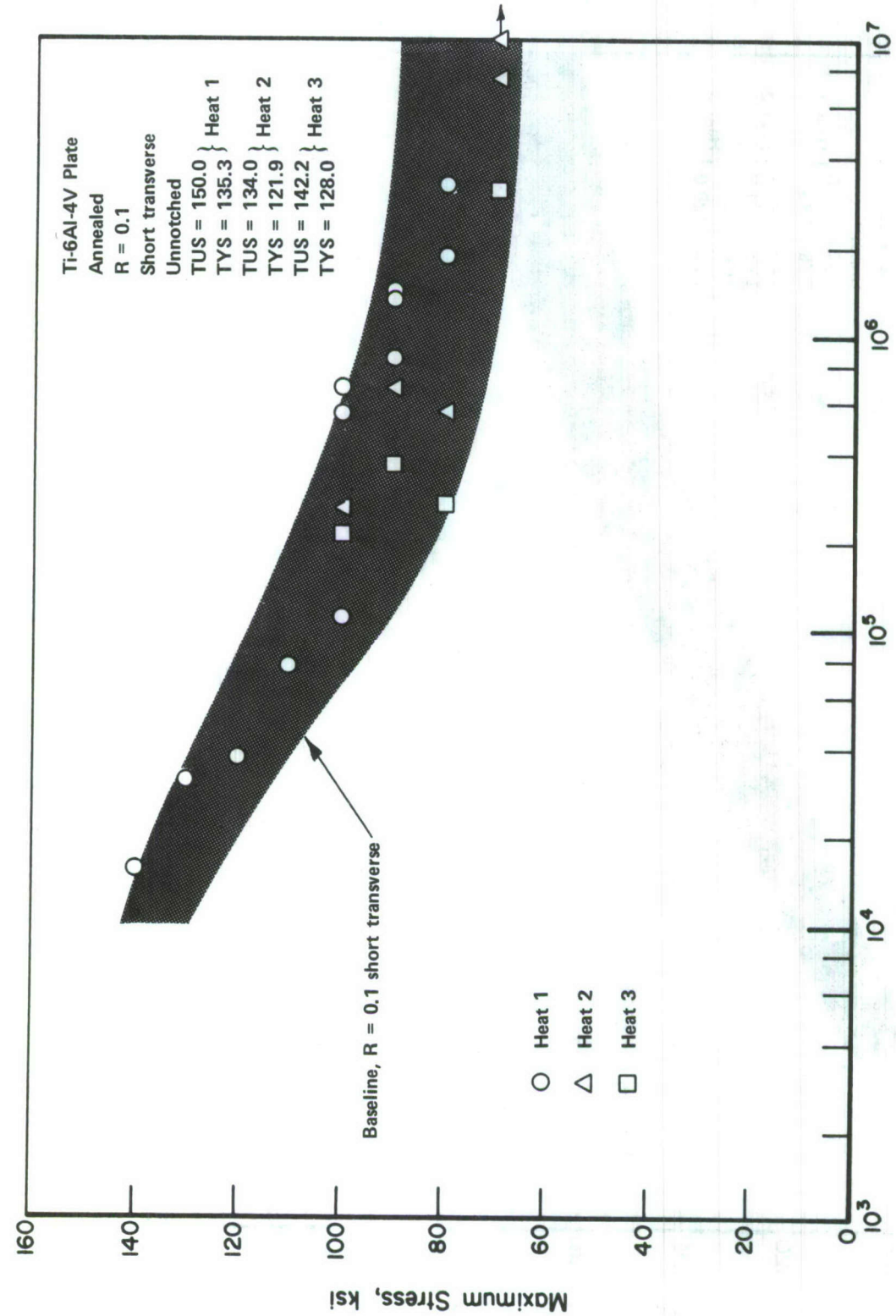

Figure 3. Axial Load Fatigue Behavior of Short Transverse, Unnotched Specimens of Baseline Material at R = 0.1

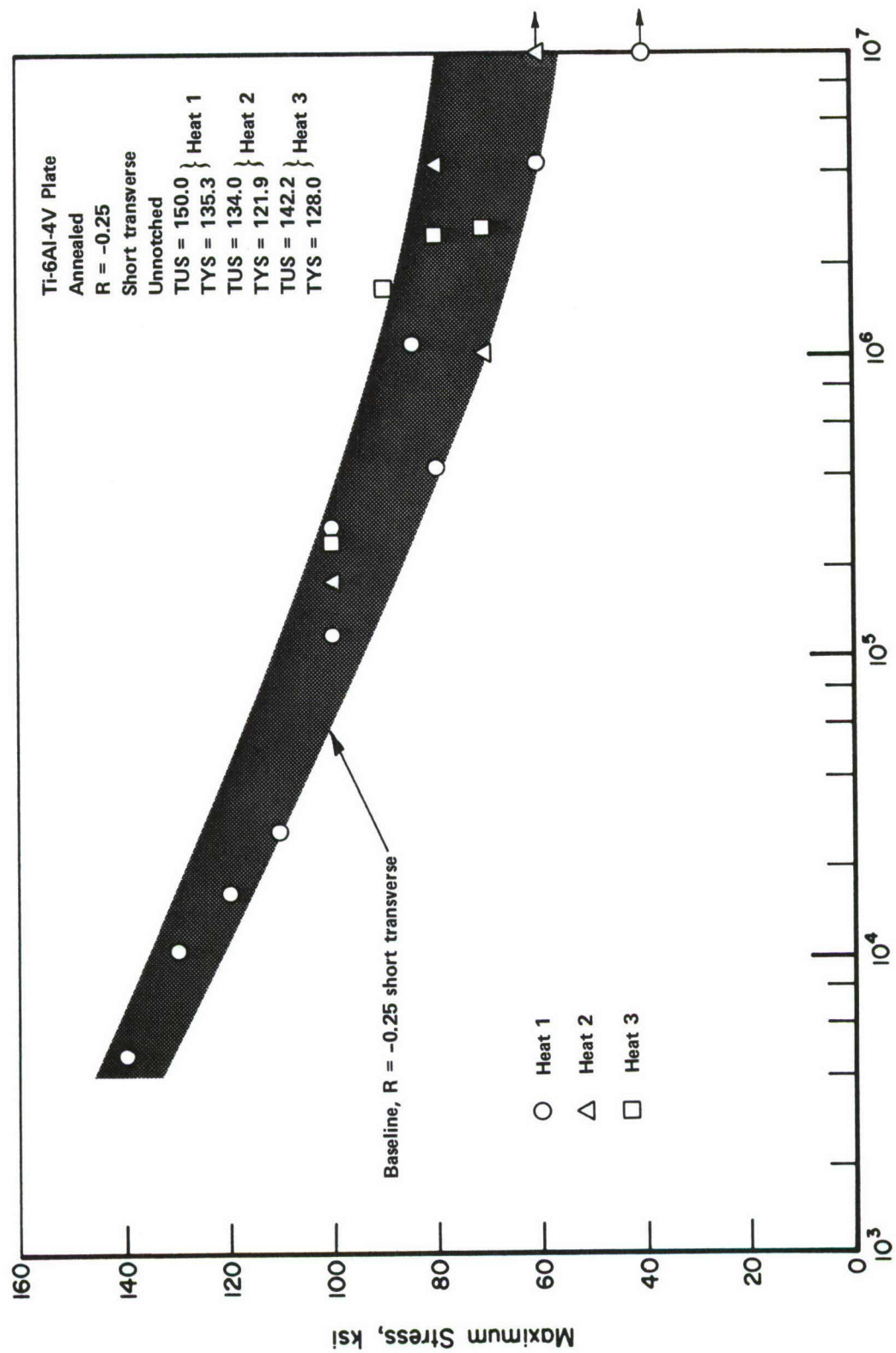

Figure 4. Axial Load Fatigue Behavior of Short Transverse, Unnotched Specimens of Baseline Material at R = -0.25

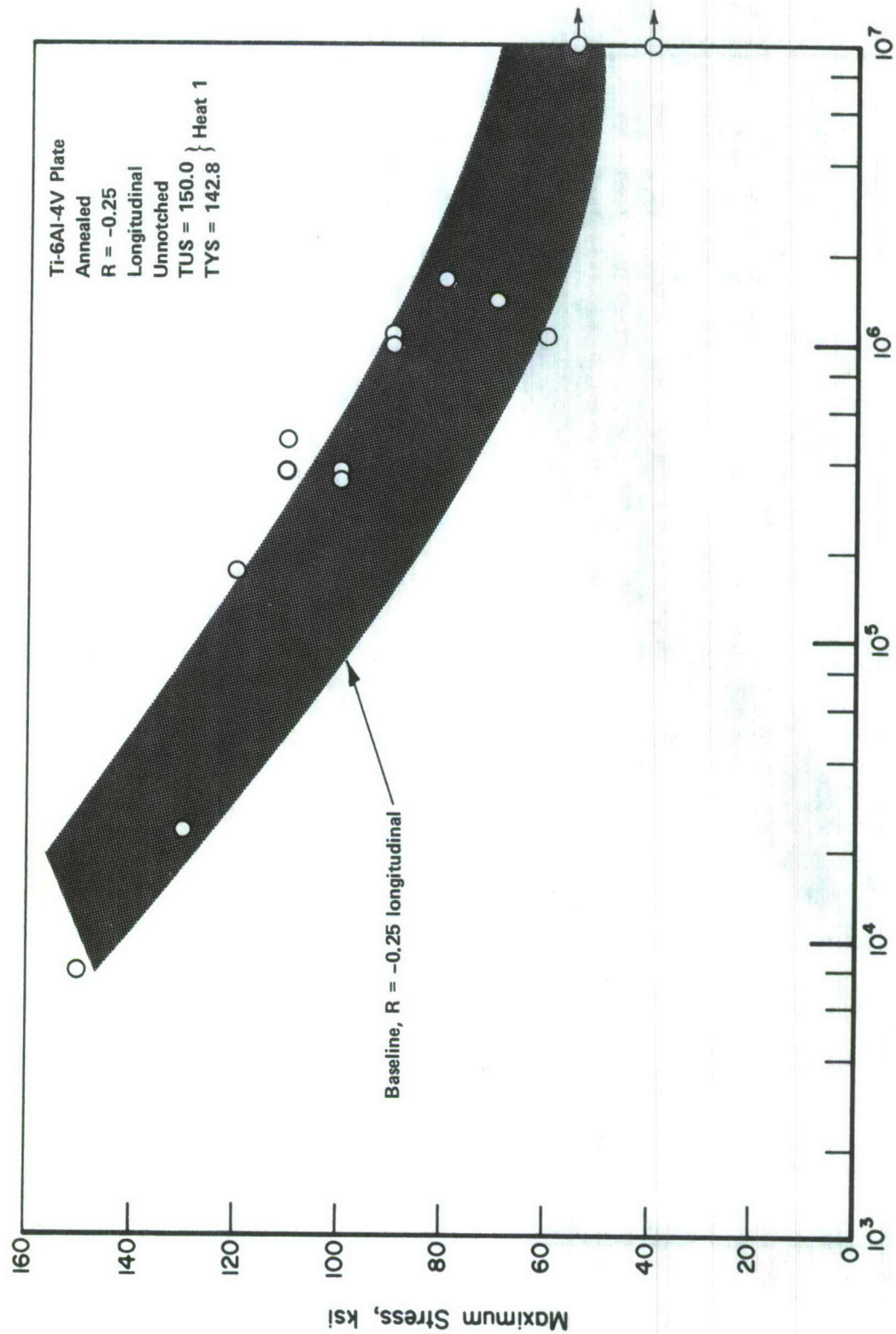

Figure 5. Axial Load Fatigue Behavior of Longitudinal, Unnotched Specimens of Baseline Material at R = -0.25

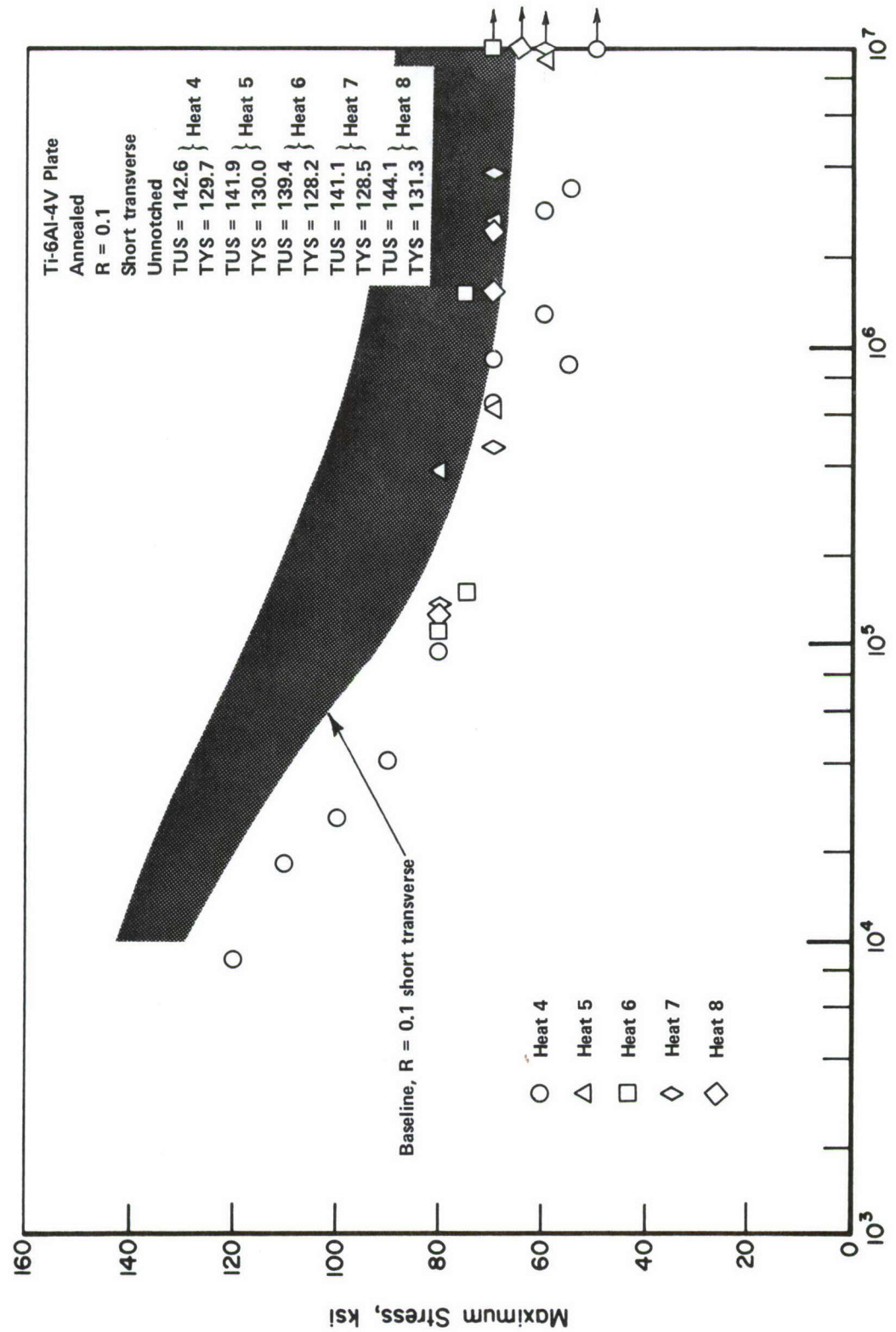

Figure 6. Axial Load Fatigue Behavior of Short Transverse, Unnotched Specimens of Plate with Yttrium at R = 0.1

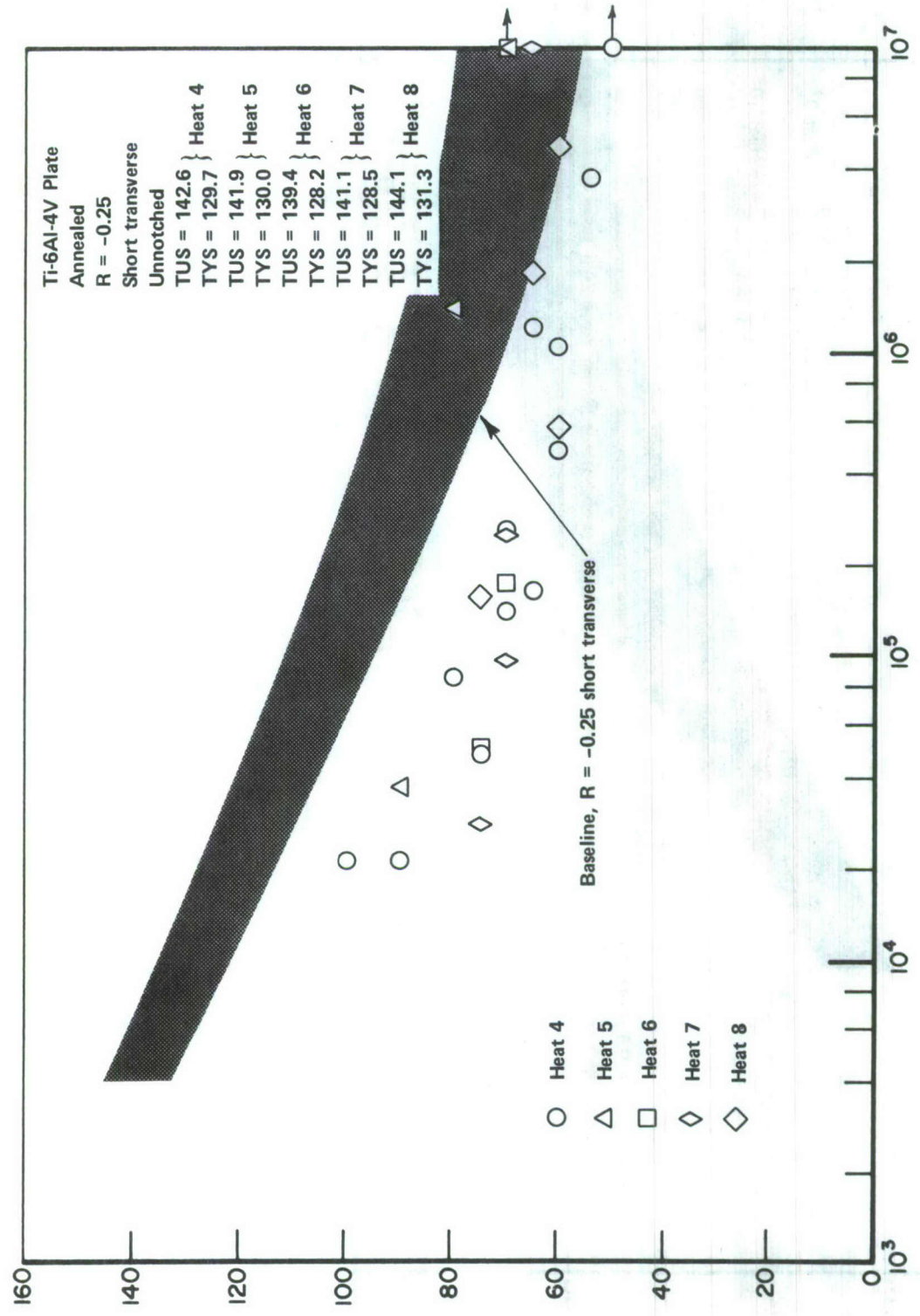

Figure 7. Axial Load Fatigue Behavior of Short Transverse, Unnotched Specimens of Plate with Yttrium at R = -0.25

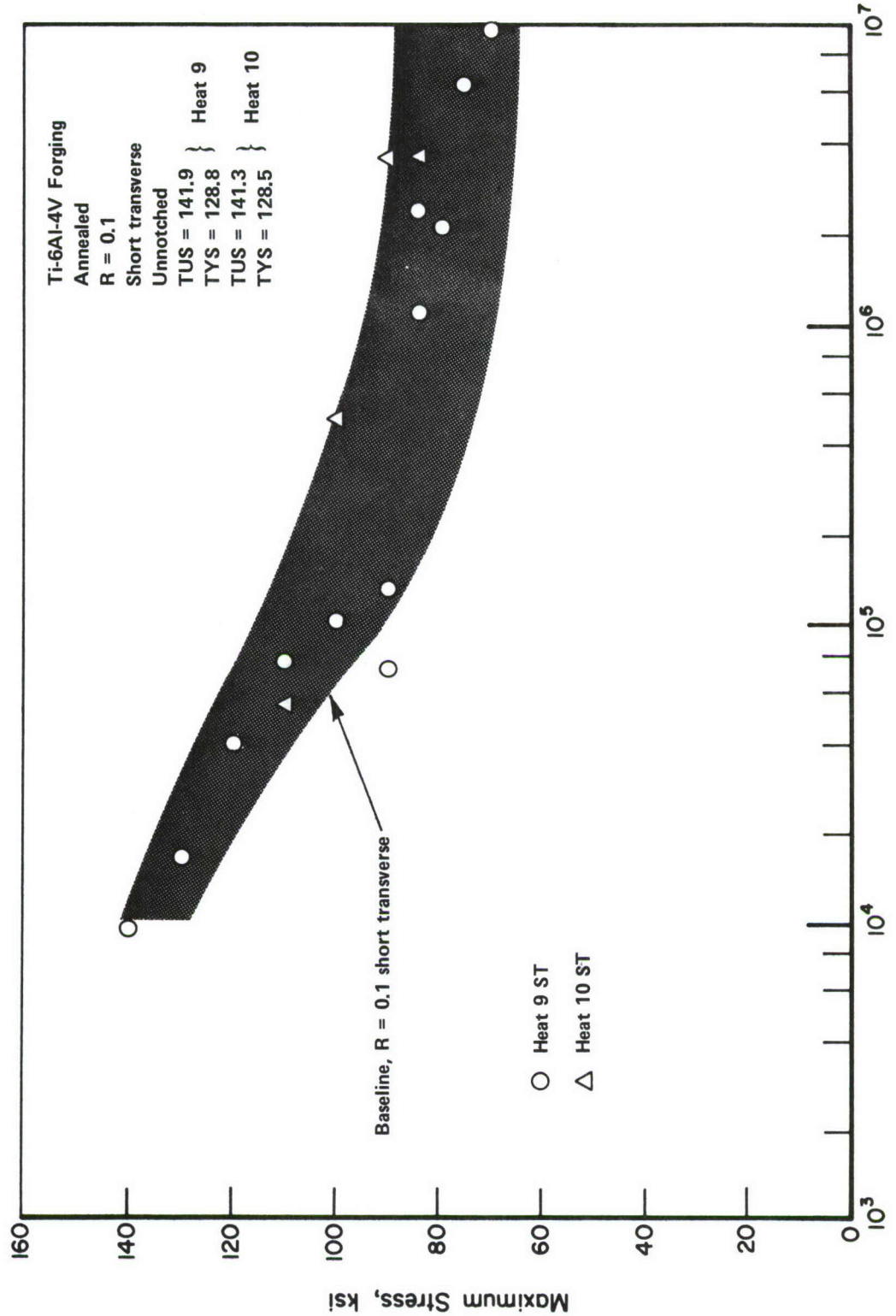

Figure 8. Axial Load Fatigue Behavior of Short Transverse, Unnotched Specimens of Forgings with Yttrium at R = 0.1

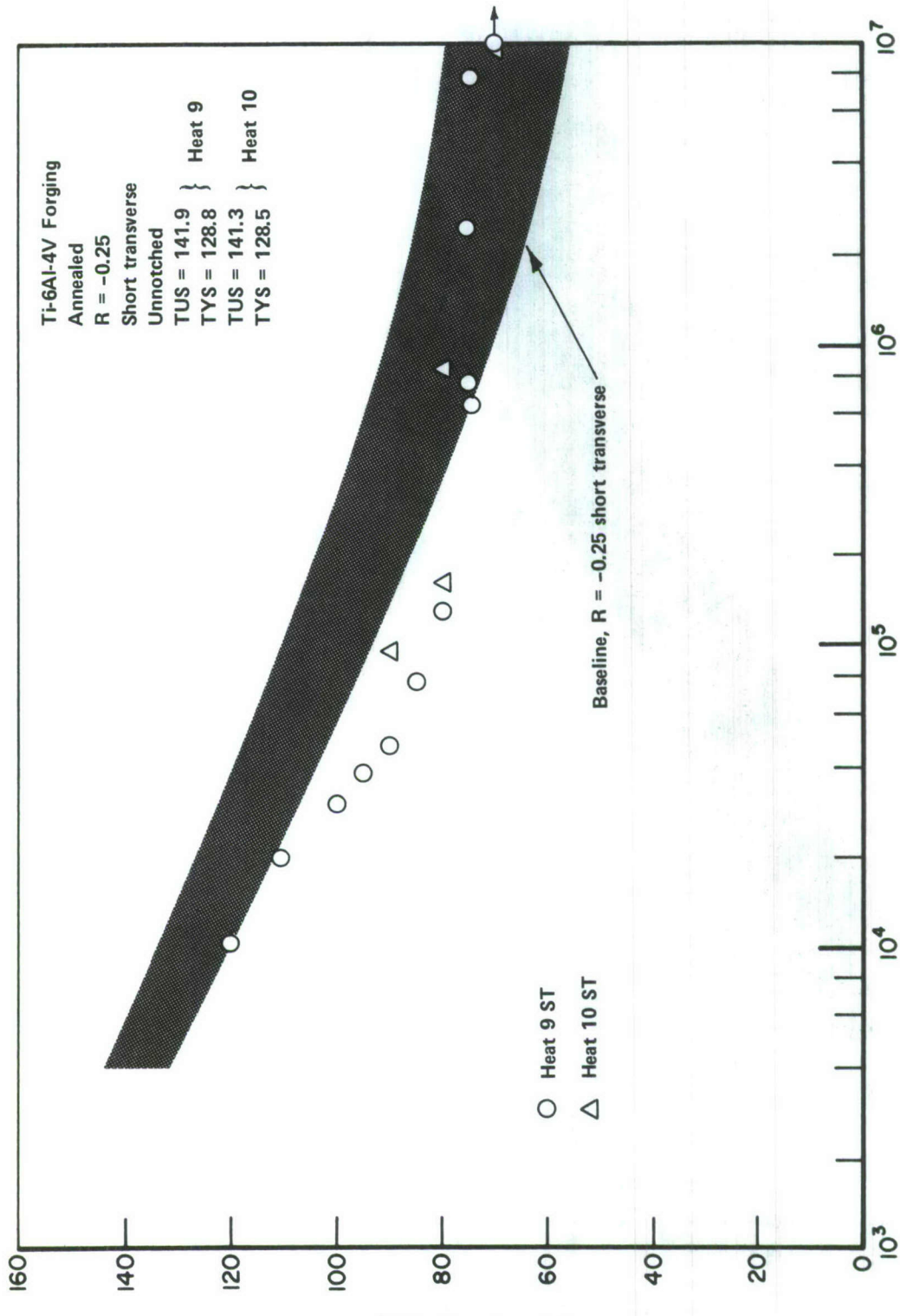

Figure 9. Axial Load Fatigue Behavior of Short Transverse, Unnotched Specimens of Forgings with Yttrium at R = -0.25

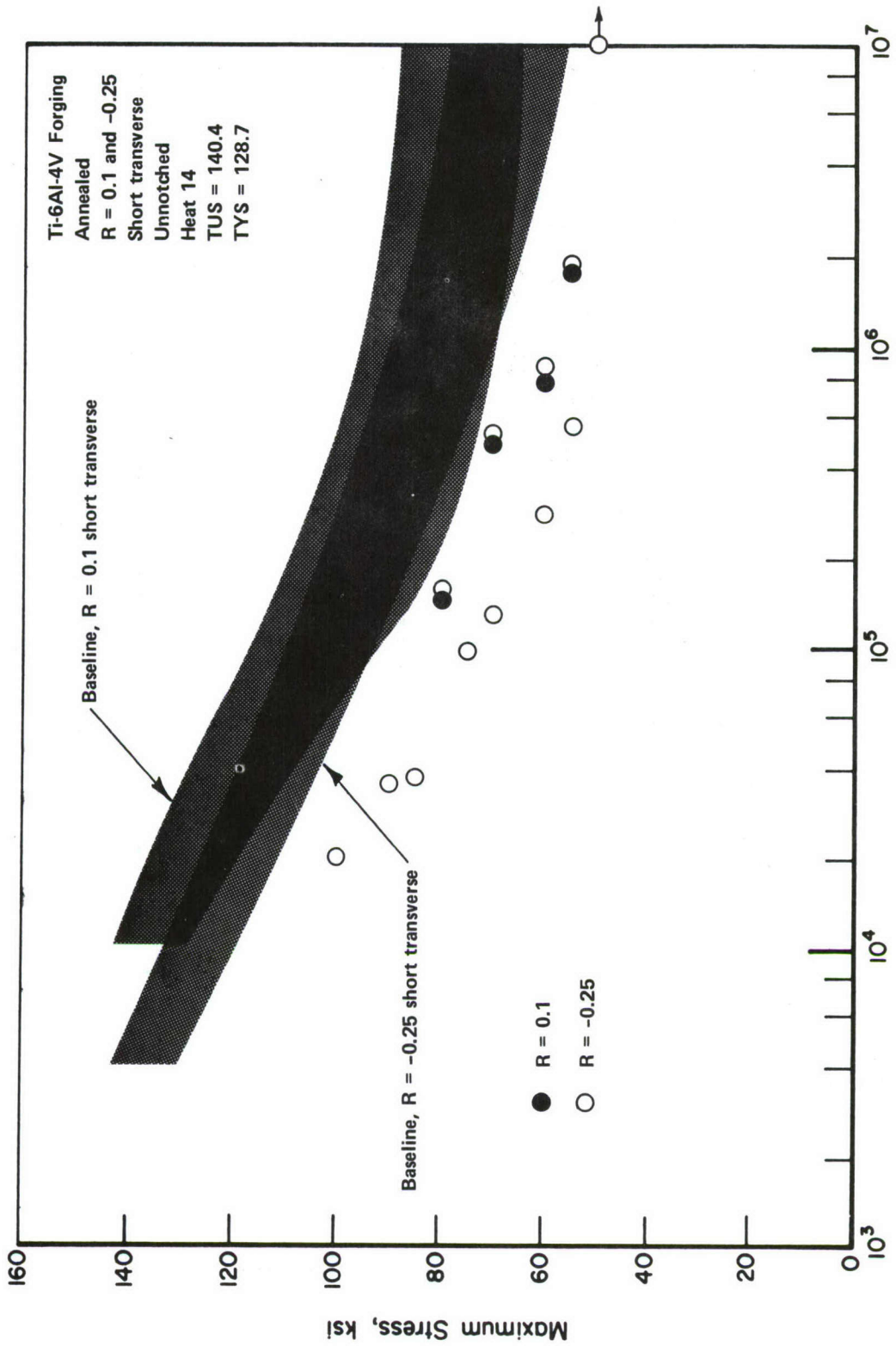

Figure 10. Axial Load Fatigue Behavior of Short Transverse, Unnotched Specimens of Heat 14 at R = 0.1 and R = -0.25 (Die Forging 61550)

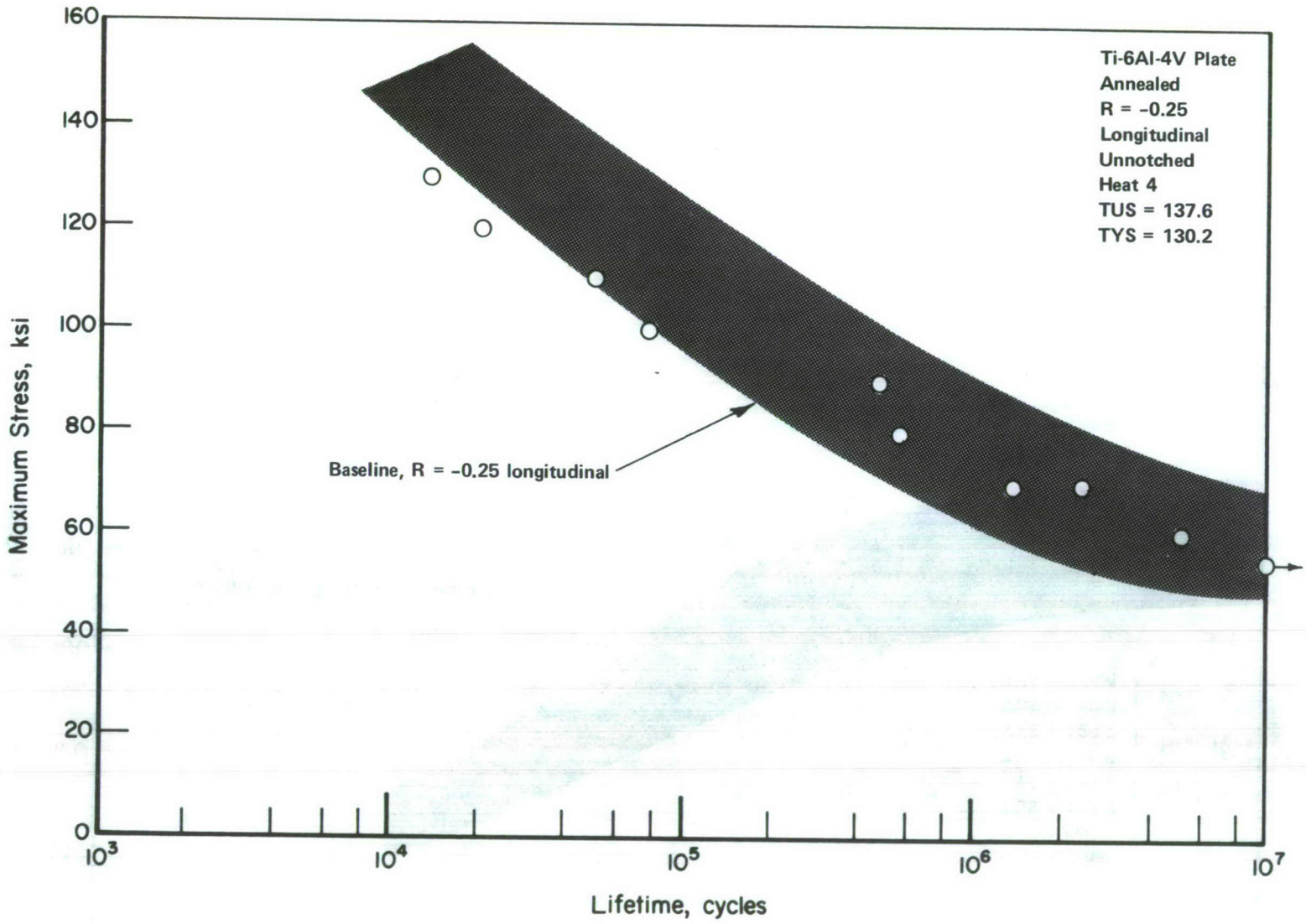

Figure 11. Axial Load Fatigue Behavior of Longitudinal, Unnotched Specimens of Plate with Yttrium of R = -0.25

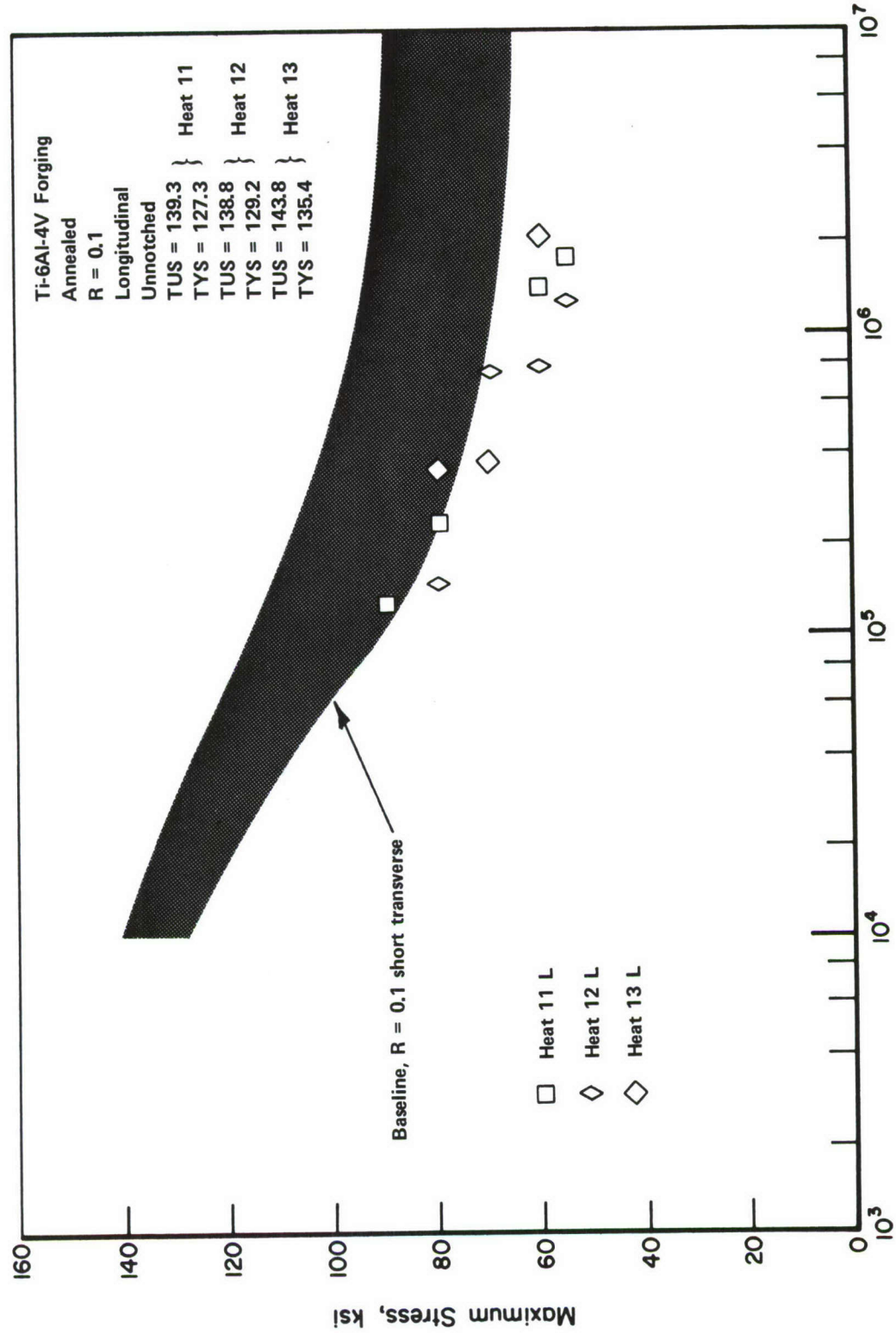

Figure 12. Axial Load Fatigue Behavior of Longitudinal, Unnotched Specimens of Forgings with Yttrium at R = 0.1

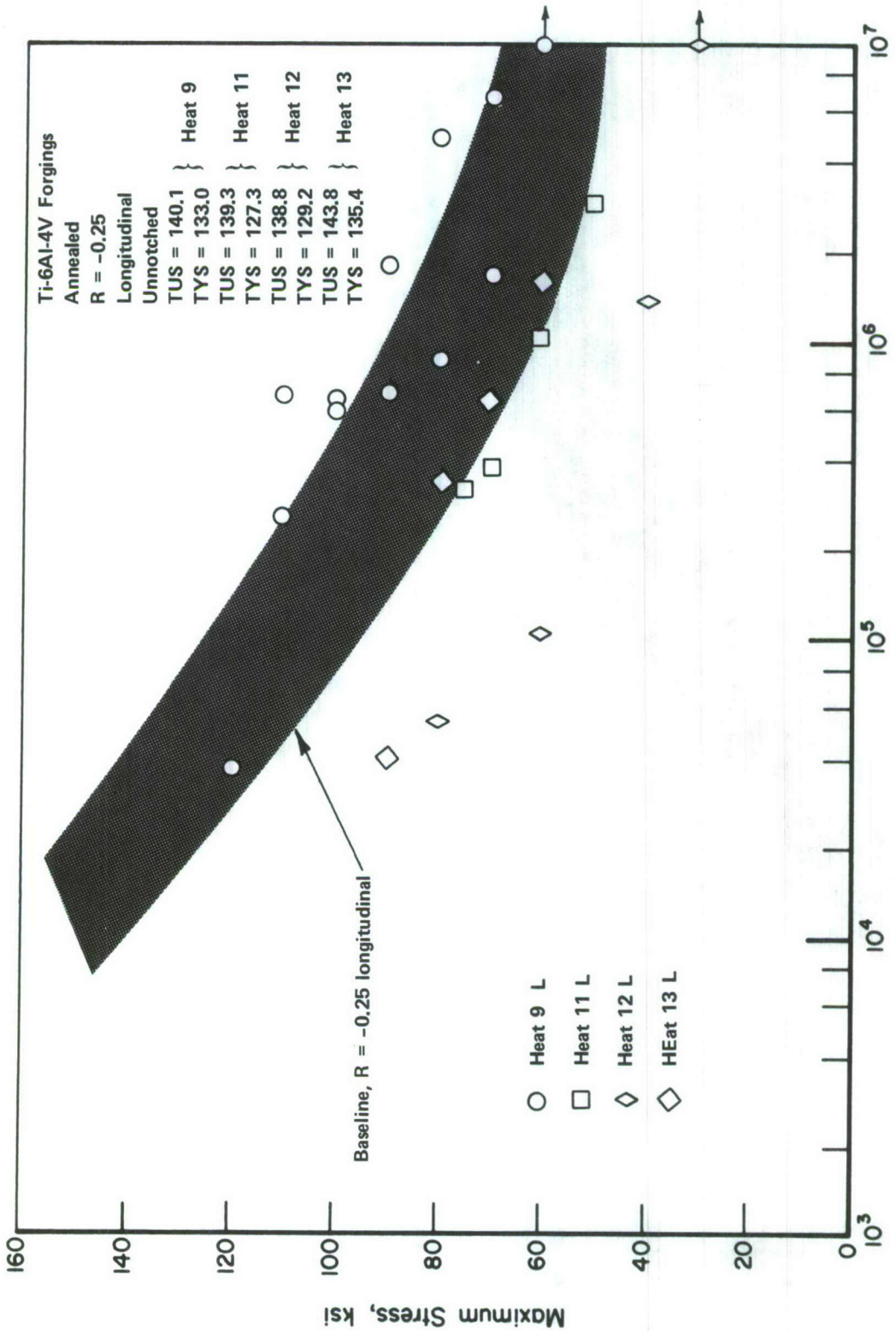

Figure 13. Axial Load Fatigue Behavior of Longitudinal, Unnotched Specimens of Forgings with Yttrium at R = -0.25

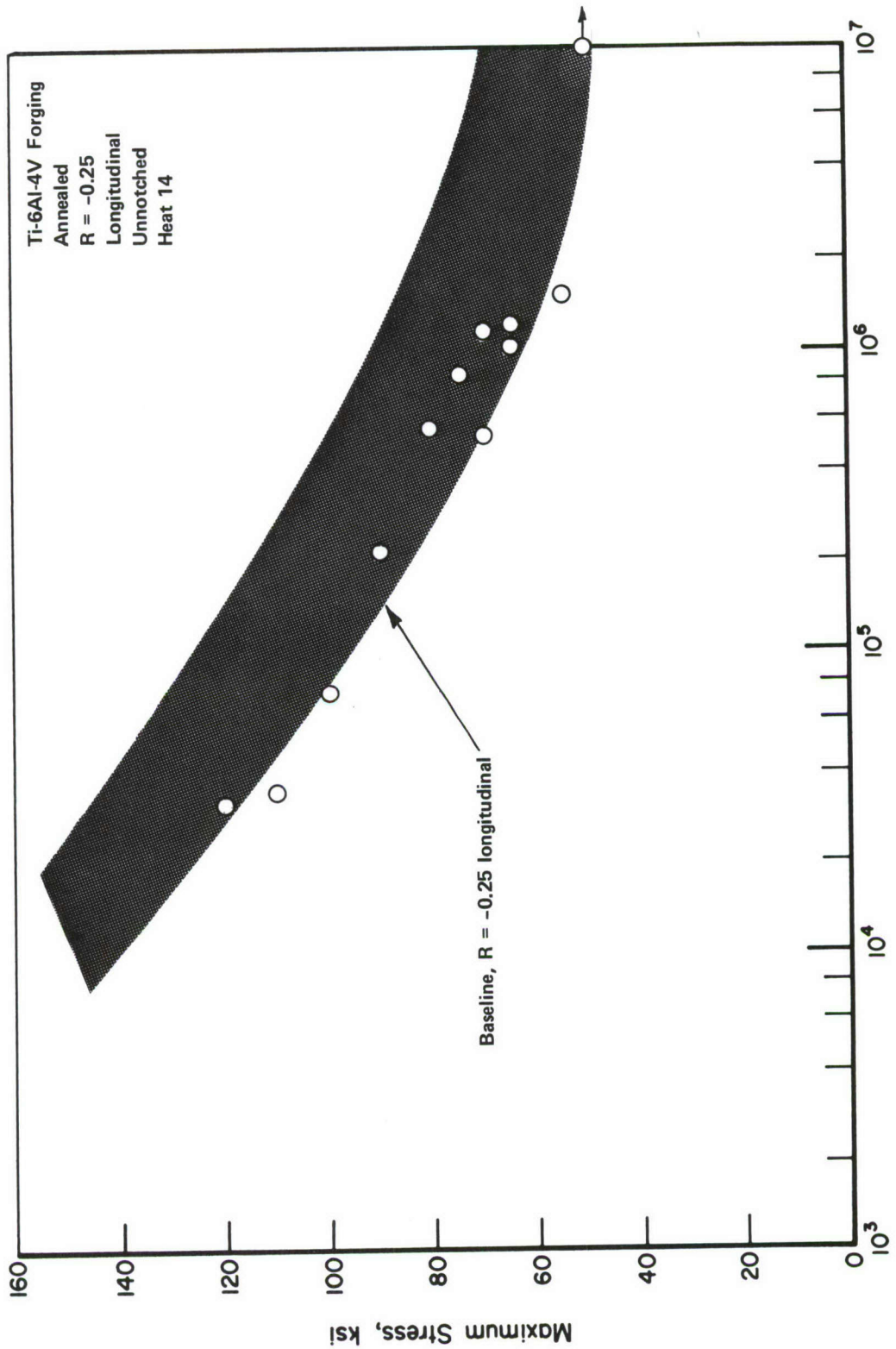

Figure 14. Axial Load Fatigue Behavior of Longitudinal, Unnotched Specimens of Heat 14 at R = -0.25 (Die Forging 61550)

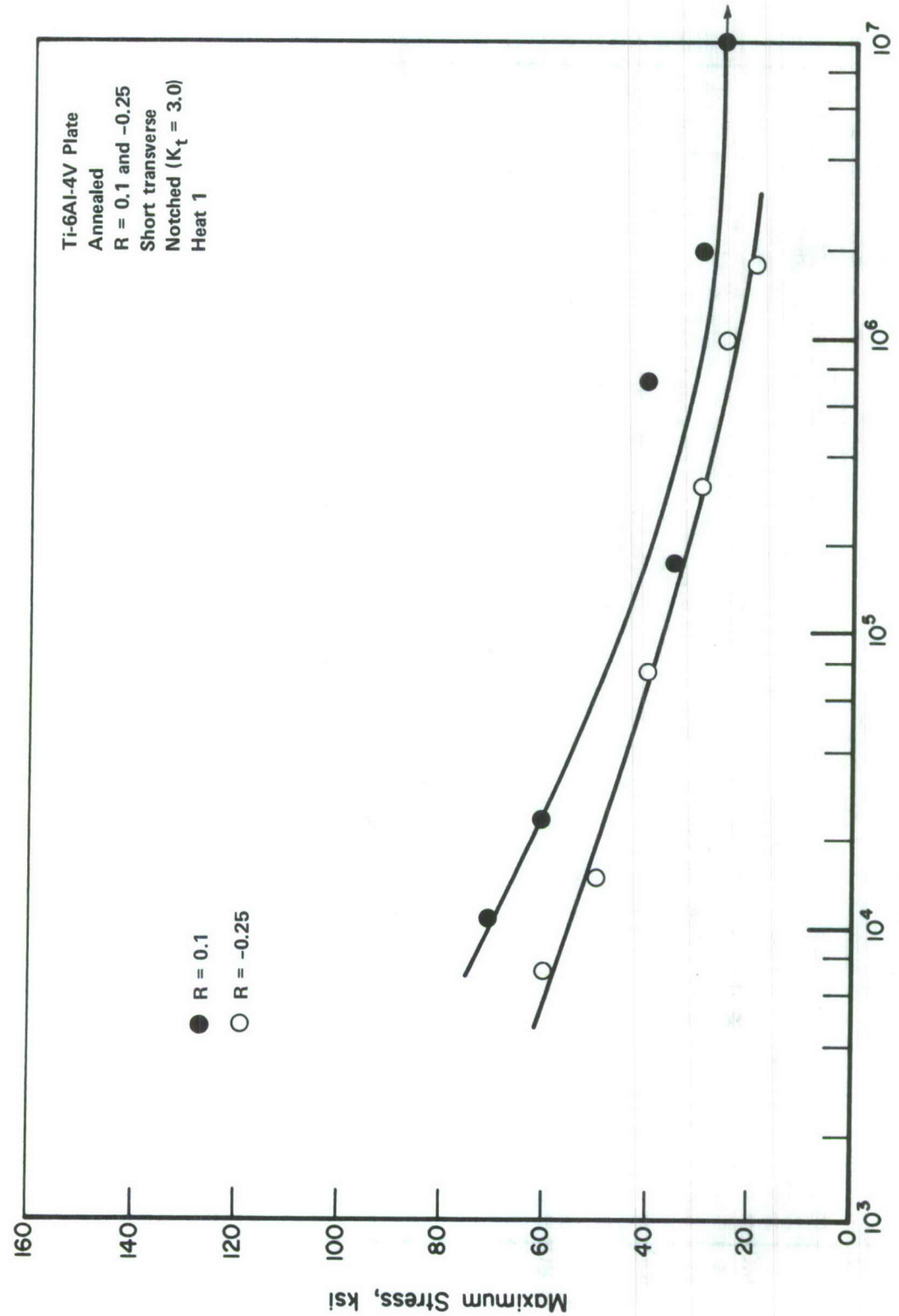

Figure 15. Axial Load Fatigue Behavior of Short Transverse, Notched (K_t = 3.0) Specimens of Baseline Material at R = 0.1 and -0.25

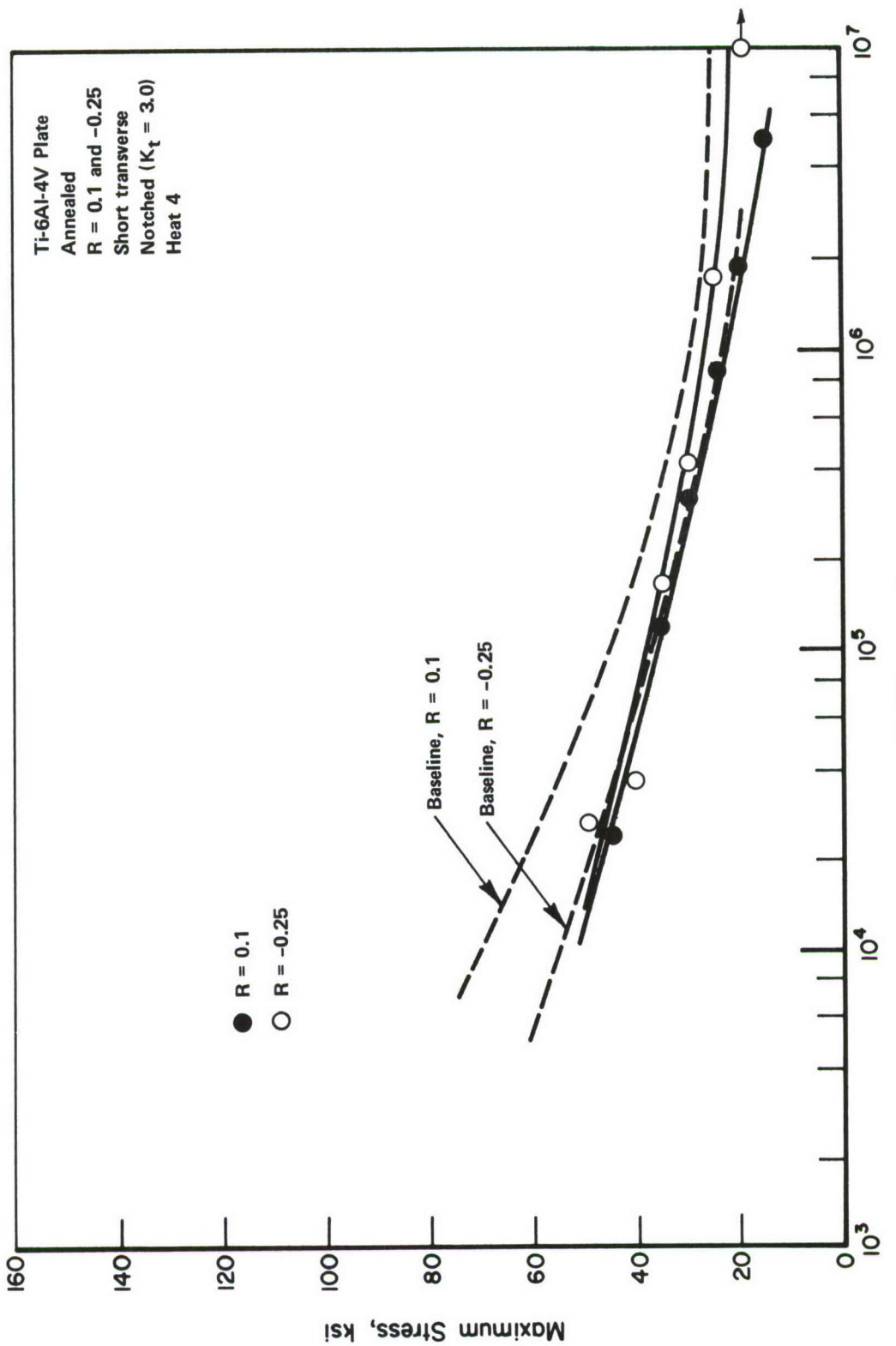

Figure 16. Axial Load Fatigue Behavior of Short Transverse, Notched (K_t = 3.0) Specimens of Plate with Yttrium at R = 0.1 and -0.25

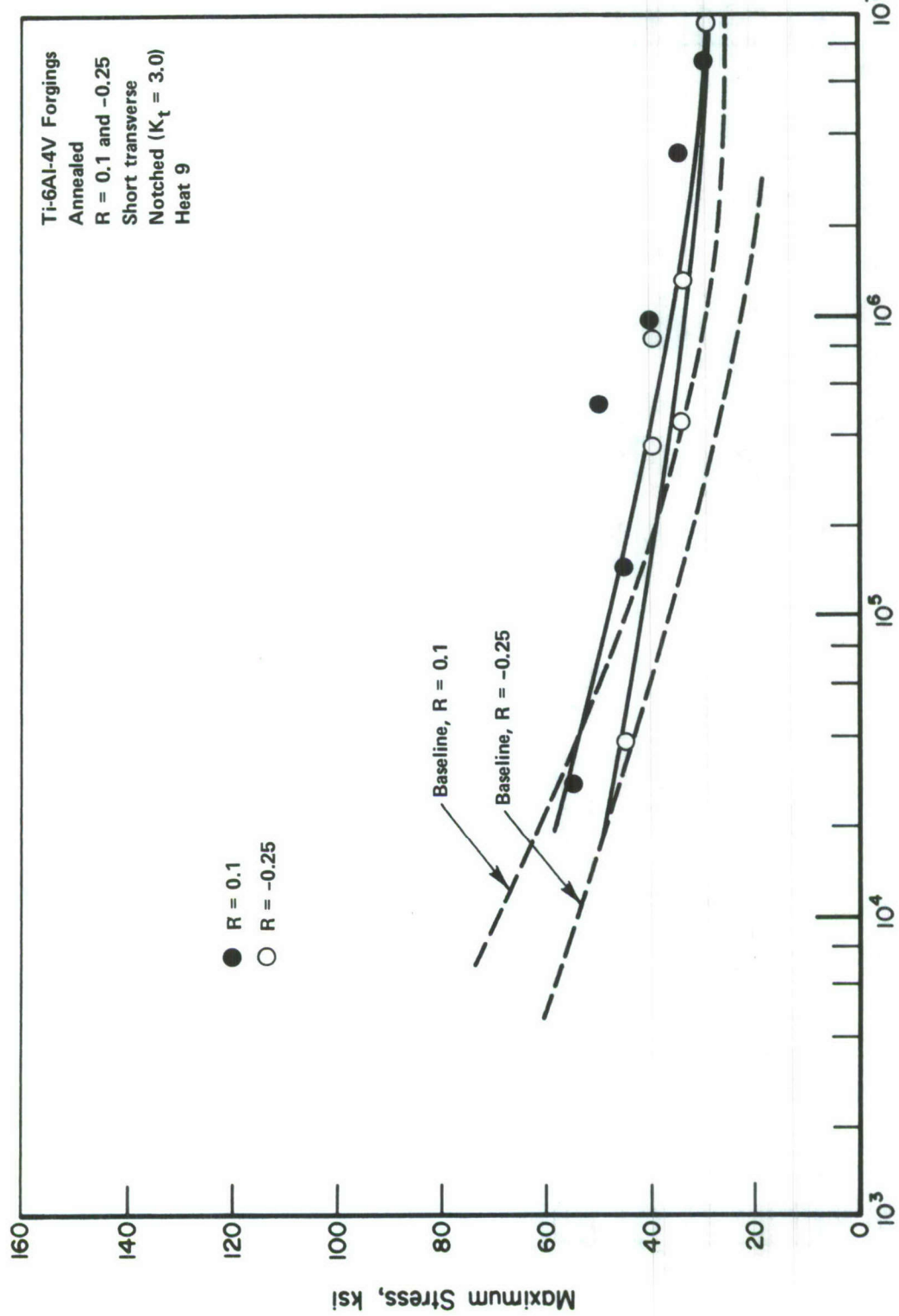

Figure 17. Axial Load Fatigue Behavior of Short Transverse, Notched (K_t = 3.0) Specimens of Forgings with Yttrium at R = 0.1 and -0.25

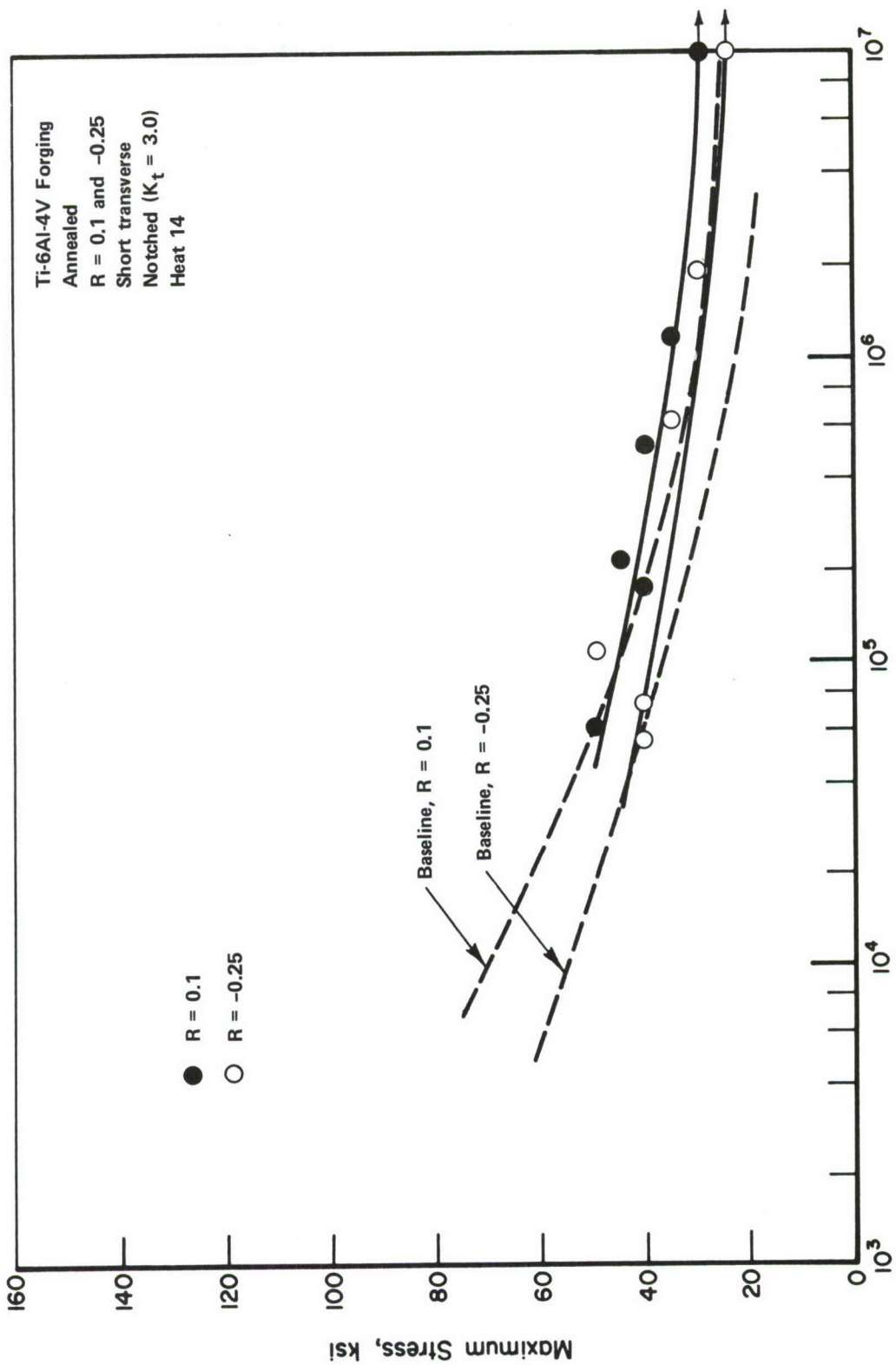

Figure 18. Axial Load Fatigue Behavior of Short Transverse, Notched (K_t = 3.0) Specimens of Heat 14 at R = 0.1 and -0.25 (Die Forging 61550)

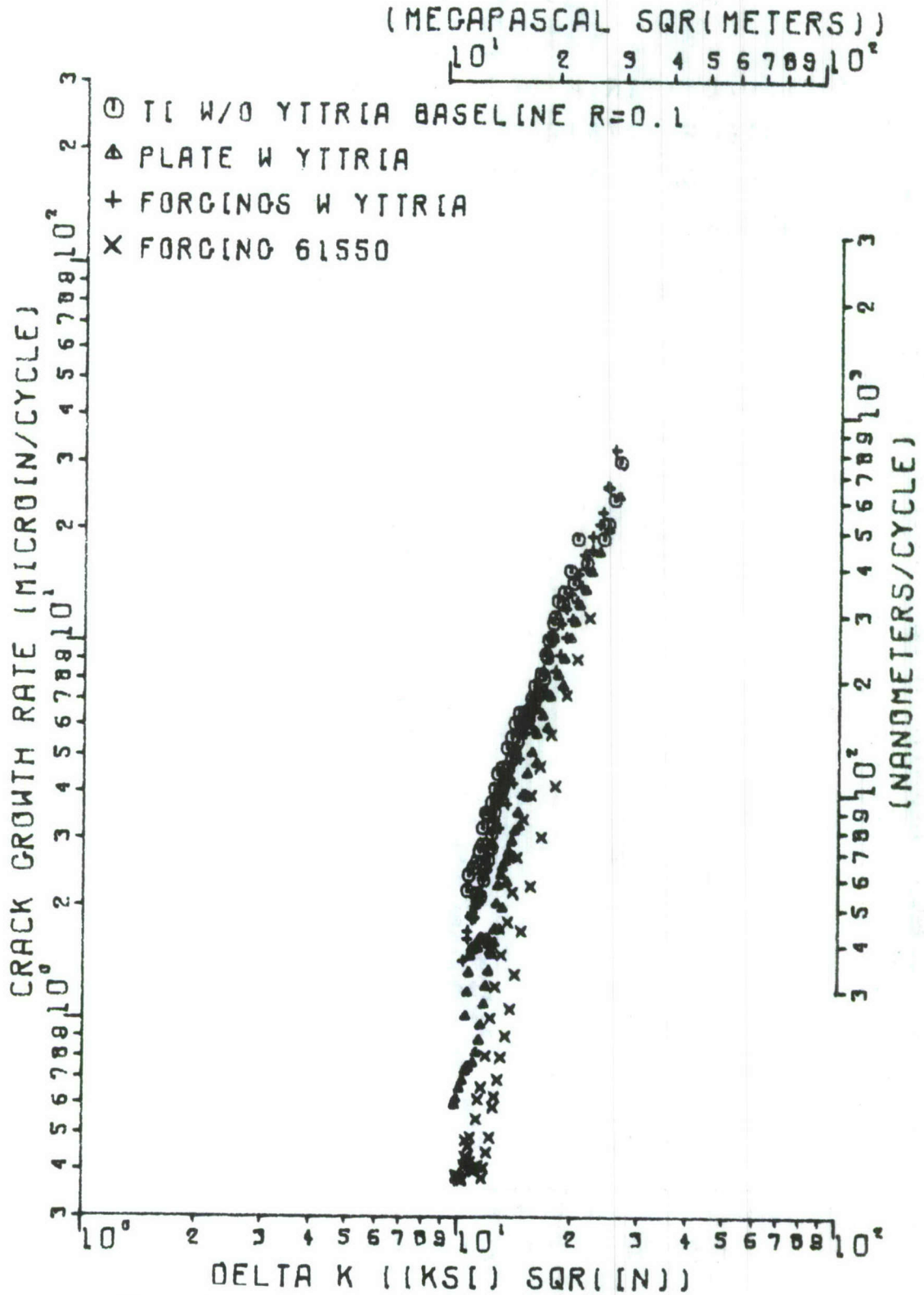

Figure 19. Crack-Growth Test Results for Baseline and Selected Yttria-Containing Heats at a Ratio of R = 0.1

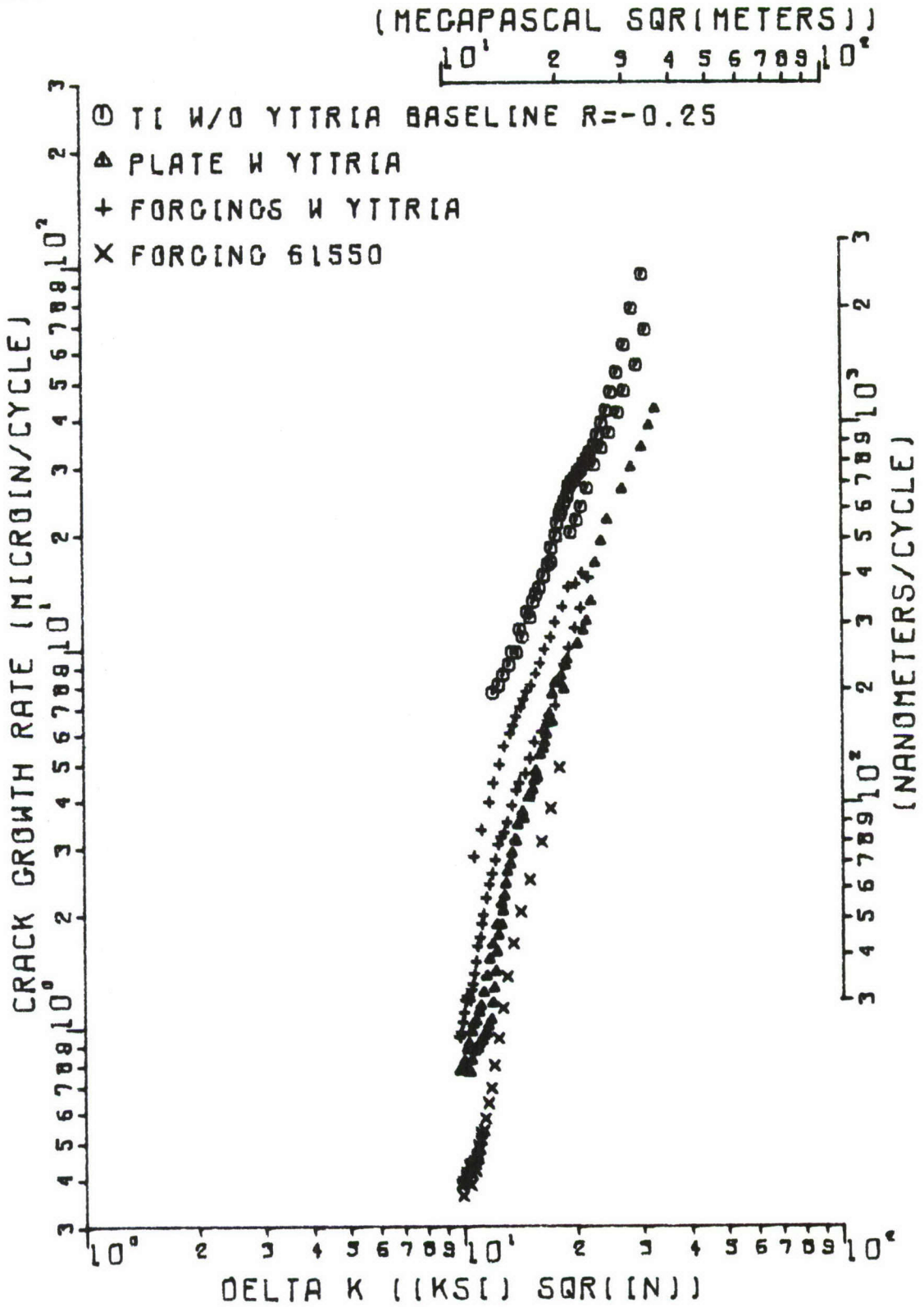

Figure 20 Crack-Growth Test Results for Baseline and Selected Yttria-Containing Heats at a Ratio of R = -0.25

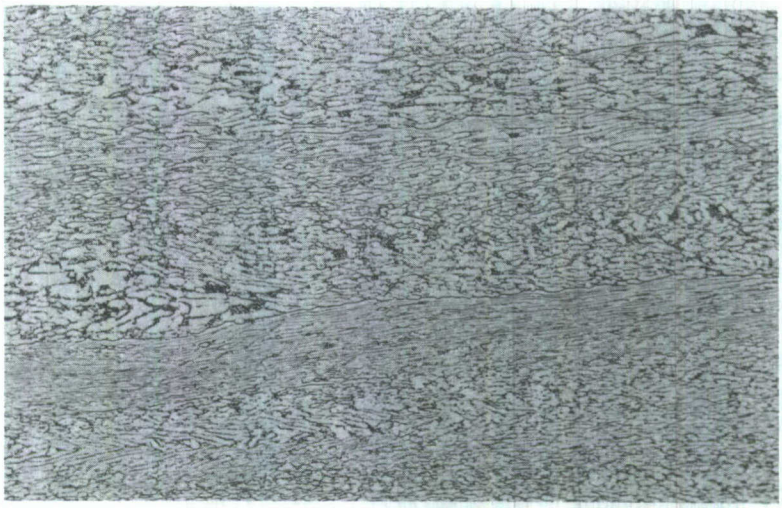

A. Heat No. 1 7H923

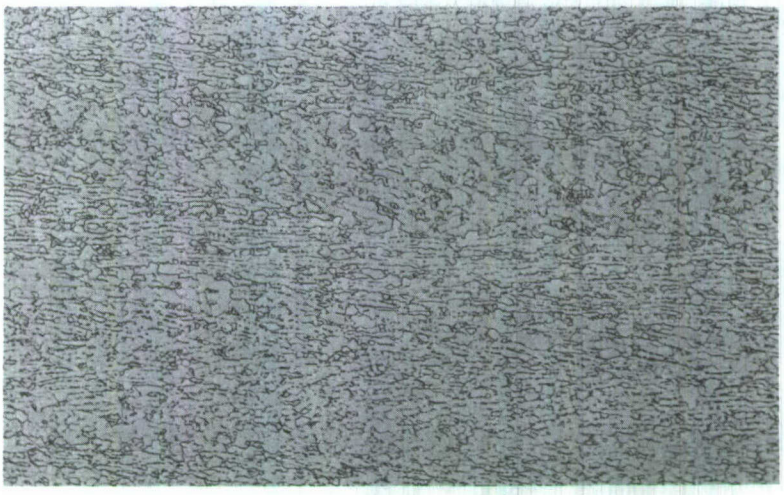

B. Heat No. 2 7H924

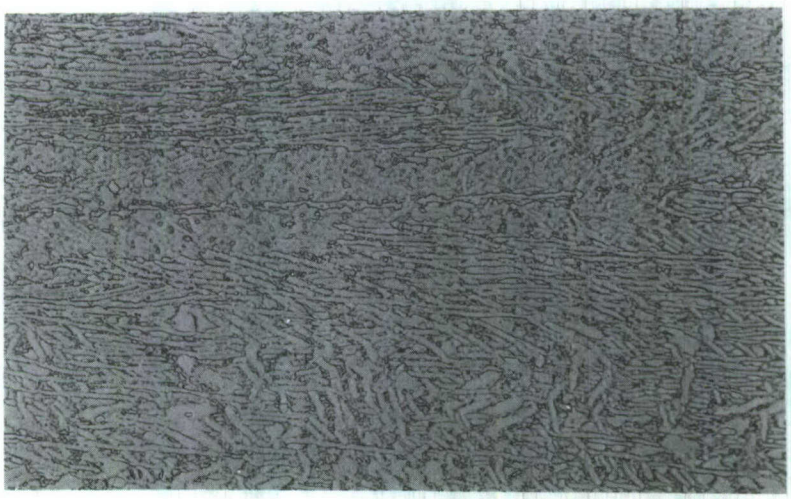

C. Heat No. 3 7H925

Figure 21. Microstructures of Baseline Plates, as Etched, 100X

100X Etched 7H297

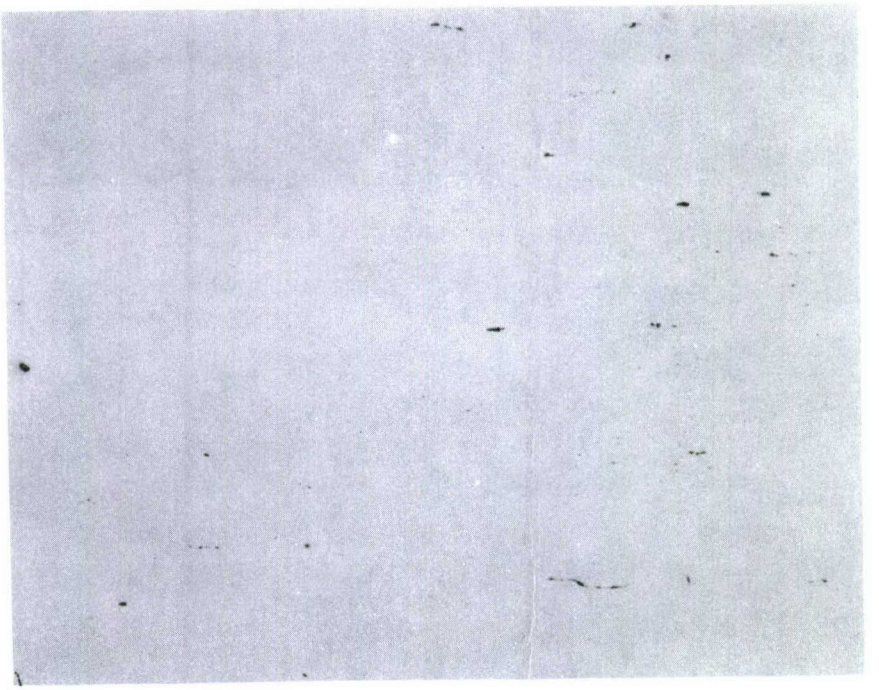

100X As Polished 7H296

Figure 22. Microstructure of Heat No. 4

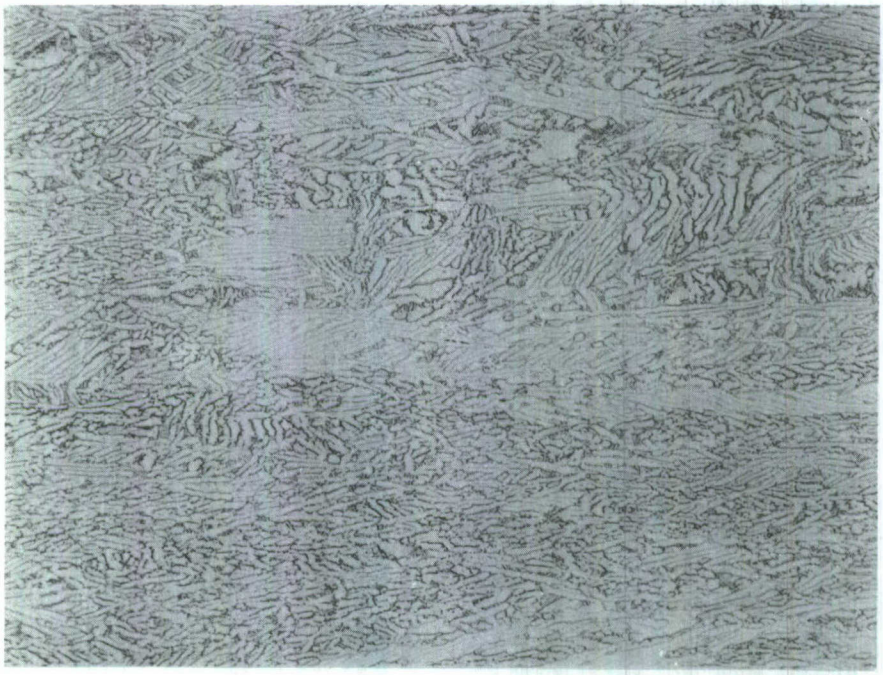

100X Etched 7H295

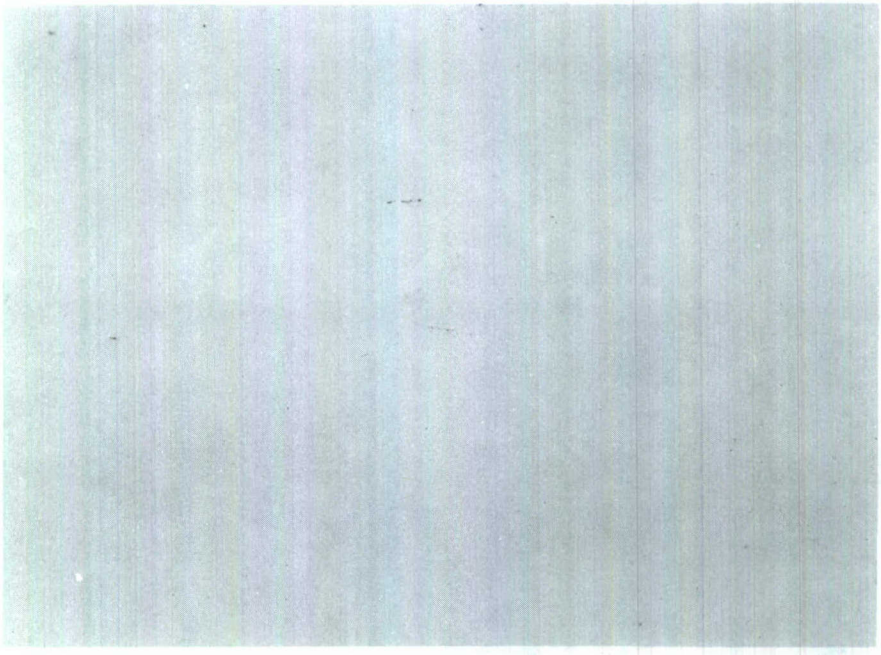

100X As Polished 7H294

Figure 23. Microstructure of Heat No. 5

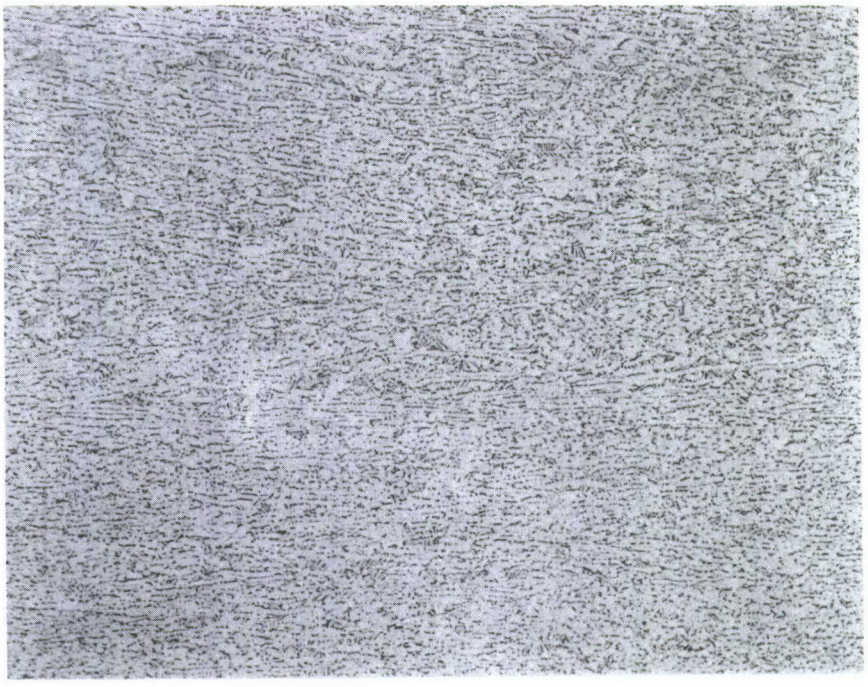

100X Etched 7H301

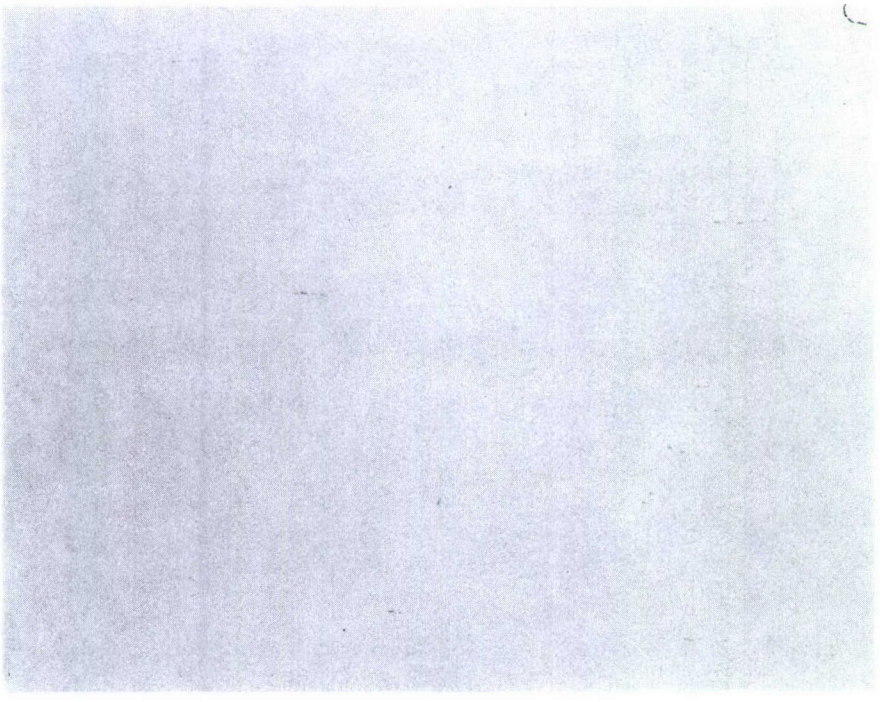

100X As Polished 7H300

Figure 24. Microstructure of Heat No. 6

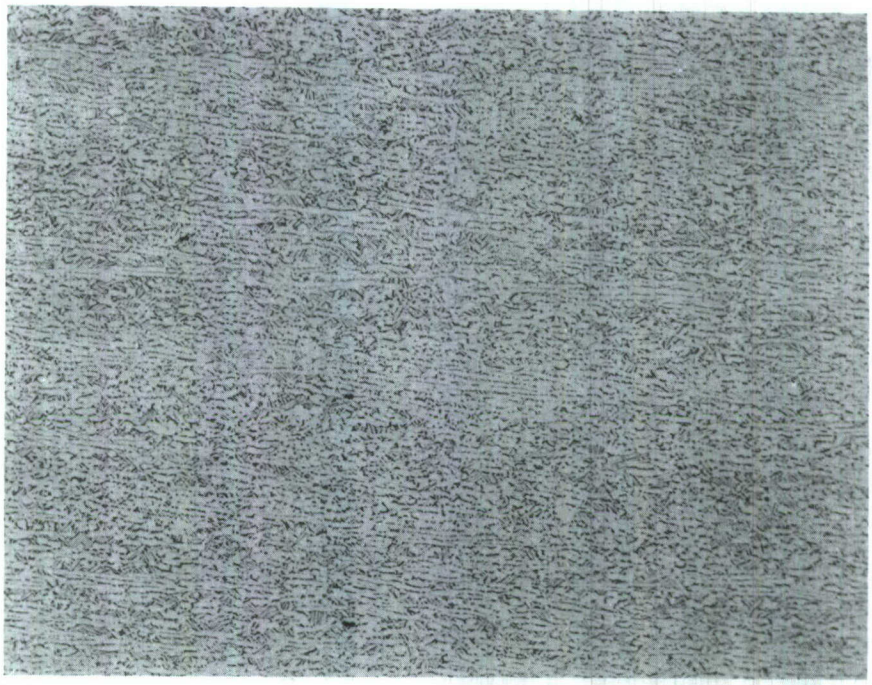

100X Etched 7H299

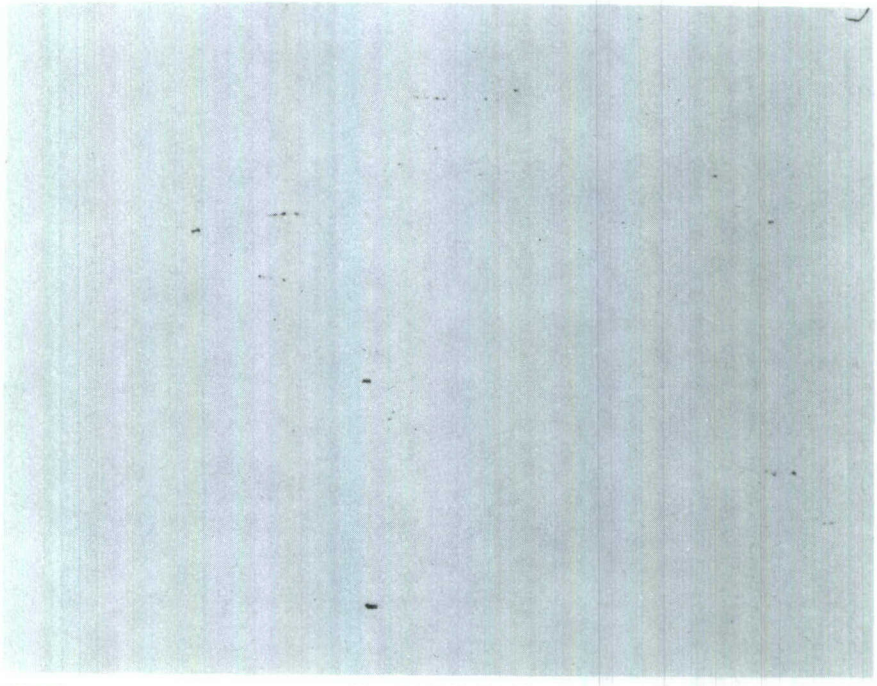

100X As Polished 7H298

Figure 25. Microstructure of Heat No. 7

100X Etched 7H303

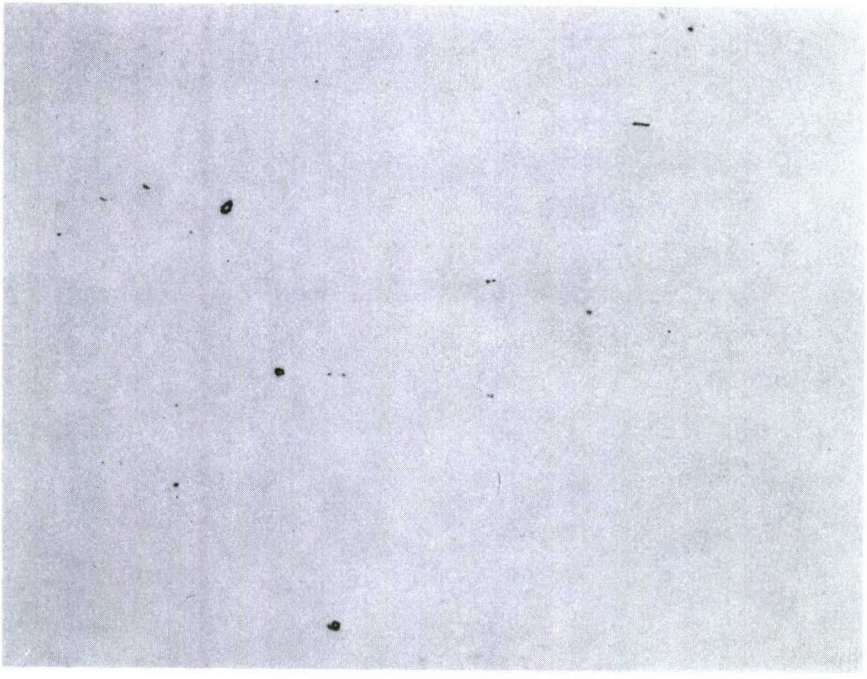

100X As Polished 7H302

Figure 26. Microstructure of Heat No. 8 (The three round particles in relief do not contain yttrium)

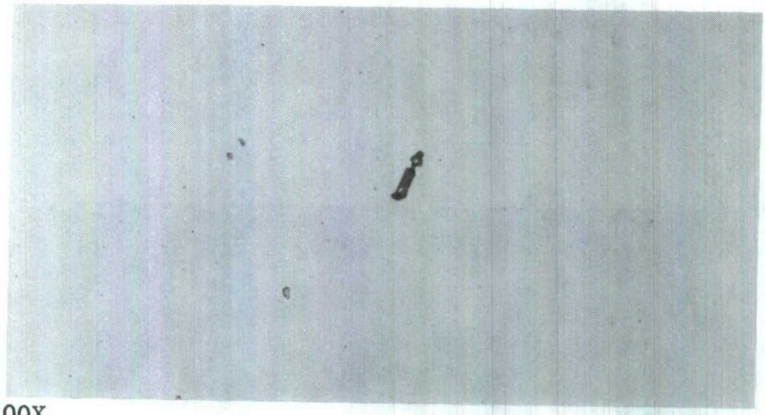

500X 16154

(a) Large yttria particle in Heat No. 4

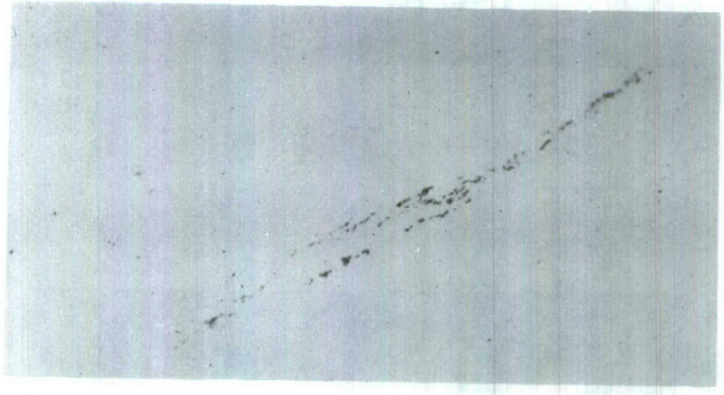

500X 16152

(b) Filigreed stringer of yttria in Heat no. 5

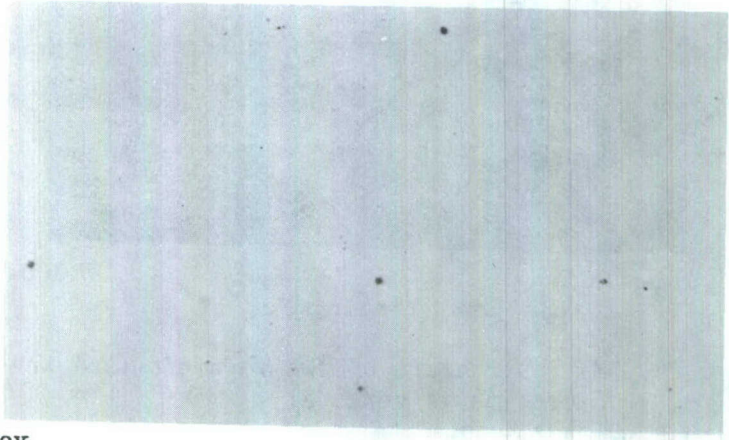

500X 16157

(c) Small rounded yttria particles in Heat No. 6

Figure 27. Photomicrographs of Yttria Particles Typical of Those Observed in the Ti-6Al-4V Plate

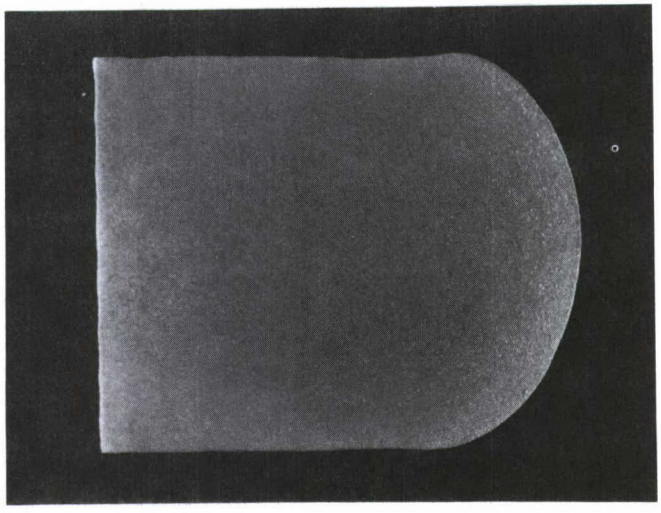

1X 7H999

(a) Pancake Forging No. 10

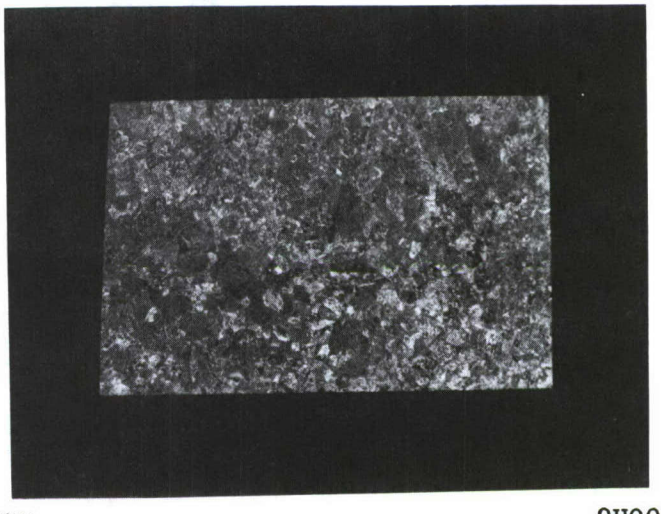

1X 9H000

(b) Hand Forging No. 12

Figure 28. Macrostructure of Two Forgings (Thickness direction is vertical)

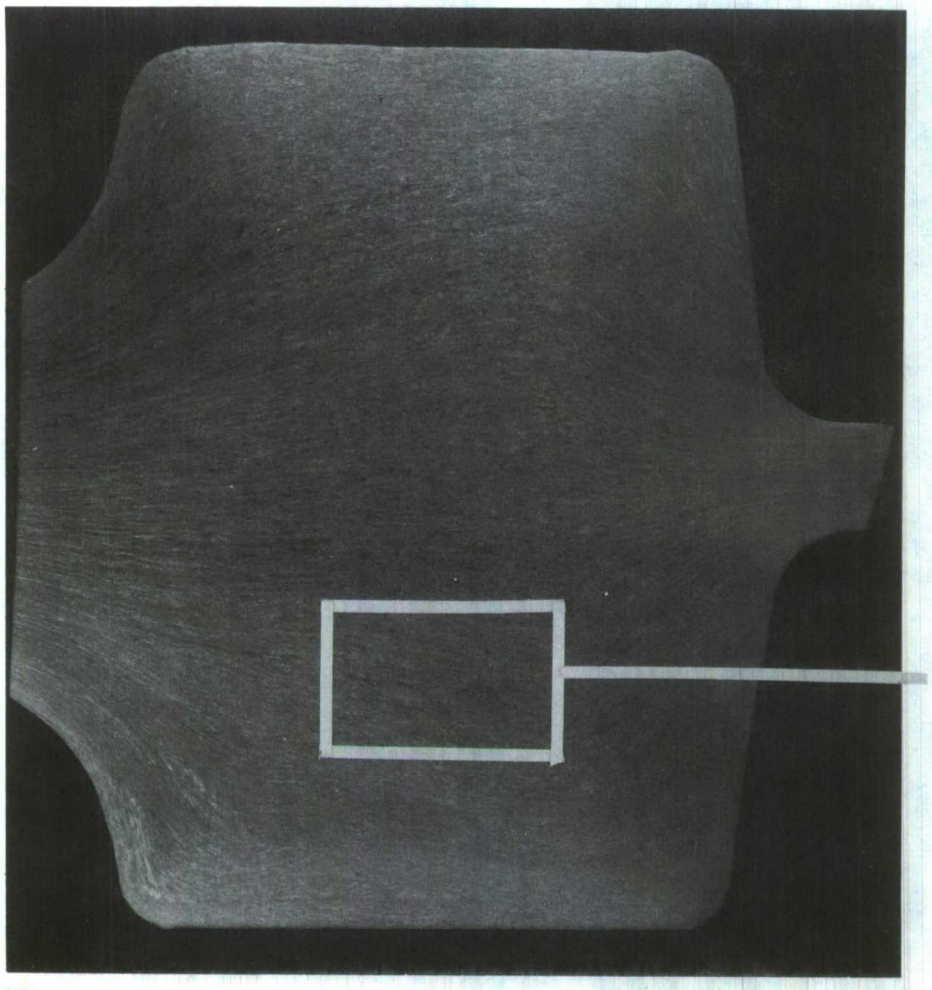

Figure 29. Macrostructure in a Section Cut from Heat No. 14

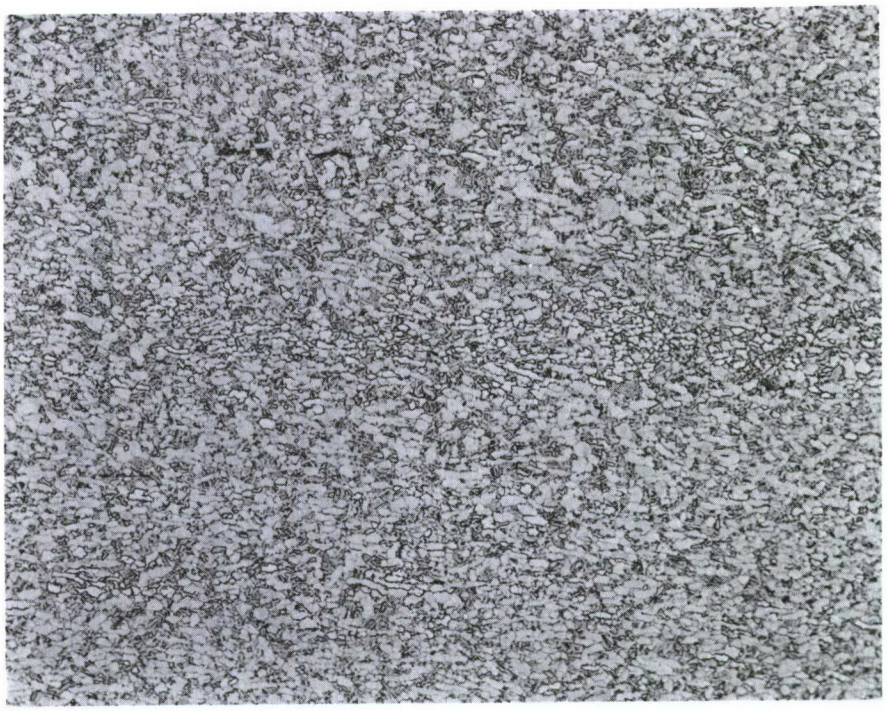

100X 9H322

Figure 30. Microstructure of Heat No. 9, As Etched

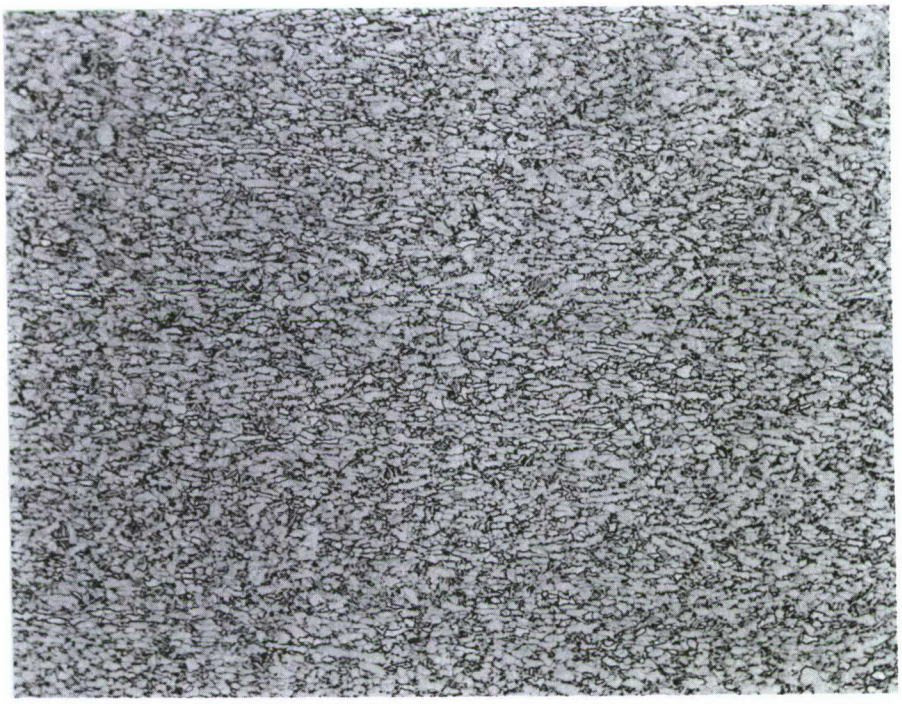

100X 9H323

Figure 31. Microstructure of Heat No. 10, As Etched

100X 9H324

Figure 32. Microstructure of Heat No. 11, As Etched

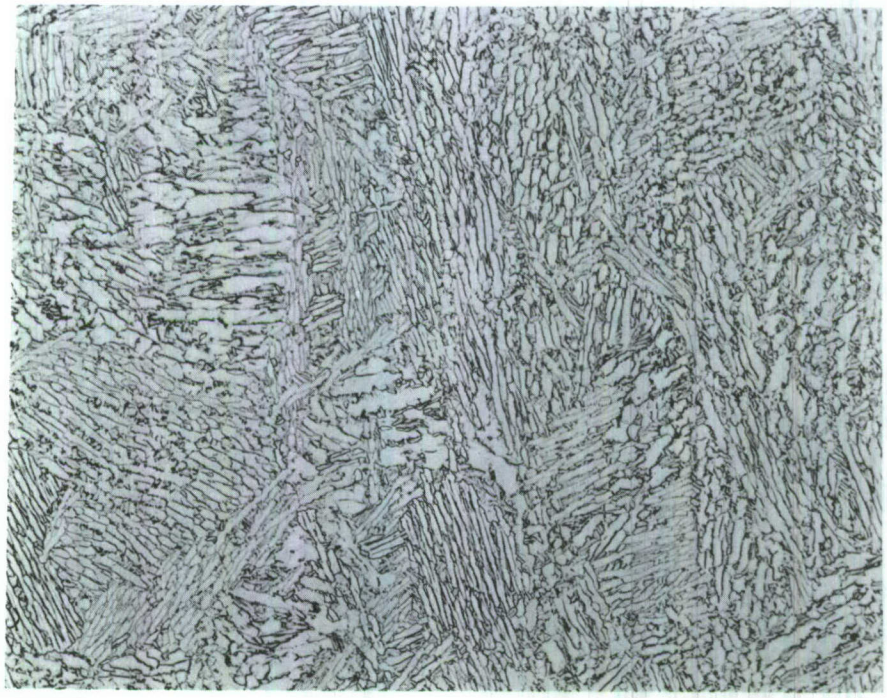

100X 9H325

Figure 33. Microstructure of Heat No. 12, As Etched

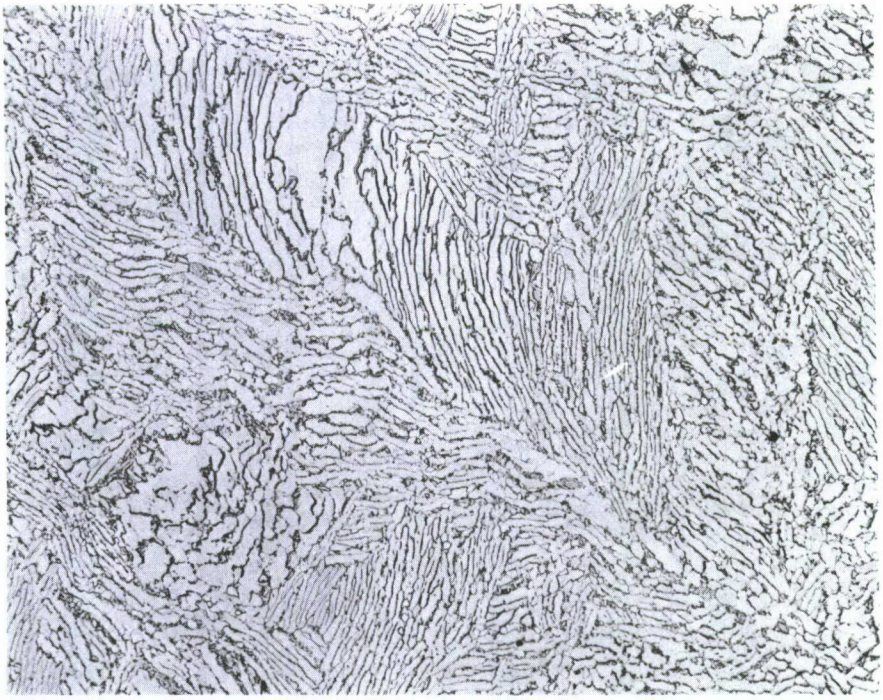

100X 9H326

Figure 34. Microstructure of Heat No. 13, As Etched

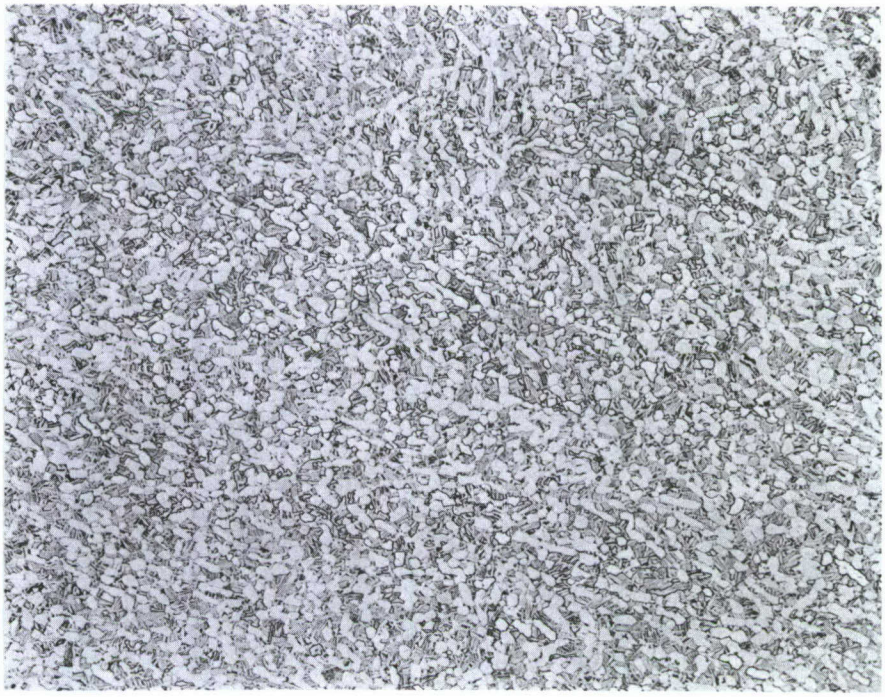

100X 9H327

Figure 35. Microstructure of Heat No. 14, As Etched

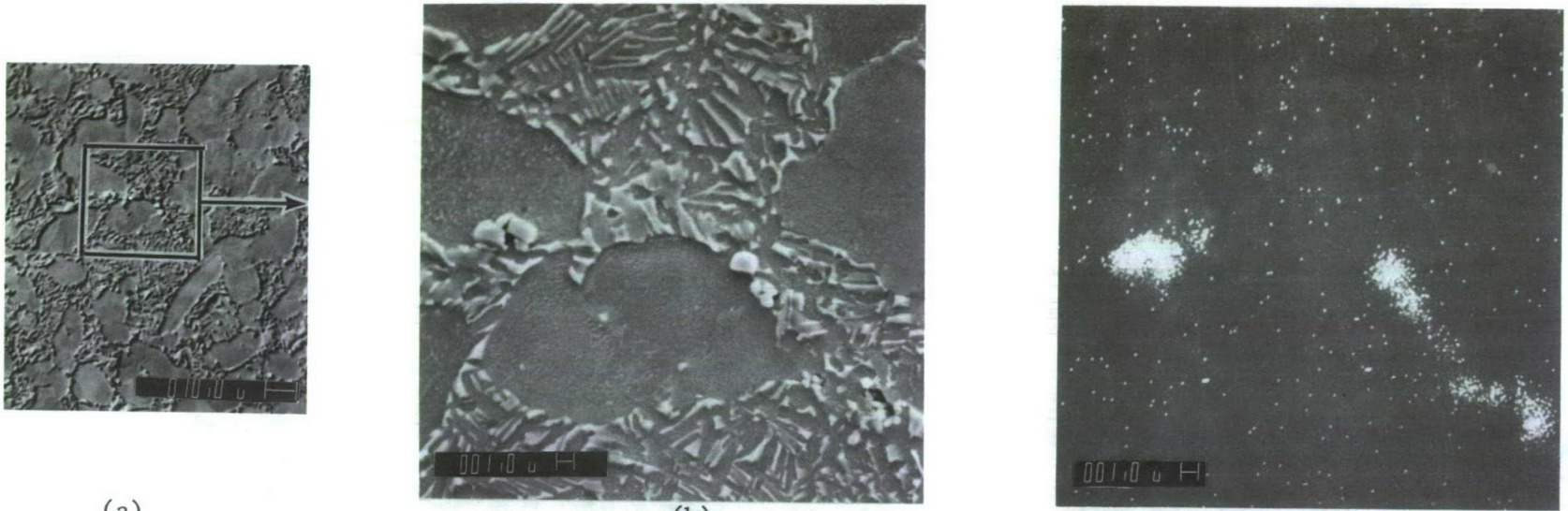

(a) (b) (c)

Figure 36. Microstructure of Pancake Forging No. 9: (a) Backscattered electron image, (b) Secondary electron image of a portion of (a) Showing 1-2 micron yttria particles at alpha grain boundaries and, (c) X-ray area scan of (b) Showing high yttrium concentrations

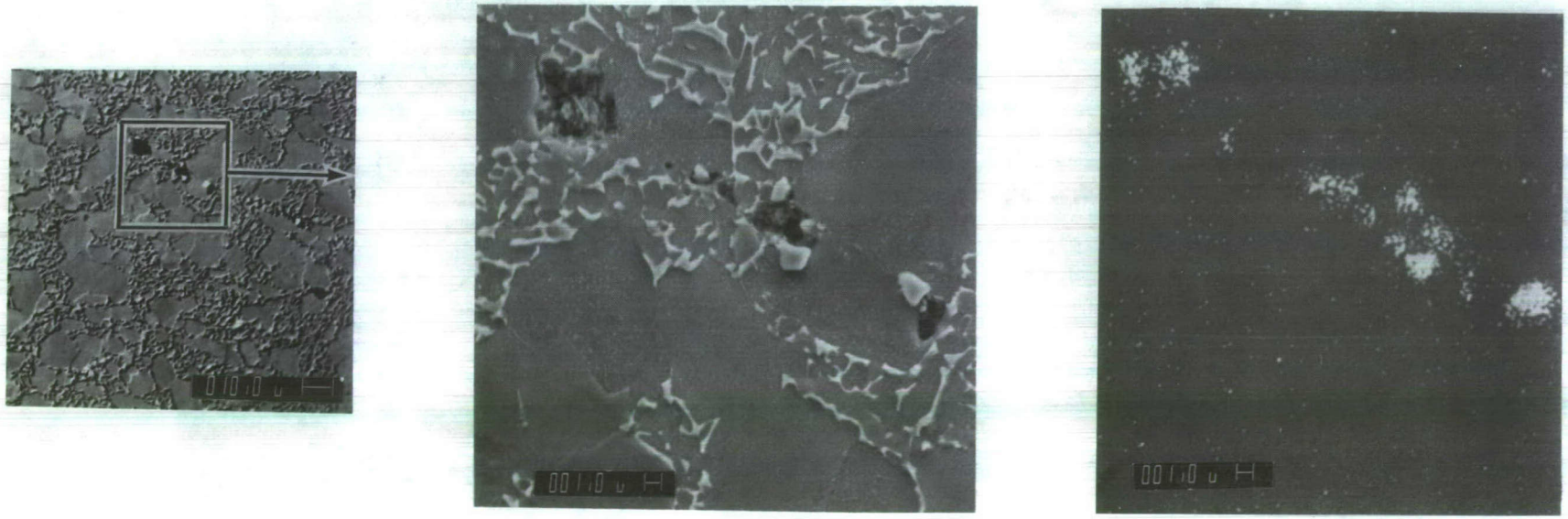

Figure 37. Microstructure of Pancake Forging No. 10. Same Sequence as Above

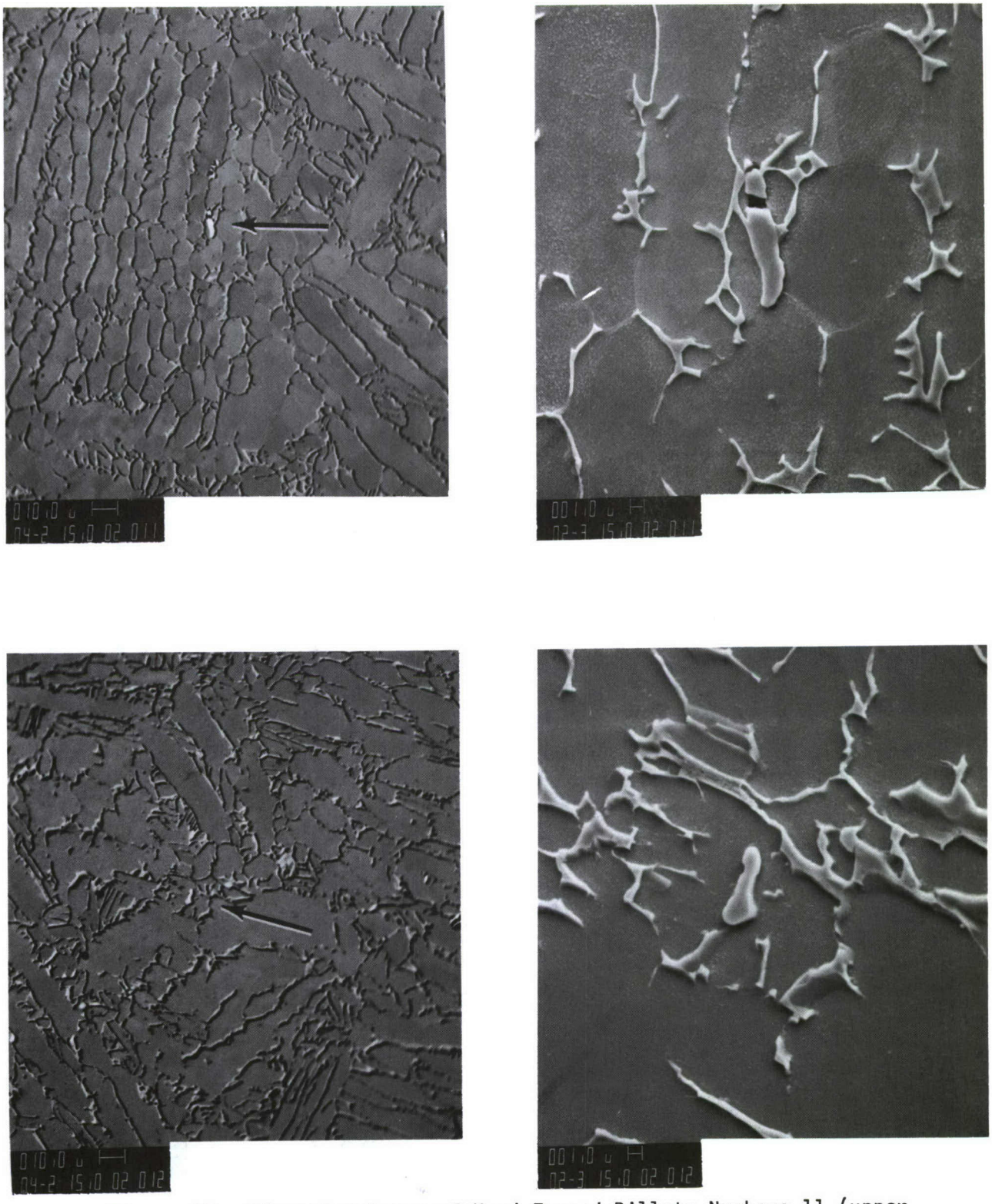

Figure 38. Microstructures of Hand Forged Billets Numbers 11 (upper micrographs) and 12 (lower micrographs). Backscattered electron images are on the left - note that yttria particles appear white due to fluorescence. Secondary electron micrographs of yttria particles are on the right.

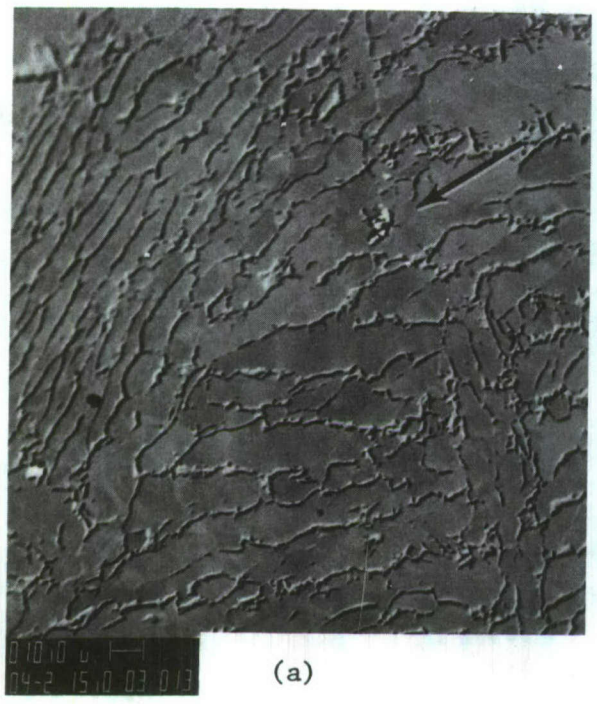

(a)

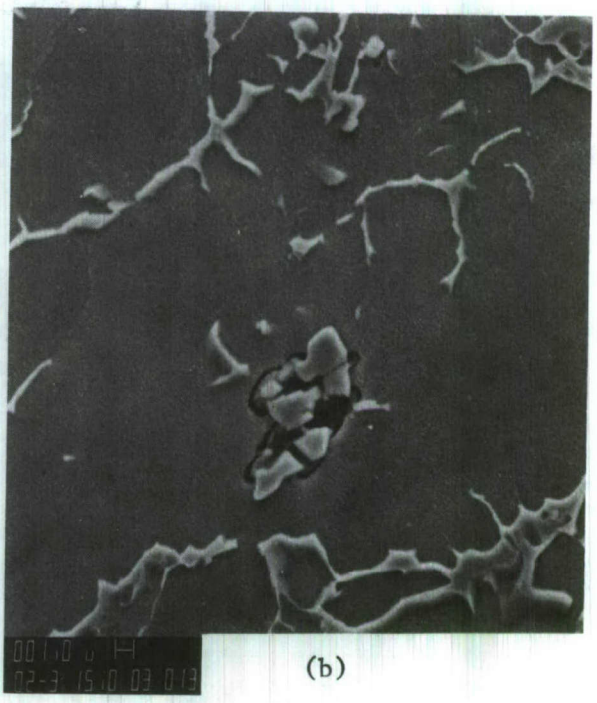

(b)

(c)

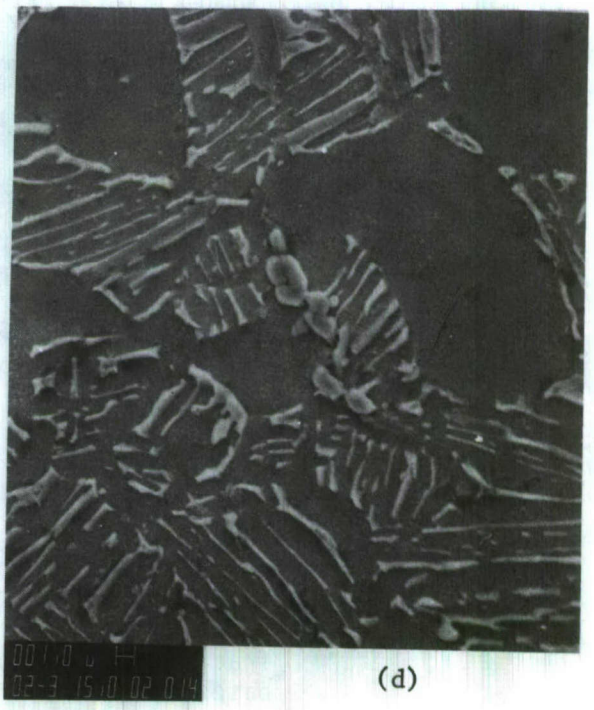

(d)

Figure 39. Microstructures of Hand Forged Billet No. 13, (a) and (b), and Die Forging No. 14, (c) and (d). Clusters of yttria particles are identified by arrows in the backscattered electron micrographs on the left and shown enlarged in the SEM's on the right.

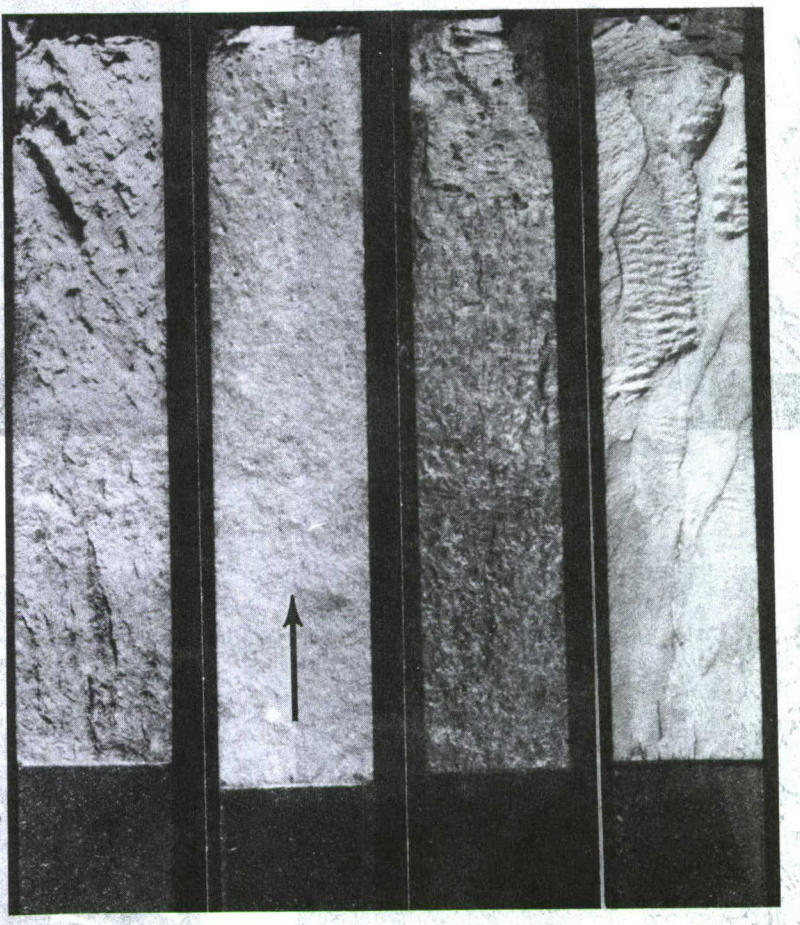

Figure 40. Fracture Surfaces of Crack Growth Rate Specimens from BCL/AFML Heat Numbers 1, 4, 9, and 14. The crack propagation direction is indicated by the arrow. Note the very large prior beta grains easily seen on the fracture surface of Specimen No. 1. (Non-yttriated baseline plate). "R" ratio = 0.1

(a)

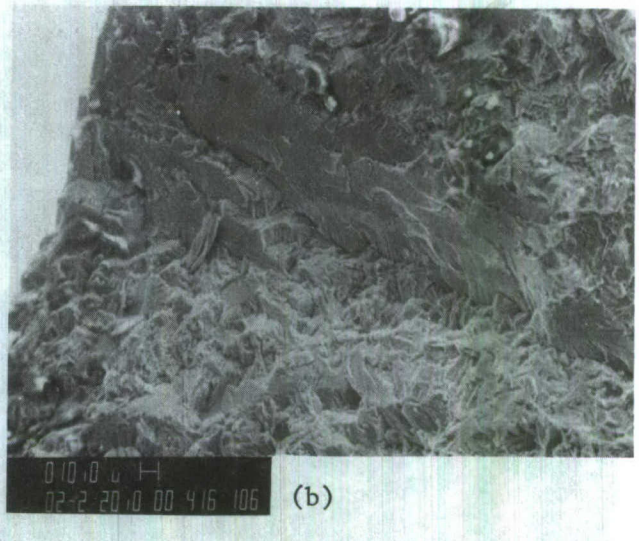

(b)

(c)

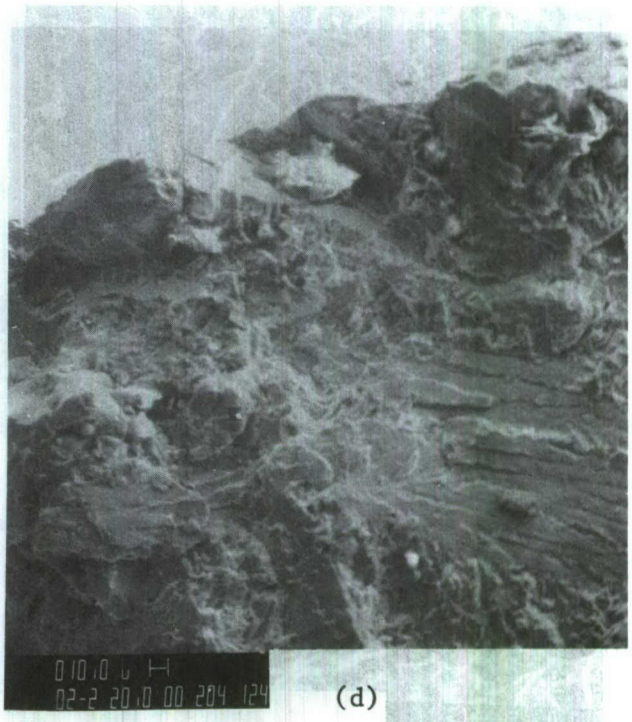

(d)

Figure 41. Scanning Electron Micrographs of the Fracture Initiation Regions of; (a) and (b) Fatigue Specimen 14-ST-16, and (c) and (d) Fatigue Specimen 12-L-4. No yttria particles were found at the multiple initiation sites; however, note the transgranular cleavage regions at each edge initiation site. The light particles are contaminants of external origin

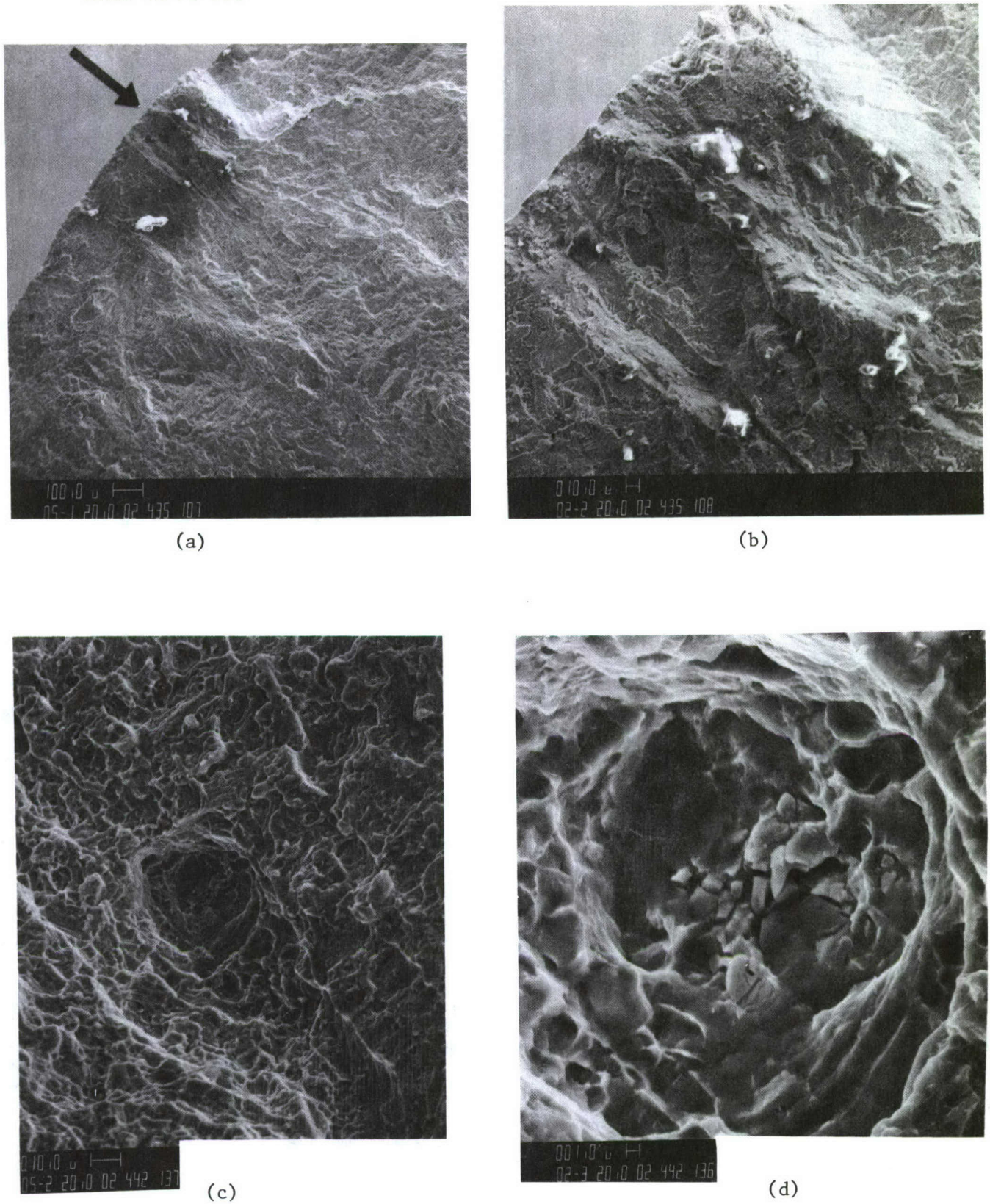

(a) (b)

(c) (d)

Figure 42. Scanning Electron Micrographs of the Fracture Surface of Fatigue Specimen 4-ST-35; (a) the fracture initiation region, (b) a higher magnification of (a) adjacent to the arrow, showing a lack of yttria particles (the light clumps and particles are contaminants), and (c) and (d) a region near the center of the specimen with yttria particles easily visible

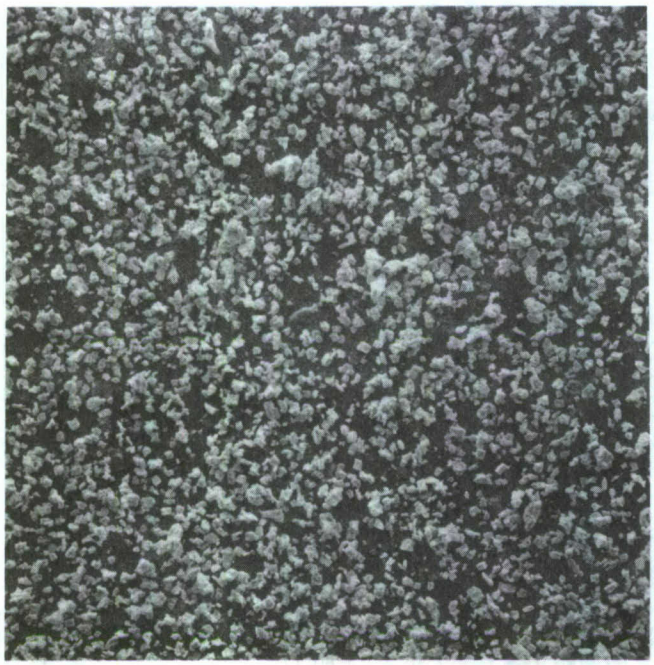

(a) 100X

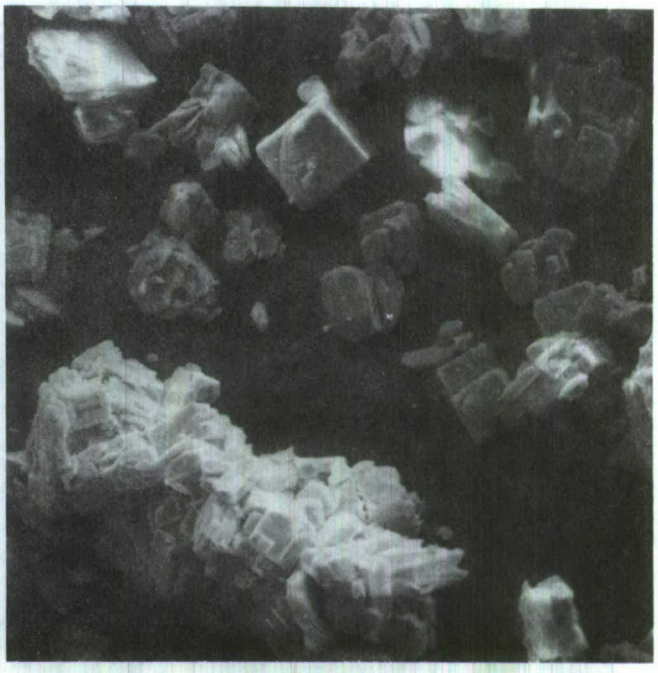

(b) 1000X

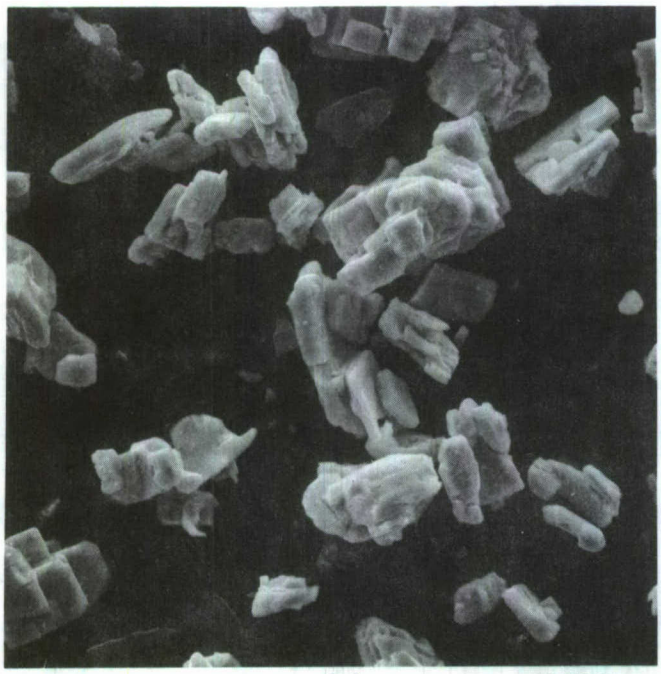

(c) 1000X

(d) 5000X

Figure 43. Scanning Electron Micrographs of the Starting Yttria Powders

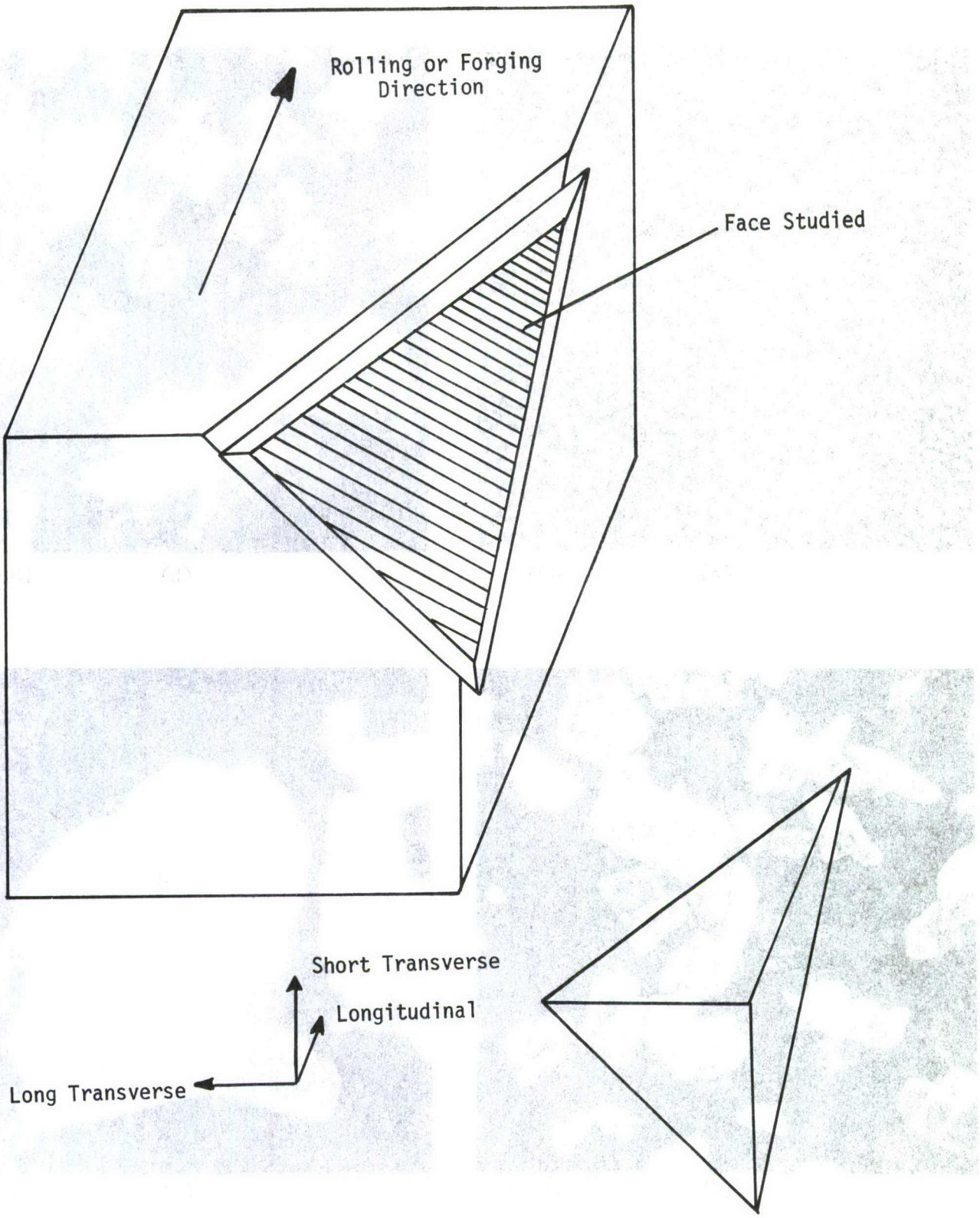

Figure 44. Illustration of the Oblique Plane Sample Cut Used for Pole Figure Determinations

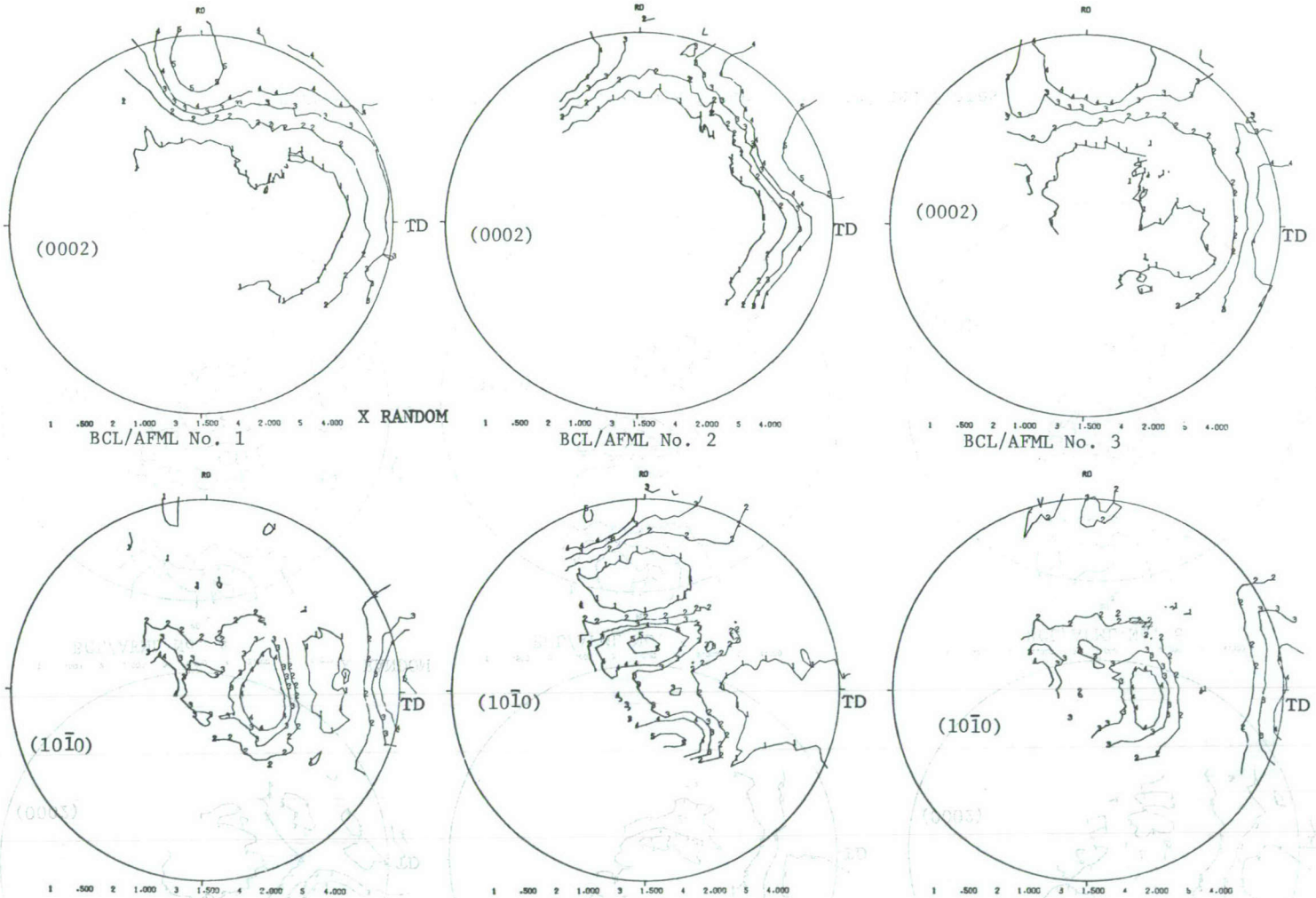

Figure 45. Basal and Prism Plane Pole Figures of Baseline Plates (Non-Yttriated)

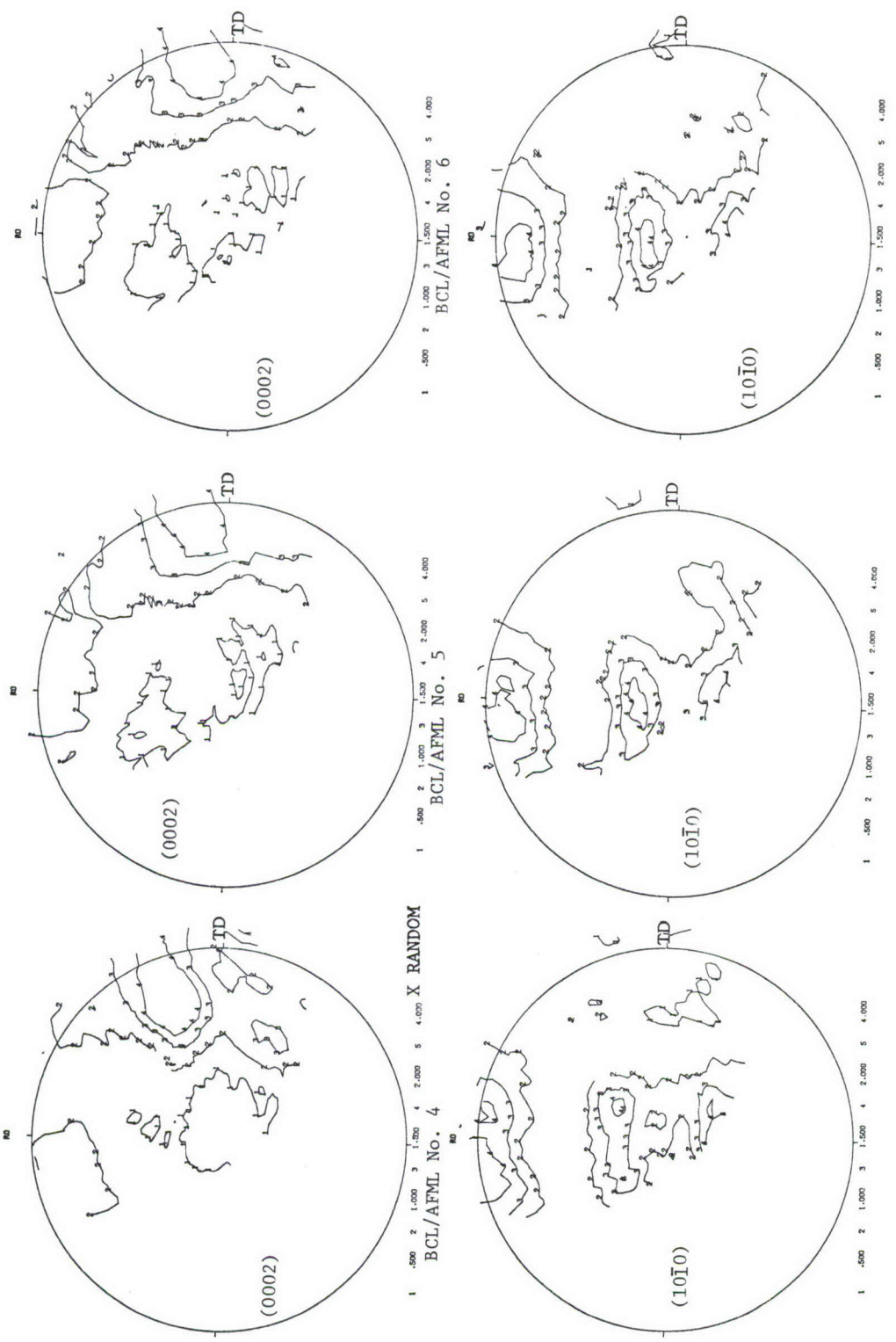

Figure 46. Basal and Prism Plane Pole Figures of Yttriated Plates

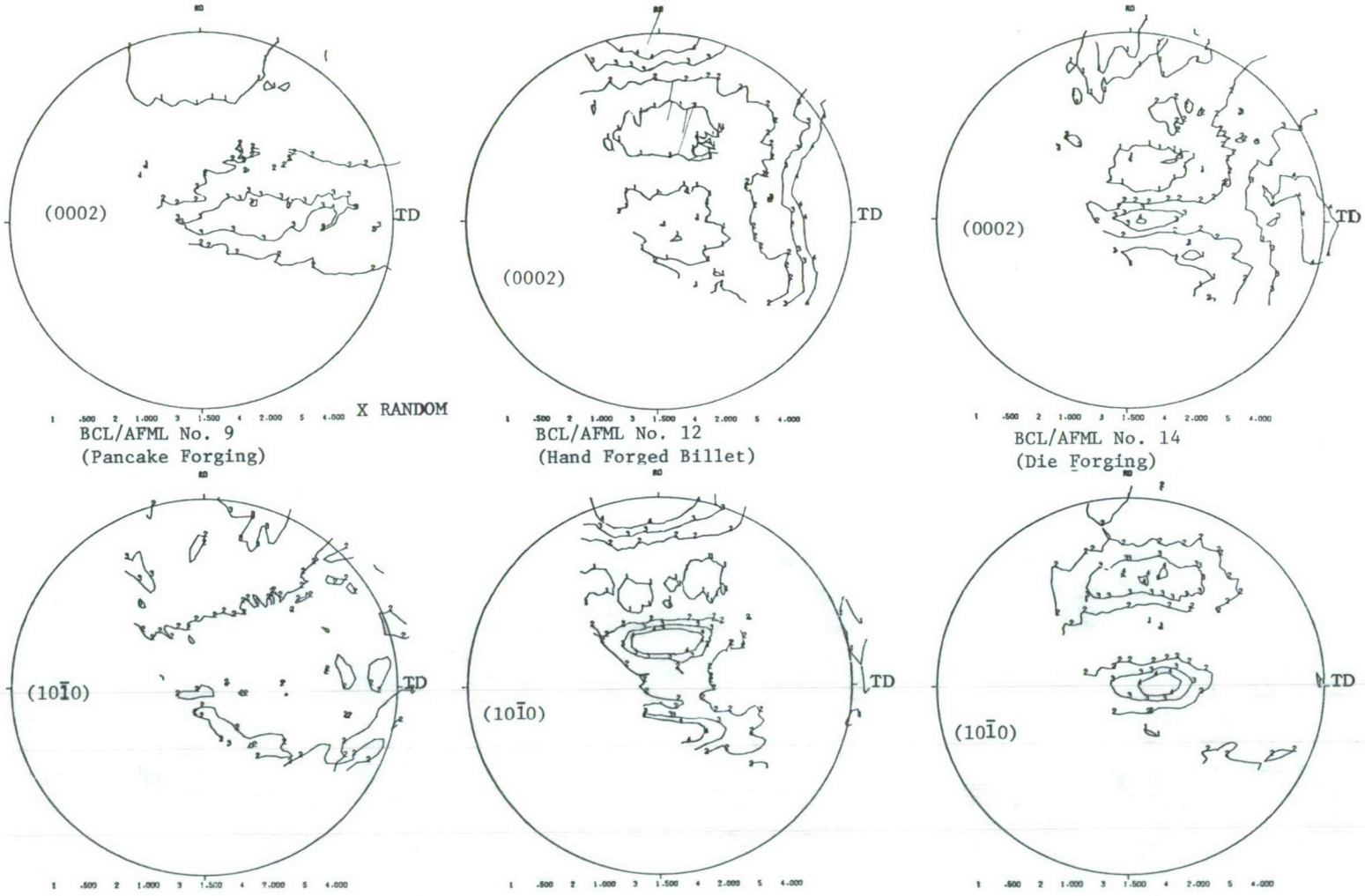

Figure 47. Basal and Prism Plane Pole Figures of Yttriated Forgings

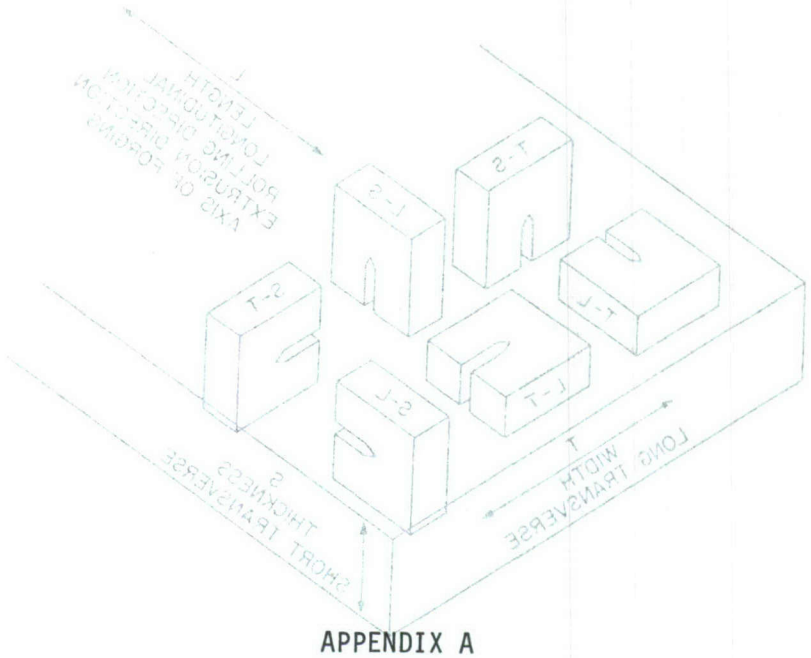

APPENDIX A

SPECIMEN DRAWINGS AND LAYOUTS

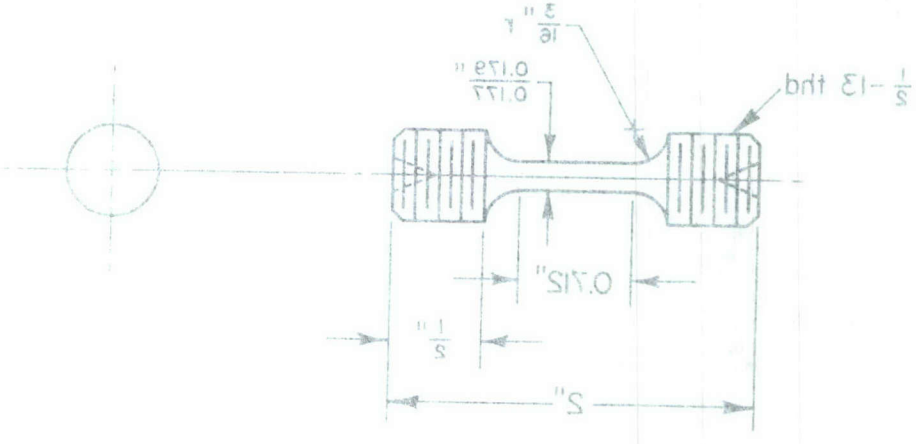

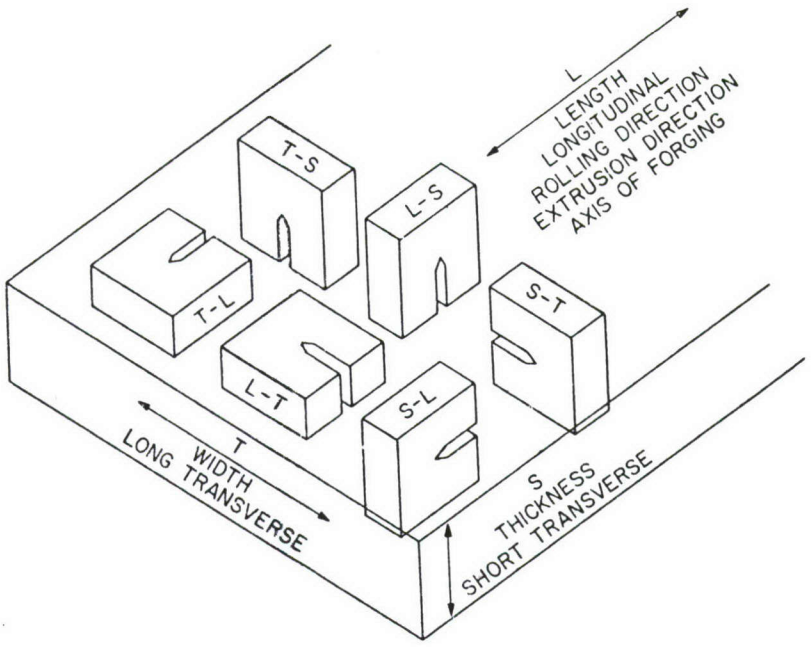

Figure 48. Standard Notations Used for Specimen Orientation

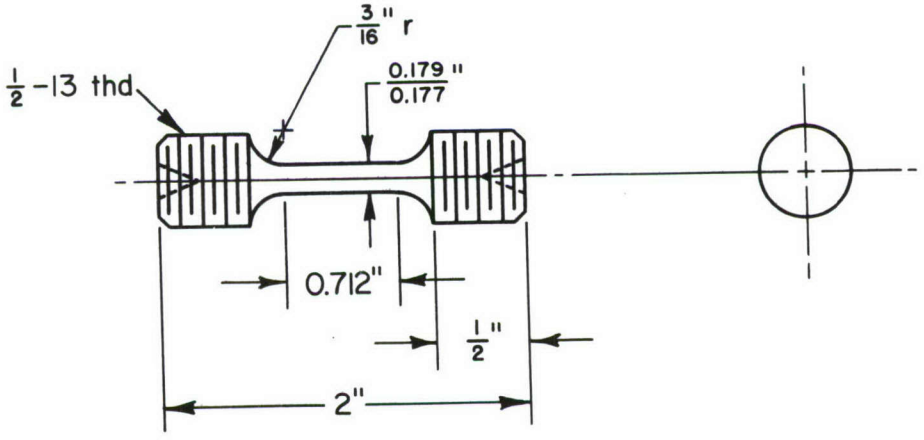

Figure 49. Tensile Specimen

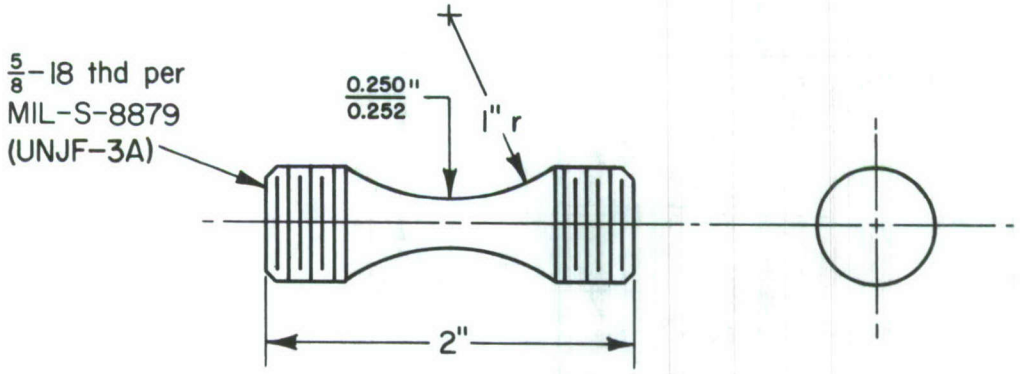

Figure 50. Unnotched Fatigue Specimen

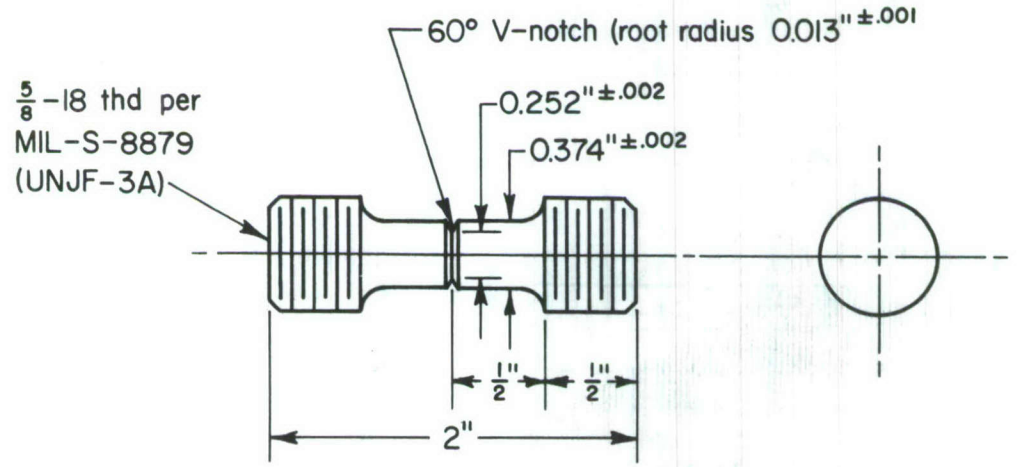

Figure 51. Notched (K_t = 3.0) Fatigue Specimen

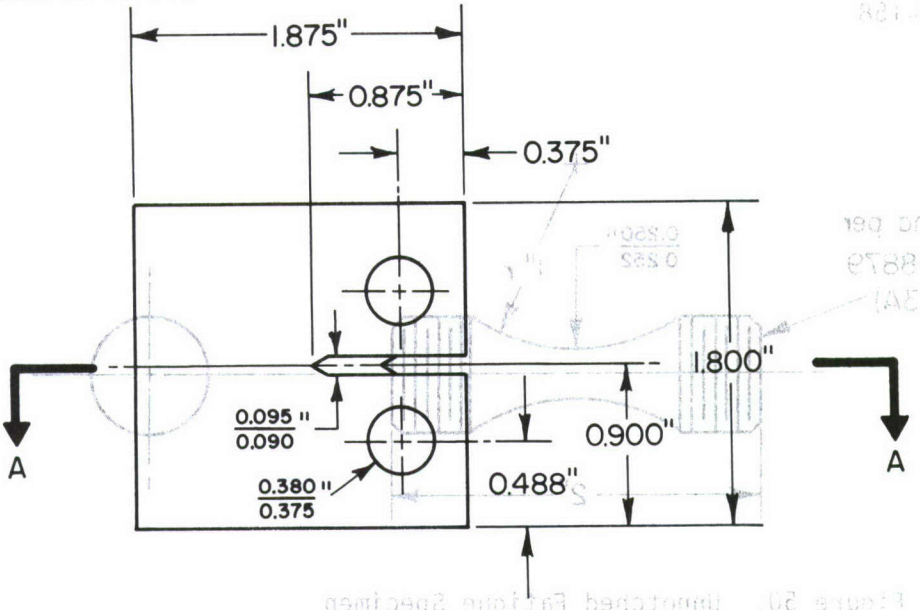

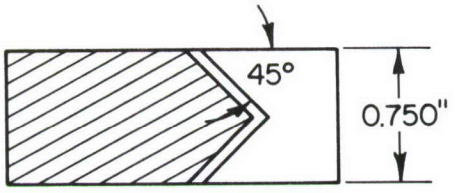

Section A–A

Figure 52. Fracture Toughness Specimen

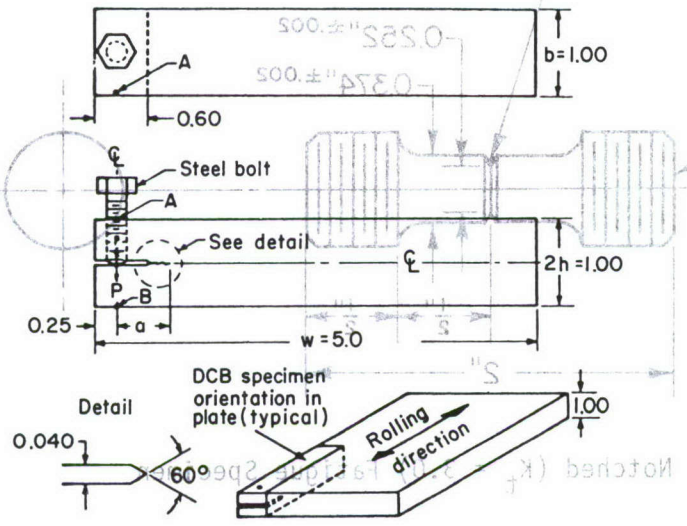

Crack opening displacement v equals the measured deflection between points A and B along the bolt centerline

Figure 53. Stress Corrosion Cracking Specimen

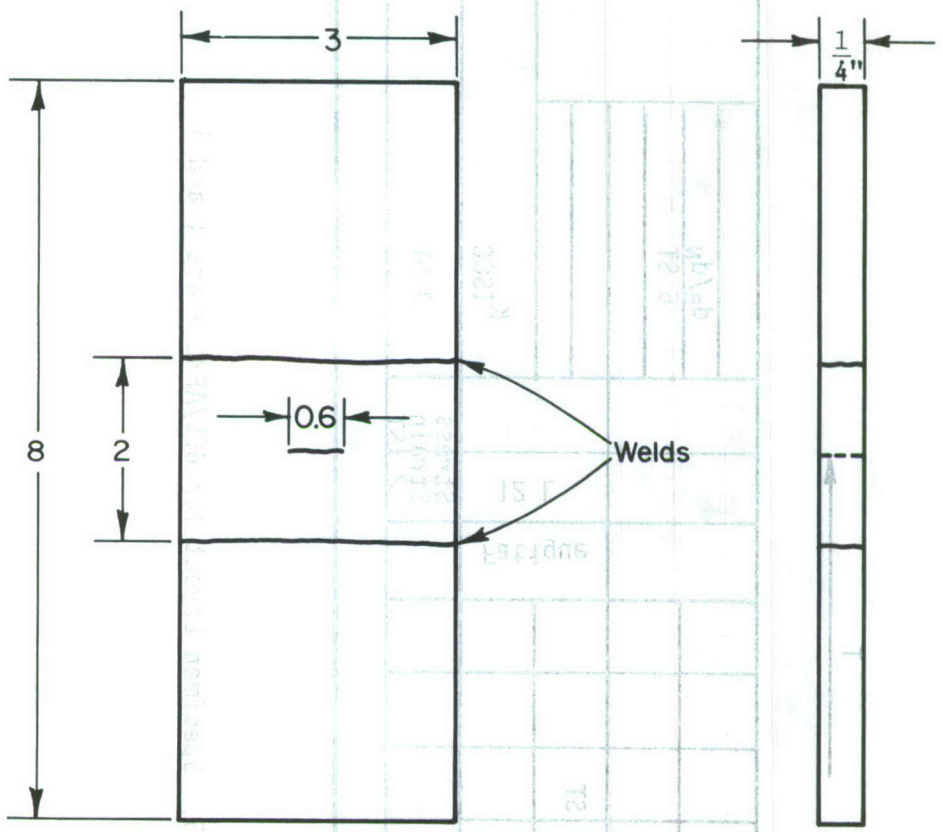

Note: Center through flaw,
0.010 x 0.6

Figure 54. Crack-Growth Specimen (All dimensions in inches)

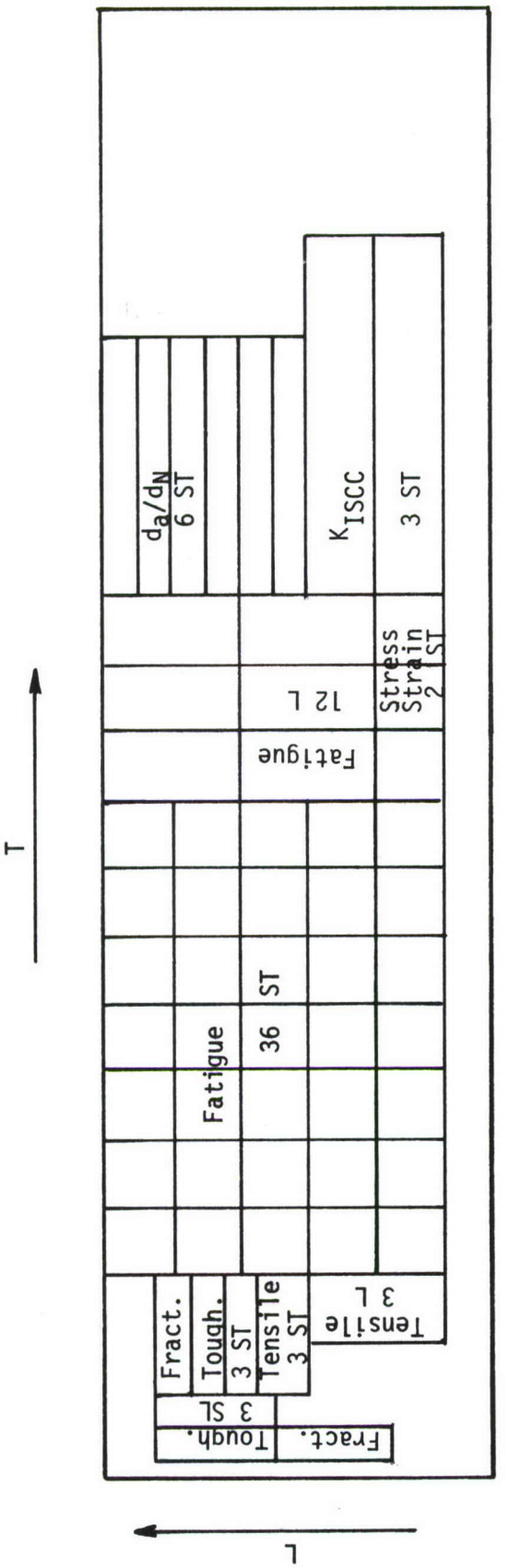

Figure 55. Specimen Layout for BCL/AFML Heats 1 and 4

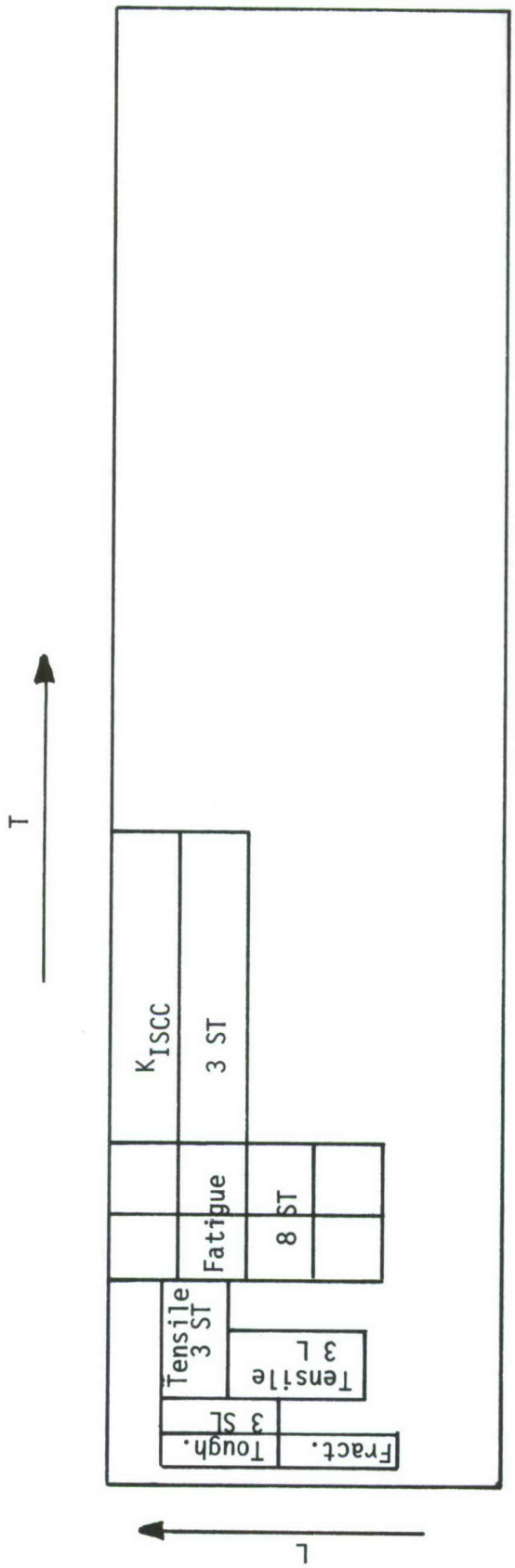

Figure 56. Specimen Layout for BCL/AFML Heats 2 and 5

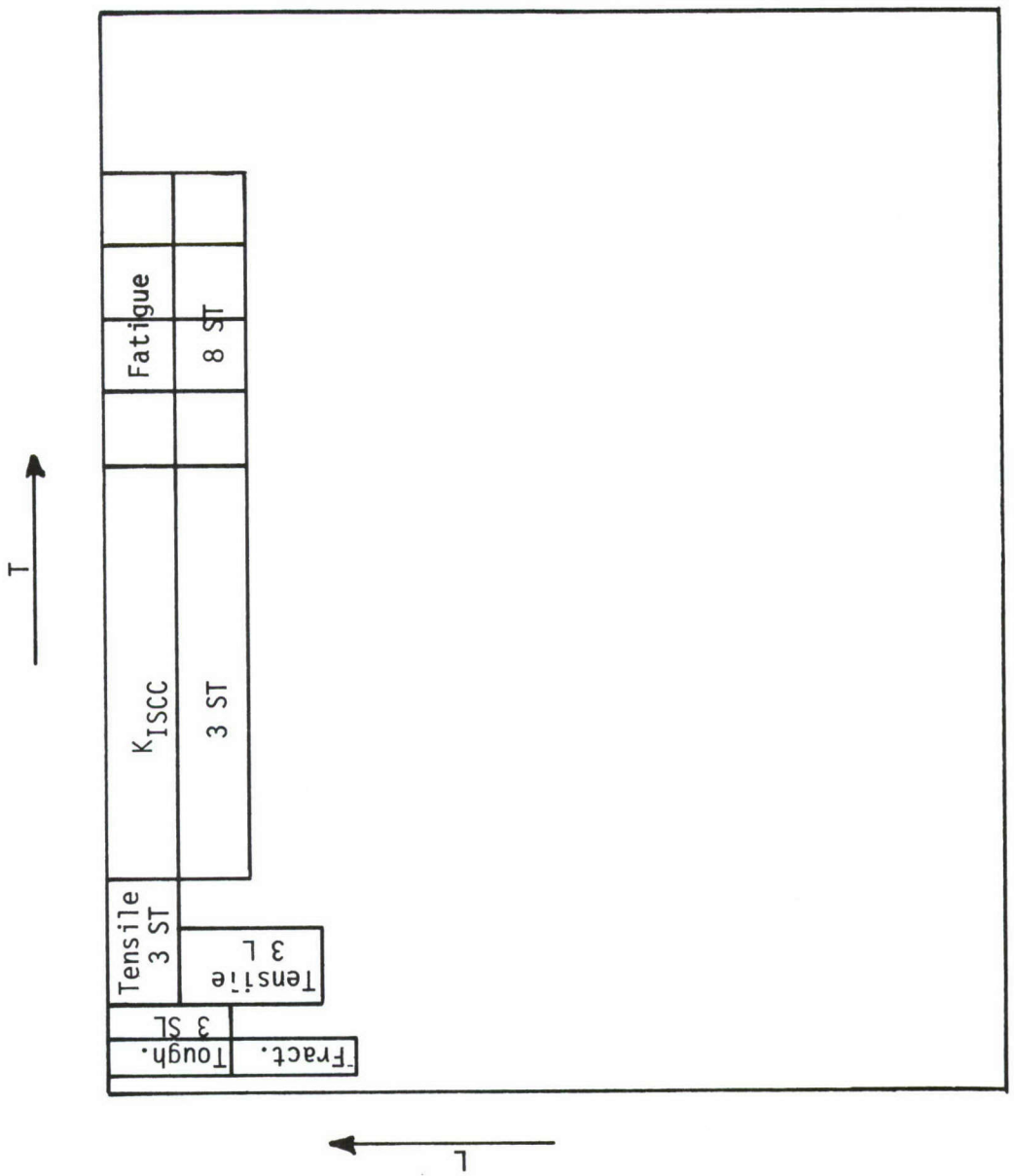

Figure 57. Specimen Layout for BCL/AFML Heat 3

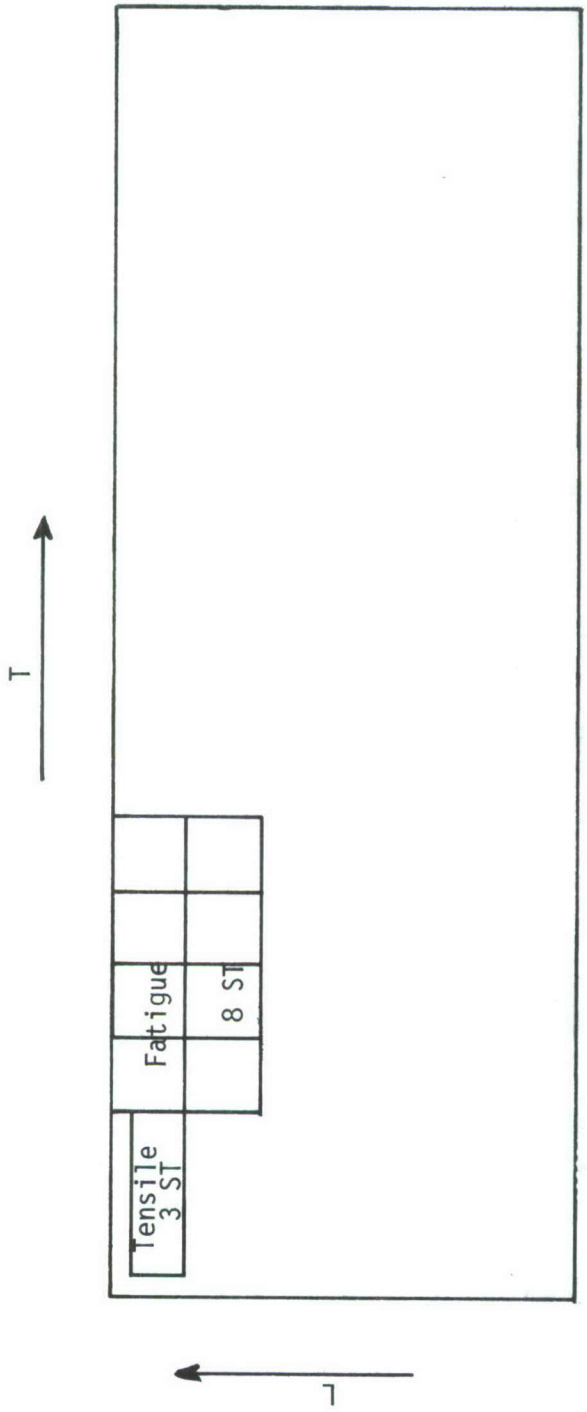

Figure 58. Specimen Layout for BCL/AFML Heats 6, 7, and 8

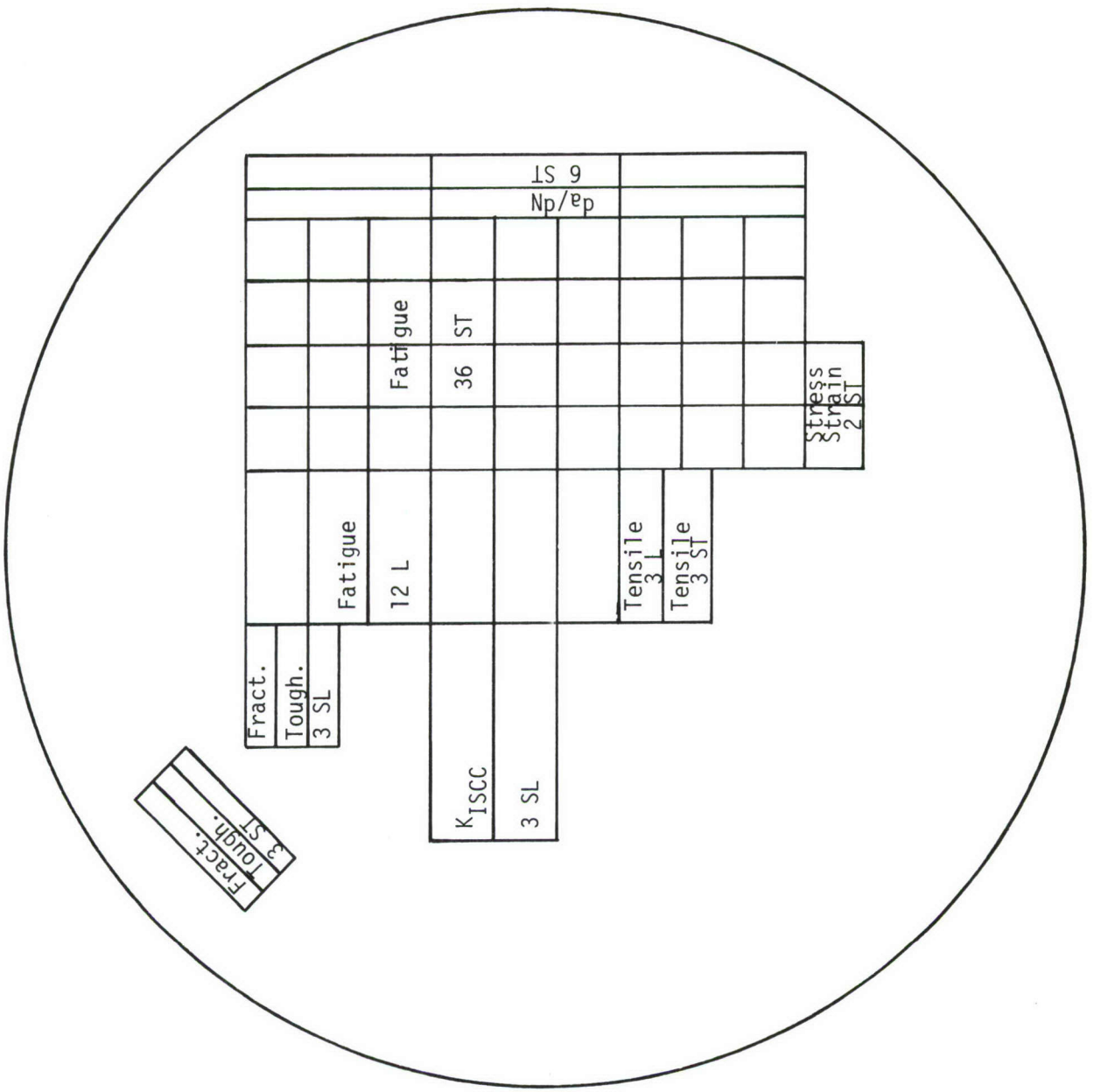

Figure 59. Specimen Layout for BCL/AFML Heat 9, Pancake Forging

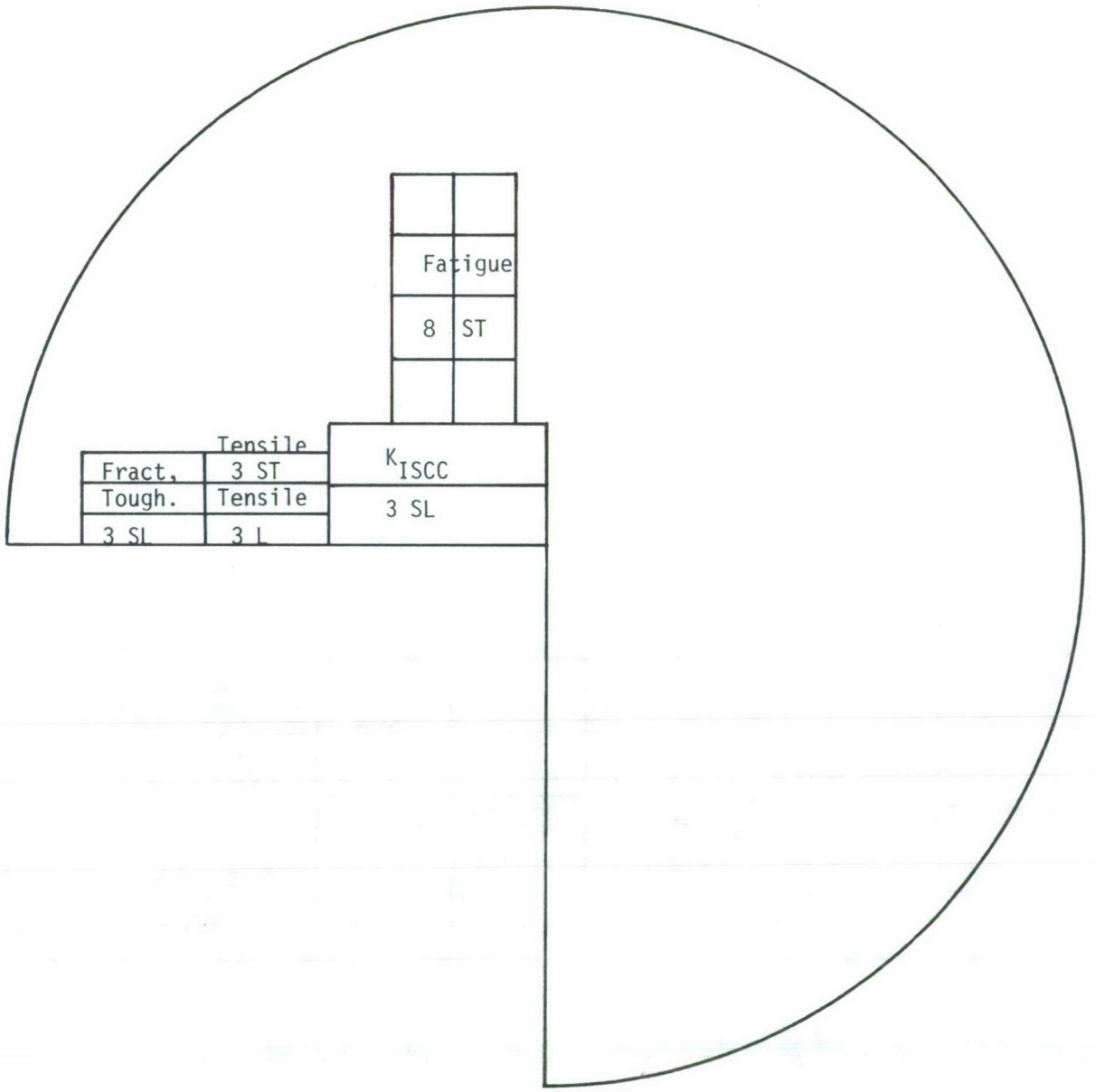

Figure 60. Specimen Layout for BCL/AFML Heat 10, Pancake Forging

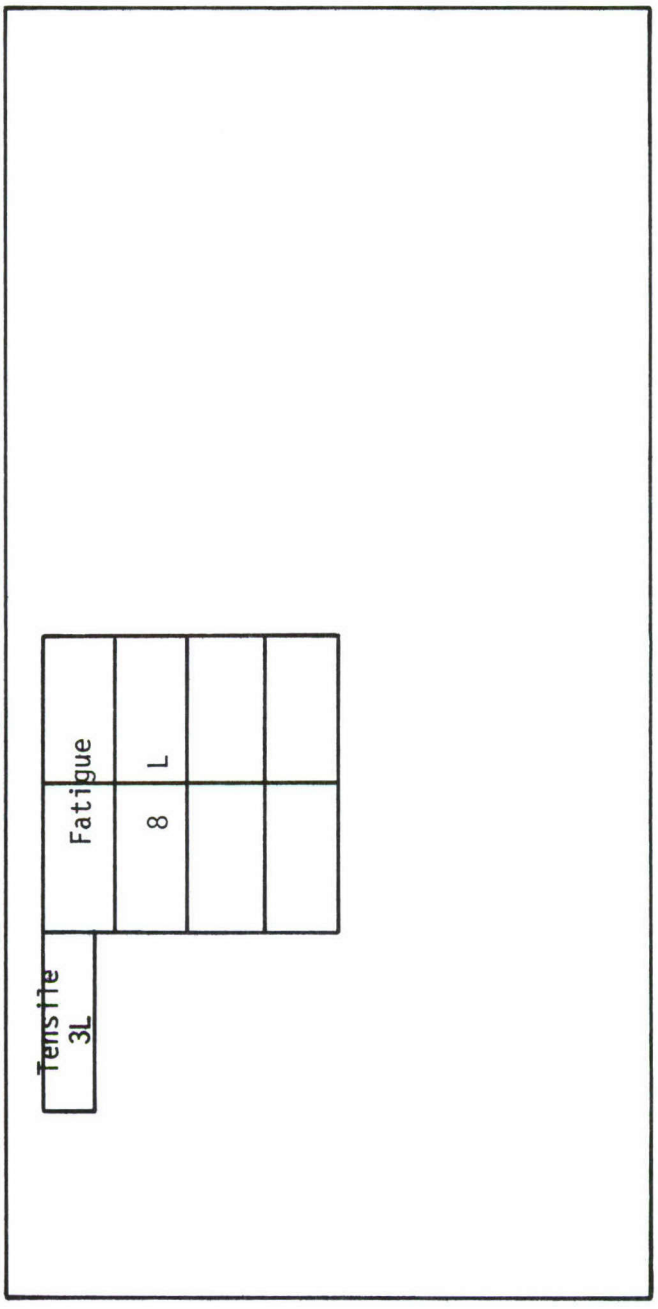

Figure 61. Specimen Layout for BCL/AFML Heats 11, 12 and 13

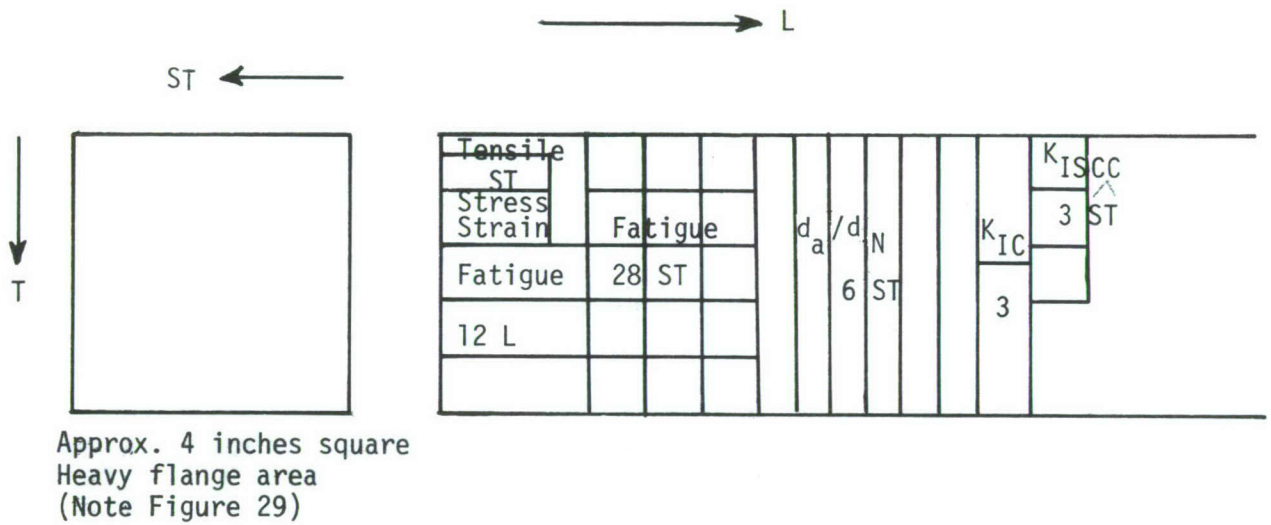

Figure 62. Specimen Layout for BCL/AFML Heat 14, Forging 61550

APPENDIX B

TABULATED MECHANICAL TEST RESULTS

TABLE 4

RESULTS OF TENSILE TESTS ON BASELINE HEATS OF ANNEALED Ti-6Al-4V PLATE

Heat Number	BCL Sequence Number	Specimen Number	Orientation	TUS, ksi	TYS, ksi	e, percent	RA, percent	E, 10^3 ksi
RMI 992141	1	1-1ST	ST	151.0	135.5	10.0	11.8	15.1
	1	1-2ST	ST	150.7	136.1	12.0	19.2	15.6
	1	1-3ST	ST	148.3	134.2	10.0	16.7	15.1
			Average	150.0	135.3	10.7	15.9	15.3
	1	1-4L	L	150.6	144.0	16.0	29.8	18.3
	1	1-5L	L	151.0	142.4	18.0	27.9	19.0
	1	1-6L	L	148.3	141.9	17.0	25.1	18.6
			Average	150.0	142.8	17.0	27.6	18.6
RMI 902099	2	2-72ST	ST	134.1	122.2	6.0	10.6	14.5
	2	2-73ST	ST	137.5	123.2	10.0	12.8	14.6
	2	2-74ST	ST	130.3	120.3	9.0	16.3	14.8
			Average	134.0	121.9	8.3	13.2	14.6
	2	2-75L	L	142.3	135.7	18.0	29.0	17.9
	2	2-76L	L	145.0	136.7	16.0	25.0	18.1
	2	2-77L	L	143.6	136.5	16.0	25.0	17.4
			Average	143.6	136.3	16.7	26.3	17.8
TIMET K-7787	3	3-95ST	ST	142.6	127.9	14.0	24.1	15.1
	3	3-96ST	ST	141.6	127.7	12.0	18.0	15.2
	3	3-97ST	ST	142.5	128.3	12.0	16.7	15.4
			Average	142.2	128.0	12.7	19.6	15.2
	3	3-92L	L	143.9	136.7	17.0	24.2	17.3
	3	3-93L	L	143.5	136.7	16.0	29.8	17.2
	3	3-94L	L	140.6	134.5	18.0	30.7	16.4
			Average	142.7	136.0	17.0	28.2	17.0

TABLE 5

RESULTS OF TENSILE TESTS ON ANNEALED Ti-6Al-4V PLATE (HEATS 4, 5, 6, 7, AND 8)

BCL Sequence Heat Number	Specimen Number	Orientation	TUS, ksi	TYS, ksi	e, percent	RA, percent	E, 10^3 ksi
4	4-1ST	ST	142.6	129.7	8.0	21.8	15.2
4	4-2ST	ST	143.1	130.1	10.0	24.7	14.9
4	4-3ST	ST	142.2	129.4	11.0	22.4	15.4
		Average	142.6	129.7	9.7	22.9	15.2
4	4-1L	L	138.3	130.2	18.0	38.1	15.8
4	4-2L	L	136.2	129.0	19.0	40.5	16.3
4	4-3L	L	138.3	131.4	17.0	38.9	16.0
		Average	137.6	130.2	18.0	39.2	16.0
5	5-1ST	ST	141.5	130.2	16.0	38.5	15.3
5	5-2ST	ST	142.2	130.1	16.0	37.4	15.5
5	5-3ST	ST	141.9	129.8	13.0	20.7	15.4
		Average	141.9	130.0	15.0	32.2	15.4
5	5-1L	L	138.6	131.7	20.0	41.9	15.9
5	5-2L	L	138.6	132.9	20.0	43.9	16.1
5	5-3L	L	141.3	133.7	19.0	41.1	16.4
		Average	139.5	132.8	19.7	42.3	16.1
6	6-1ST	ST	137.4	127.7	5.0	5.7	14.7
6	6-2ST	ST	139.9	128.5	12.0	25.1	14.9
6	6-3ST	ST	140.9	128.5	10.0	17.3	15.4
		Average	139.4	128.2	9.0	16.0	15.0
7	7-1ST	ST	141.0	128.9	15.0	34.7	15.2
7	7-2ST	ST	141.4	128.0	12.0	19.9	14.8
7	7-3ST	ST	141.0	128.5	8.0	23.0	15.0
		Average	141.1	128.5	11.7	25.9	15.0
8	8-1ST	ST	143.9	131.4	10.0	21.3	15.2
8	8-2ST	ST	144.4	131.4	14.0	28.3	14.9
8	8-3ST	ST	144.1	131.1	12.0	20.3	15.0
		Average	144.1	131.3	12.0	23.3	15.0

TABLE 6

RESULTS OF TENSILE TESTS ON ANNEALED Ti-6Al-4V FORGINGS (HEATS 9, 10, 11, 12, 13, AND 14)

BCL Sequence Heat Number	Specimen Number	Orientation	TUS, ksi	TYS, ksi	e, percent	RA, percent	E, 10^3 ksi
9	9-1ST	ST	145.9	128.9	15.0	33.5	15.5
9	9-2ST	ST	140.3	128.9	14.0	34.0	15.5
9	9-3ST	ST	139.5	128.5	14.0	29.7	15.4
		Average	141.9	128.8	14.3	32.4	15.5
9	9-4L	L	139.3	132.4	18.0	37.6	16.5
9	9-5L	L	141.3	133.9	18.0	34.4	17.1
9	9-6L	L	139.8	132.8	18.0	36.0	16.4
		Average	140.1	133.0	18.0	36.0	16.7
10	10-1ST	ST	141.7	129.0	12.0	18.4	15.8
10	10-2ST	ST	141.4	128.3	14.0	24.1	15.5
10	10-3ST	ST	140.8	128.1	15.0	25.8	15.8
		Average	141.3	128.5	13.7	22.8	15.7
10	10-4L	L	143.5	135.4	19.0	39.0	16.5
10	10-5L	L	142.0	133.9	18.0	44.3	16.4
10	10-6L	L	142.2	134.1	19.0	41.8	16.5
		Average	142.6	134.5	18.7	41.7	16.5
11	11-1L	L	136.4	126.1	14.0	23.9	16.5
11	11-2L	L	142.3	129.4	11.0	27.2	16.7
11	11-3L	L	139.3	126.3	14.0	16.9	16.4
		Average	139.3	127.3	13.0	22.7	16.5
12	12-1L	L	138.1	129.1	16.0	22.9	17.3
12	12-2L	L	138.5	129.5	17.0	27.2	16.7
12	12-3L	L	139.9	128.9	14.0	26.5	17.0
		Average	138.8	129.2	15.7	25.5	17.0
13	13-1L	L	140.7	131.7	15.0	28.1	17.5
13	13-2L	L	145.8	136.9	15.0	24.1	17.3
13	13-3L	L	144.9	137.6	14.0	24.9	17.2
		Average	143.8	135.4	14.6	25.7	17.3
14	14-1ST	ST	141.8	129.1	6.0	8.8	16.2
14	14-2ST	ST	140.5	128.7	7.0	8.7	16.2
14	14-3ST	ST	139.0	128.3	11.0	21.3	16.4
		Average	140.4	128.7	8.0	12.9	16.3

TABLE 7

FRACTURE TOUGHNESS TEST RESULTS FOR BASELINE AND SELECTED YTTRIA CONTAINING HEATS (COMPACT TENSION SPECIMENS)

Heat Number	Specimen Number	Orientation	P_{max}, lb	P_Q, lb	W, in.	a, in.	B, in.	K_Q, ksi$\sqrt{in.}$
1	1-7ST	S-T	7350	6700	1.5	.7635	.75	72.6(a)
1	1-8ST	S-T	5600	5425	1.5	.7549	.75	57.8
1	1-9ST	S-T	7600	7100	1.5	.7688	.75	77.8(a)
1	1-10SL	S-L	5500	5200	1.5	.7804	.75	58.4
1	1-11SL	S-L	5300	4900	1.5	.7863	.75	55.7
1	1-12SL	S-L	5220	5000	1.5	.7771	.75	55.8
2	2-78SL	S-L	8100	7200	1.5	.7671	.75	78.6(a)
2	2-79SL	S-L	7740	6550	1.5	.7666	.75	71.5(a)
2	2-80SL	S-L	7200	6750	1.5	.7751	.75	74.9(a)
3	3-98SL	S-L	7000	6400	1.5	.7690	.75	70.2
3	3-99SL	S-L	6000	5600	1.5	.7671	.75	61.2
3	3-100SL	S-L	6800	6350	1.5	.7673	.75	69.4
4	4-1ST	S-T	5200	4700	1.5	.7781	.75	52.5
4	4-2ST	S-T	5100	4675	1.5	.7981	.75	54.5
4	4-3ST	S-T	5000	4800	1.5	.8206	.75	58.9
4	4-1SL	S-L	6650	6500	1.5	.7536	.75	69.1
4	4-2SL	S-L	5800	5600	1.5	.7875	.75	63.9
4	4-3SL	S-L	6275	5950	1.5	.7574	.75	63.7
5	5-1SL	S-L	5900	5700	1.5	.7590	.75	61.2
5	5-2SL	S-L	5650	5450	1.5	.7813	.75	61.3
9	9-10ST	S-T	5675	5350	1.5	.7139	.75	52.4
9	9-11ST	S-T	5525	5450	1.5	.7301	.75	54.6
9	9-12ST	S-T	6100	5920	1.5	.7139	.75	57.6
9	9-7SL	S-L	5900	5500	1.5	.7126	.75	50.0
9	9-8SL	S-L	5950	5720	1.5	.7120	.75	55.6
9	9-9SL	S-L	5820	5700	1.5	.7031	.75	61.8
10	10-7SL	S-L	5900	5650	1.5	.7277	.75	56.5
10	10-8SL	S-L	5100	4950	1.5	.8029	.75	57.7
10	10-9SL	S-L	6300	6100	1.5	.7060	.75	58.5
14	14-6SL	S-L	6500	6350	1.5	.7150	.75	61.9
14	14-7SL	S-L	6940	6940	1.5	.6986	.75	65.7
14	14-8SL	S-L	6550	6200	1.5	.7172	.75	60.7

(a) Invalid per E-399.

TABLE 8

RESULTS OF AXIAL LOAD FATIGUE TESTS FOR UNNOTCHED SHORT TRANSVERSE SPECIMENS AT A RATIO OF R = 0.1 FOR HEATS 1, 2, AND 3

Specimen Number	Maximum Stress, ksi	Cycles to Failure
	Heat 1	
1-30ST	140	15,600
1-33ST	130	30,200
1-28ST	120	38,600
1-34ST	110	76,500
1-36ST	100	675,600
1-71ST	100	525,000
1-29ST	100	108,200
1-37ST	90	1,327,900
1-39ST	90	828,000
1-70ST	90	1,373,000
1-38ST	80	3,112,400
1-31ST	80	1,875,300
1-32ST	70	10,000,000(a)
	Heat 2	
2-89ST	100	250,000
2-88ST	90	684,000
2-90ST	80	550,200
2-91ST	70	7,220,200
	Heat 3	
3-111ST	100	202,700
3-112ST	90	369,300
3-113ST	80	276,500
3-114ST	70	3,059,600

(a) Did not fail.

TABLE 9

RESULTS OF AXIAL LOAD FATIGUE TESTS FOR UNNOTCHED SHORT TRANSVERSE SPECIMENS AT A RATIO OF R = -0.25 FOR HEATS 1, 2, AND 3

Specimen Number	Maximum Stress, ksi	Cycles to Failure
	Heat 1	
1-19ST	140	4,600
1-20ST	130	10,200
1-21ST	120	16,500
1-24ST	110	24,300
1-23ST	100	116,900
1-18ST	100	257,000
1-22ST	85	1,064,500
1-27ST	80	401,300
1-17ST	60	4,149,400
1-40ST	55	10,000,000(a)
1-16ST	40	10,000,000(a)
	Heat 2	
2-84ST	100	179,800
2-85ST	80	4,031,300
2-86ST	70	961,700
2-87ST	60	10,481,400(a)
	Heat 3	
3-107ST	100	222,300
3-110ST	90	1,618,100
3-108ST	80	2,308,300
3-109ST	70	2,454,600

(a) Did not fail.

TABLE 10

RESULTS OF AXIAL LOAD FATIGUE TESTS FOR UNNOTCHED LONGITUDINAL SPECIMENS AT A RATIO OF R = -0.25 FOR HEAT 1

Specimen Number	Maximum Stress, ksi	Cycles to Failure
1-53L	150	7,600
1-52L	130	22,400
1-58L	120	166,700
1-59L	110	446,500
1-54L	110	386,100
1-57L	100	338,200
1-60L	100	315,600
1-61L	90	1,088,500
1-56L	90	941,100
1-55L	80	1,568,400 *
1-62L	70	1,397,900
1-63L	60	1,030,400
1-40L	55	10,000,000(a)

TABLE 11

RESULTS OF AXIAL LOAD FATIGUE TESTS FOR NOTCHED (K_t=3.0) SHORT TRANSVERSE SPECIMENS AT A RATIO OF R = 0.1 FOR HEAT 1

Specimen Number	Maximum Stress, ksi	Cycles to Failure
1-40ST	70	10,540
1-41ST	60	23,370
1-42ST	40	706,500
1-43ST	35	179,600
1-48ST	30	1,900,500
1-49ST	25	10,000,000(a)

(a) Did not fail.

* Thread Failure

TABLE 12

RESULTS OF AXIAL LOAD FATIGUE TESTS FOR NOTCHED (K_t=3.0) SHORT TRANSVERSE SPECIMENS AT A RATIO OF R = -0.25 FOR HEAT 1

Specimen Number	Maximum Stress, ksi	Cycles to Failure
1-44ST	60	7,000
1-47ST	50	14,700
1-45ST	40	72,200
1-46ST	30	308,000
1-51ST	25	996,400
1-50ST	20	1,710,200

TABLE 13

RESULTS OF AXIAL LOAD FATIGUE TESTS FOR UNNOTCHED SHORT TRANSVERSE SPECIMENS AT A RATIO OF R = 0.1 FOR HEATS 4, 5, 6, 7, and 8

Specimen Number	Maximum Stress, ksi	Cycles to Failure
	Heat 4	
4-32ST	120	8,400
4-29ST	110	17,500
4-28ST	100	24,300
4-33ST	90	40,100
4-30ST	80	92,500
4-31ST	70	895,700
4-37ST	70	617,400
4-34ST	60	2,732,200
4-38ST	60	1,250,800
4-35ST	55	851,000
4-39ST	55	3,163,300
4-36ST	50	10,000,000(a)
	Heat 5	
5-10ST	80	371,600
5-9ST	70	2,445,700
5-11ST	70	601,200
5-8ST	60	8,875,300
	Heat 6	
6-9ST	80	104,600
6-11ST	75	159,300
6-10ST	75	1,539,300
6-8ST	70	11,566,700(a)
	Heat 7	
7-8ST	80	123,700
7-18ST	70	3,630,600
7-11ST	70	422,600
7-9ST	60	10,000,000(a)
	Heat 8	
8-8ST	80	124,100
8-11ST	70	1,458,600
8-9ST	70	2,215,700
8-10ST	65	10,000,000(a)

(a) Did not fail.

TABLE 14

RESULTS OF AXIAL LOAD FATIGUE TESTS FOR UNNOTCHED SHORT TRANSVERSE SPECIMENS AT A RATIO OF R = -0.25 FOR HEATS 4, 5, 6, 7, AND 8

Specimen Number	Maximum Stress, ksi	Cycles to Failure
	Heat 4	
4-16ST	100	21,500
4-22ST	90	21,200
4-17ST	80	83,400
4-25ST	75	48,300
4-26ST	70	249,000
4-18ST	70	136,700
4-21ST	65	63,500
4-23ST	65	1,193,000
4-19ST	60	1,018,000
4-24ST	60	486,800
4-27ST	55	3,641,000
4-20ST	50	10,000,000(a)
	Heat 5	
5-6ST	90	37,700
5-7ST	80	1,390,300
5-5ST	70	10,600,000(a)
5-4ST	60	16,536,000(a)
	Heat 6	
6-5ST	75	49,870
6-4ST	70	181,970
6-7ST	70	12,198,300(a)
6-6ST	65	10,696,600(a)
	Heat 7	
7-5ST	75	28,300
7-7ST	70	95,600
7-4ST	70	246,000
7-6ST	65	15,772,700
	Heat 8	
8-5ST	75	160,810
8-4ST	70	594,650
8-6ST	65	1,818,200
8-7ST	60	4,557,400

(a) Did not fail.

TABLE 15

RESULTS OF AXIAL LOAD FATIGUE TESTS FOR UNNOTCHED LONGITUDINAL SPECIMENS AT A RATIO OF R = -0.25 FOR HEAT 4

Specimen Number	Maximum Stress, ksi	Cycles to Failure
4-3L	130	14,800
4-12L	120	20,700
4-10L	110	49,400
4-8L	100	74,300
4-7L	90	50,400
4-11L	90	463,000
4-5L	80	544,300
4-1L	70	1,464,300
4-4L	70	2,130,000
4-2L	60	4,963,700
4-6L	55	13,740,000(a)

(a) Did not fail.

TABLE 16

RESULTS OF AXIAL LOAD FATIGUE TESTS FOR NOTCHED (K_t = 3.0) SHORT TRANSVERSE SPECIMENS AT A RATIO OF R = 0.1 FOR HEAT 4

Specimen Number	Maximum Stress, ksi	Cycles to Failure
4-11ST	45	25,000
4-14ST	35	121,200
4-12ST	30	314,900
4-13ST	25	835,400
4-4ST	20	1,965,100
4-15ST	15	4,933,800

TABLE 17

RESULTS OF AXIAL LOAD FATIGUE TESTS FOR NOTCHED (K_t = 3.0) SHORT TRANSVERSE SPECIMENS AT A RATIO OF R = -0.25 FOR HEAT 4

Specimen Number	Maximum Stress, ksi	Cycles to Failure
4-10ST	50	27,700
4-6ST	40	35,310
4-7ST	35	177,800
4-9ST	30	408,800
4-5ST	25	1,850,990
4-8ST	20	11,623,000[a]

(a) Did not fail.

TABLE 18

RESULTS OF AXIAL LOAD FATIGUE TESTS FOR UNNOTCHED SPECIMENS AT A STRESS RATIO OF R = 0.1 FOR HEATS 9, 10, 11, 12, AND 13

Specimen Number	Maximum Stress, ksi	Cycles to Failure
	Heat 9	
9-32ST	140	9,600
9-16ST	130	17,000
9-18ST	120	40,300
9-26ST	110	76,300
9-24ST	100	101,600
9-19ST	90	122,100
9-25ST	90	72,400
9-17ST	85	2,209,000
9-37ST	85	1,029,500
9-20ST	80	2,015,600
9-28ST	75	6,163,600
9-30ST	70	9,353,600
	Heat 10	
10-15ST	110	53,600
10-14ST	100	498,100
10-13ST	90	3,484,400
10-19ST	85	3,698,400
	Heat 11	
11-6L	90	125,400
11-11L	80	213,600
11-7L	60	1,452,600
11-10L	55	1,758,000
	Heat 12	
12-11L	80	150,400
12-5L	70	721,600
12-6L	60	795,500
12-8L	55	1,298,100
	Heat 13	
13-5L	90	172,000
13-4L	80	333,300
13-7L	70	360,600
13-10L	60	2,083,400

TABLE 19

RESULTS OF AXIAL LOAD FATIGUE TESTS FOR UNNOTCHED SPECIMENS AT A STRESS RATIO OF R = -0.25 FOR HEATS 9, 10, 11, 12, AND 13

Specimen Number	Maximum Stress, ksi	Cycles to Failure
	Heat 9	
9-23ST	120	11,000
9-39ST	110	20,200
9-27ST	100	31,100
9-34ST	95	39,000
9-33ST	90	48,400
9-35ST	85	78,000
9-29ST	80	125,400
9-36ST	75	876,800 (a)
9-38ST	75	746,500 (a)
9-22ST	75	2,372,900 (a)
9-31ST	75	7,590,800
9-21ST	70	16,540,300 (b)
	Heat 10	
10-17ST	90	96,720
10-18ST	80	164,090
10-20ST	80	826,800 (a)
10-16ST	70	10,000,000 (b)
	Heat 11	
11-4L	75	319,500
11-5L	70	393,600
11-8L	60	1,005,100
11-9L	50	2,915,000
	Heat 12	
12-10L	80	54,000
12-9L	60	101,000
12-4L	40	1,452,400
12-7L	30	10,000,000 (b)
	Heat 13	
13-6L	90	41,070
13-8L	80	342,760
13-9L	70	654,520
13-1L	60	1,748,900

(a) Failed in grip.

(b) Did not fail.

TABLE 20

RESULTS OF AXIAL LOAD FATIGUE TESTS FOR UNNOTCHED LONGITUDINAL SPECIMENS AT A STRESS RATIO OF R = -0.25 FOR HEAT 9

Specimen Number	Maximum Stress, ksi	Cycles to Failure
9-56L	120	37,490
9-60L	110	607,660
9-63L	110	247,000
9-54L	100	584,170
9-57L	100	620,970
9-58L	90	1,868,670
9-53L	90	650,590
9-62L	80	848,420
9-61L	80	4,860,270
9-59L	70	1,622,600
9-55L	70	6,618,860
9-52L	60	16,636,500(a)

(a) Did not fail.

TABLE 21

RESULTS OF AXIAL LOAD FATIGUE TESTS FOR NOTCHED (K_t = 3.0) SHORT TRANSVERSE SPECIMENS AT A STRESS RATIO OF R = 0.1 FOR HEAT 9

Specimen Number	Maximum Stress, ksi	Cycles to Failure
9-45ST	55	28,800
9-43ST	50	499,400
9-42ST	45	144,700
9-41ST	40	953,100
9-44ST	35	3,228,800
9-40ST	30	6,675,900

TABLE 22

RESULTS OF AXIAL LOAD FATIGUE TESTS FOR NOTCHED (K_t = 3.0) SHORT TRANSVERSE SPECIMENS AT A STRESS RATIO OF R = -0.25 FOR HEAT 9

Specimen Number	Maximum Stress, ksi	Cycles to Failure
9-49ST	45	39,600
9-51ST	40	822,500
9-46ST	40	373,800
9-50ST	35	429,500
9-47ST	35	1,317,900
9-48ST	30	9,043,900

TABLE 23

RESULTS OF AXIAL LOAD FATIGUE TESTS FOR UNNOTCHED SHORT TRANSVERSE SPECIMENS AT A RATIO OF R = 0.1 FOR HEAT 14

Specimen Number	Maximum Stress, ksi	Cycles to Failure
14-17ST	80	141,100
14-21ST	70	471,600
14-19ST	60	755,400
14-20ST	55	1,877,000

TABLE 24

RESULTS OF AXIAL LOAD FATIGUE TESTS FOR UNNOTCHED SHORT TRANSVERSE SPECIMENS AT A RATIO OF R = -0.25 FOR HEAT 14

Specimen Number	Maximum Stress, ksi	Cycles to Failure
14-18ST	100	21,600
14-24ST	90	35,800
14-16ST	85	37,700
14-23ST	80	155,900
14-15ST	75	98,140
14-13ST	70	126,000
14-14ST	70	500,000
14-25ST	60	269,500
14-11ST	60	871,800
14-10ST	55	1,700,000
14-12ST	55	515,800
14-22ST	50	10,000,000 (a)

(a) Did not fail.

TABLE 25

RESULTS OF AXIAL LOAD FATIGUE TESTS FOR UNNOTCHED LONGITUDINAL SPECIMENS AT A RATIO OF R = -0.25 FOR HEAT 14

Specimen Number	Maximum Stress, ksi	Cycles to Failure
14-40L	120	30,640
14-42L	110	33,640
14-46L	100	72,040
14-41L	90	203,300
14-39L	80	513,840
14-38L	75	801,140
14-43L	70	1,257,330
14-45L	70	500,230
14-44L	65	1,247,490
14-47L	65	1,061,000
14-48L	55	1,515,560
14-49L	50	10,000,000 (a)

(a) Did not fail.

TABLE 26

RESULTS OF AXIAL LOAD FATIGUE TESTS FOR NOTCHED (K_t = 3.0) SHORT TRANSVERSE SPECIMENS AT A STRESS RATIO OF R = 0.1 FOR HEAT 14

Specimen Number	Maximum Stress, ksi	Cycles to Failure
14-29ST	50	62,400
14-28ST	45	207,800
14-26ST	40	178,400
14-31ST	40	500,600
14-27ST	35	1,193,900
14-30ST	30	10,000,000(a)

(a) Did not fail.

TABLE 27

RESULTS OF AXIAL LOAD FATIGUE TESTS FOR NOTCHED (K_t = 3.0) SHORT TRANSVERSE SPECIMENS AT A RATIO OF R = -0.25 FOR HEAT 14

Specimen Number	Maximum Stress, ksi	Cycles to Failure
14-33ST	45	108,630
14-32ST	40	54,330
14-35ST	40	72,210
14-37ST	35	607,170
14-34ST	30	1,986,800
14-36ST	25	10,000,000(a)

(a) Did not fail.

REFERENCES

1. F. R. Schwartzberg, "Rare-Earth Elements in Titanium and Zirconium," Special Report to the Rare-Earth Research Group, Battelle Memorial Institute, Columbus, Ohio, March 31, 1958.

2. K. A. Gschneidner, Jr., Rare Earth Alloys, D. Van Nostrand Company, Inc., Princeton, N. J. 1961.

3. F. H. Spedding and A. H. Daane, The Rare Earths, John Wiley & Sons, Inc., New York, 1961.

4. H. B. Bomberger and S. R. Seagle, "Method of Improving Macrostructure of Titanium-Base Alloy Products," U.S. Patent No. 3,679,403, July 25, 1972, assigned to RMI Company, Niles, Ohio.

5. M. J. Buczek, G. S. Hall, and S. R. Seagle, Grain Refinement of Titanium Alloys, AFML-TR-74-255, November 1974, Air Force Materials Laboratory, Wright-Patterson AFB, Ohio.

6. H. B. Bomberger, and S. R. Seagle, "Method of Producing a Hot-Worked Titanium Product," U. S. Patent No. 3,963,525, June 15, 1976, assigned to RMI Company, Niles, Ohio.

7. M. Hoch, "The Solubility of Yttrium Oxide (Y_2O_3) in Liquid and Solid Titanium," unpublished work, University of Cincinnati, August, 1977.

8. R. P. Simpson, "Controlled Weld-Pool Solidification Structure and Resultant Properties with Yttrium Inoculation of Ti-6Al-6V-2Sn Welds," Welding Research Supplement to the Welding Journal, March, 1977, pp 67s - 77s.

9. S. R. Lyon, S. Inouye, C. A. Alexander, and D. E. Niesz, "The Interaction of Titanium with Refractory Oxides," in Titanium Science and Technology, Vol. 1, pp 271 - 284, edited by R. I. Jaffee and H. M. Burte, Plenum Press, New York, 1973.

10. W. R. Kerr, Private communication with R. F. Geisendorfer of unpublished work, AFML, April 1977.

11. D. R. Schuyler, J. A. Petrusha, G. S. Hall, and S. R. Seagle, Development of Titanium Casting Technology, Final Report AFML-TR-76-80 (AD A031776), AiResearch Mfg. Co. of Arizona, Phoenix, AZ and RMI, Inc., Niles, Ohio, Contract No. F33615-74 C-5055, August, 1976.

12. B. B. Rath, Private communication with R. F. Geisendorfer on the interaction of yttria with Ti-6Al-4V.

13. S. M. L. Sastry, Informal presentation to AFML personnel, AFML, Wright-Patterson AFB, Ohio, 18 May 1977.

REFERENCES (CONTINUED)

14. A. W. Sommer and M. Creager, Research Toward Developing an Understanding of Crystallographic Texture on Mechanical Properties of Titanium Alloys, Technical Report AFML-TR-76-222, Air Force Materials Laboratory, Wright-Patterson AFB, Ohio 45433, January, 1977.

15. S. L. Lopata and E. B. Kula, "A Reflection Method of Pole Figure Determination," Transactions of the Metallurgical Society of AIME Vol. 224, 1962, p 865.

16. R. H. Olsen, Metallography, 5, p 369, 1972.

17. A. W. Bowen, "The Effect of Testing Direction on the Fatigue and Tensile Properties of a Ti-6Al-4V Bar," Titanium Science and Technology, Volume 2, p 1271, R. I. Jaffee and H. M. Burte, Editors, Plenum Press, New York, 1973.

18. F. Larson and A. Zarkades, "Properties of Textured Titanium Alloys," Metals and Ceramics Information Center Document MCIC-74-20, June 1974, Available from NTIS, Springfield, VA 22151.

19. J. C. Williams and M. J. Blackburn, "The Identification of a Non-Basal Slip Vector in Titanium and Titanium-Aluminum Alloys," Phys Stat Sol Vol 25, P K-1, 1968.

☆U.S.Government Printing Office: 1979 — 657-002/718